



Rapid Solution Exchange to Neuronal Culture Grown on Multi Electrode Arrays

by Nitzan Herzog

Thesis submitted to The University of Nottingham
for the degree of Doctor of Philosophy, January 2017

Contents

List of Figures	4
Abstract	7
Acknowledgements	8
1 Introduction	9
1.1 The MEA culture model for network activity in neuronal ensembles	9
1.1.1 Notable achievements of the neuronal culture on MEA model	9
1.2 Volume transmission in neuroscience	9
1.2.1 Neuromodulator transmission and plasticity	9
1.3 Microfluidics for cell culture	9
1.3.1 Rapid drug delivery	9
1.3.2 Microfluidics in neuroscience	10
1.3.3 Neurons and flow	10
1.4 Ph.D objectives	10
2 Methods	11
2.1 Basic fabrication elements	11
2.1.1 PDMS preparation	11
2.1.2 Thin film spinning	11
2.1.3 Soft lithography	11
2.1.4 PDMS extraction	11
2.2 Bonding techniques	12
2.2.1 Plasma bonding	12
2.2.2 Double sided silicone tape	12
2.3 Surface coating	13
2.3.1 Open surface	13
2.3.2 Devices - Bond-then-PLL	13
2.3.3 Devices - PEI-then-bond	13
2.4 Seeding and maintaining of Neuronal cultures	13
2.5 MEA recording and stimulation	13
2.5.1 Spike detection and noise removal	13

2.5.1.1	Automatic quantification of active channels	13
2.5.2	Electrical stimulation	14
2.5.2.1	Automatic detection of responsive channels	14
2.5.3	Correlation maps	14
2.5.4	Burst detection	14
2.5.5	Functional connectivity analysis	14
2.6	Plasticity protocol	18
2.7	Conditioned media production	18
2.8	Flow experiments	18
2.8.1	Heated chamber	18
2.8.2	Steady flow	18
2.8.3	Pulsing	19
2.9	Immunohistochemistry	20
3	Establishment of a culture model for network activity in neuronal ensembles	21
3.1	Introduction	21
3.2	Development of spontaneous activity in Mouse cultures	22
3.2.1	Statistics of activity and synchronicity measures	25
3.2.2	Comparison between mouse and rat cultures	29
3.3	Evoked activity	30
3.4	Plasticity induction in the presence of dopamine	33
3.4.1	Examining changes in response to stimulation	35
3.4.2	Examining changes in functional connectivity	39
3.5	Chapter conclusion	41
4	Viability of neuronal cultures in microfluidic devices in static conditions and under steady flow	43
4.1	Introduction	43
4.2	Long term neuronal cultures in microfluidic devices	45
4.2.1	Development of protocol	45
4.2.1.1	Evaporation and surface chemistry considerations	47
4.2.1.2	Considerations of factor circulation	47
4.2.1.3	Alternative bonding methods	51
4.2.1.4	Extraction of PDMS	52
4.2.2	Growing microcultures in plasma bonded devices	55
4.3	Viability of neuronal cultures under steady microfluidic flow	59
4.3.1	Pilot flow study	59
4.3.2	Quantitative viability analysis	61
4.4	Chapter conclusion	66

5 Activity under steady microfluidic flow	67
5.1 Introduction	67
5.2 Neuronal cultures in cross flow devices on MEAs	68
5.3 Activity under flow for young cultures	71
5.3.1 Effect of flow rate	71
5.3.2 The semi-permeable membrane approach for shear reduction	74
5.3.3 Considerations of diffusive flux	77
5.4 Activity under flow for old cultures	79
5.4.1 The effect of the media source	80
5.4.2 How old conditioned media performs on young cultures	83
5.5 Interpretation of the activity under flow results	86
5.6 Chapter conclusion	91
6 Rapid Programmatic Drug Delivery to a Neuronal Microculture	92
6.1 Pulsing performance in microculture devices	92
6.1.1 Analysis of pulsing visualized by fluorescein	93
6.1.2 Numerical simulation of drug pulsing	93
6.1.3 Effect of well depth on pulsing performance (optional)	93
6.2 Establishment of long term Neuronal microcultures	96
6.2.1 PEI-then-all-tape devices	96
6.2.2 PEI-then-PDMS-tape device	96
6.2.3 Activity in normal conditions	96
6.3 Behaviour under flow	100
6.4 Glutamate pulsing	100
6.5 Dopamine pulses	101
7 Discussion	106
7.1 The utility of the culture model	106
7.2 The shear protection vs. conditioning protection issue	106
7.2.1 Limitation uncovered by the conducted experiments	106
7.2.2 Avenues for further expansion of the model	106
7.3 Importance of extrasynaptic environment	106
7.4 Prospects of the <i>in vitro</i> volume transmission model	107
A Appendix	108
A.1 MEA Data sheets	108
A.2 Heat transfer for water flowing in a PTFE tube	108
Bibliography	108

Chapter 3

Establishment of a culture model for network activity in neuronal ensembles

3.1 Introduction

As reviewed in section 1.1, neuronal cultures grown on multi electrode arrays have emerged as a successful model for studying generic properties of neuronal ensembles at the network level. The overall purpose of this Ph.D work is to provide this model system with an added functionality of phasic volume transmission, thus achieving a novel experimental platform for studying how fine temporal feature of extrasynaptic agonist concentrations interact with the activity. In this first chapter we describe the establishment of the standard neuronal cultures on MEA model system within our laboratory group. We followed their development for over 3 weeks *in vitro* and demonstrated that they develop normally and exhibit hallmark network activity, both spontaneous and evoked, and comply in characteristics with the literature^{old} standard.

To date, MEA investigation have been dominated by use of primary cultures derived from rat. However, mouse is generally a more popular neuroscience model and offers a greater library of molecular and genetic tools so using it as a tissue source might be beneficial. Thus, an additional contribution presented in this chapter is the examination of mouse based cultures and comparison with rat preparations in the context of MEA investigations. We found that the mouse cultures were difficult to culture on the MEA surface and exhibited a delayed synaptic maturation as compared to their rat counterparts. Nevertheless, mouse cortical cultures that were able to develop exhibited all the richness of network phenomena described in rat literature.

Finally, prior to engaging in the development of the microfluidics system for rapid pulsing

we took the chance to explore generating a slower phasic dopamine signalling model in these traditional experimental systems by manually pipetting the agonist (in this case dopamine) onto the culture followed by replacement of the media. We used this approach to revisit the long standing issue of plasticity in these systems.

Synaptic plasticity without neuromodulation in neuronal cultures on MEA has been controversial as multiple reports produced contradictory or negative results (reviewed further in section 3.4). This contrast to slices and *in vivo* systems where activity dependent plasticity induced through stimulation or behavioural paradigms is well established [1]. It should be noted that spike timing dependent plasticity had been demonstrated in hippocampal cultures for pre and post synaptic neuron pairs explicitly controlled and monitored via patch clamp [2]. The lack of success on MEAs cannot, therefore, be attributed so a skewed biology of neurons in culture and it is not yet clear if it is related to the poorer sensitivity of the extracellular recordings (sensitive only to super-threshold processes), to the culture network topology which needs to be accounted for in the stimulation protocols, or to the absence of neuromodulators. Indeed that dopamine modulates plasticity in culture has been established but using bath application therefore only interrogating tonic effects [3, 4].

Thus, as a final step in this chapter, we revisited the question of plasticity induction and found that a standard tetanization protocol does not produce a measurable change in evoked responses or in functional connectivity in our cultures. We then explored whether slow pulsing of dopamine by manually adding it during the plasticity-induction phase (tetanization) and washing it away immediately after could have an enabling effect on plasticity. We found that the altered protocol results in a change to activity and connectivity measures but argue that the effect of the washing cannot be easily separated from that of the dopamine, hence confusing the interpretation. This chapter thus serves to establish the multi electrode array electrophysiology technique and to provide motivation for the development of the microfluidics technology in the following chapters.

3.2 Development of spontaneous activity in Mouse cultures

Primary mouse embryonic cortical cultures were seeded on pre-coated MEAs as described in sections 2.3 and 2.4. All MEAs used for the work undertaken in this chapter are of 8x8 configuration with $30\mu m$ electrodes and $200\mu m$ electrode spacing (see appendix A.1 for data sheets).

Figure 3.1 A-C shows microscope images of a representative culture over 18 days in culture. The images show how over the first few days the cells became polarized and extended neurites and dendrites. As these continued to grow, branch and generate synaptic contacts the culture obtained a weblike appearance. In later days of development an obvious mass of extracellular tissue was evident in between the cells covering the previously bare glass

and engulfing the fine cellular processes. In the case of the mouse cultures, many of the preparations did not develop properly whereby, despite good initial adhesion, the majority of the plated cells did not continue differentiating and after a few days detached from the surface and degenerated (figure 3.1 D). This was the case for over half of plated cultures and these were discarded during the experiment. Cultures prepared from rat embryos did not present this sort of inconsistency and generally developed at a high success rate despite using the same MEAs and generally same coating and seeding procedures.

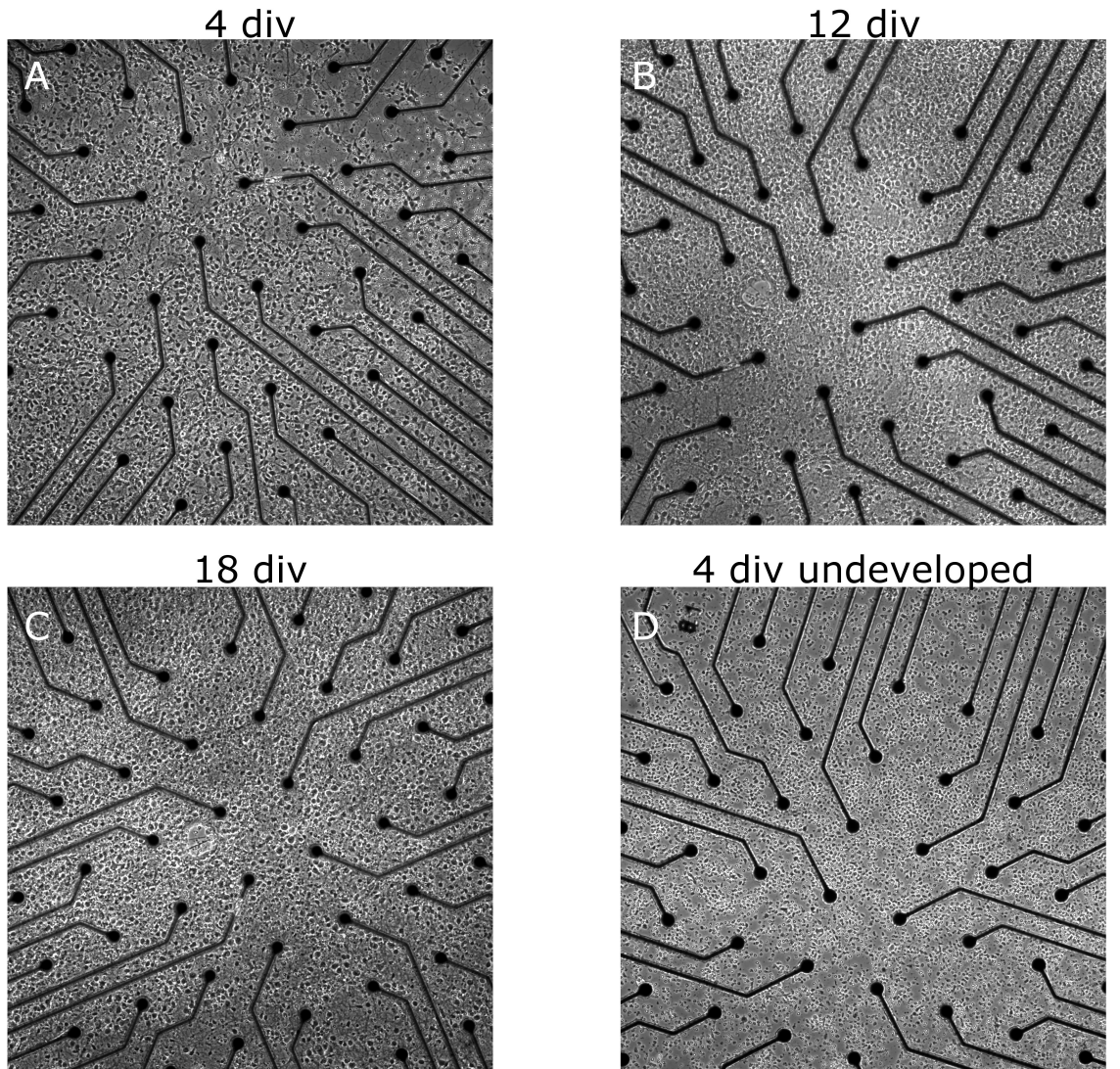


Figure 3.1: Cortical mouse cultures develop to become a densely interconnected neural tissue. (A-C) Cortical culture prepared from mice embryos and plated on micro-electrode arrays imaged on several time points over development. by 4 days *in vitro* most of the cells show an obvious polarized neuronal morphology and extended neurites. At 12 days *in vitro* a thick ECM tissue is evident between the cells (D) Example of a seeded culture that didn't show proper development. The electrodes are $30\mu m$ wide and spaced $200\mu m$ apart.

We monitored the activity of the mouse cultures for 3 weeks in *in vitro*. The analysis

performed throughout this thesis is restricted solely to spiking activity and lower frequencies associated with local field potentials were filtered out of the data. Spike detection was performed through a combination of match filtering and simple threshold crossing. A second pre-analysis step detected and removed erroneous spike waveforms induced by electromagnetic noise and which generated synchronized spiking events across several channels (see section 2.5 for full description of the pre-analysis). No spike sorting was attempted as this was shown to be ineffective in culture [5].

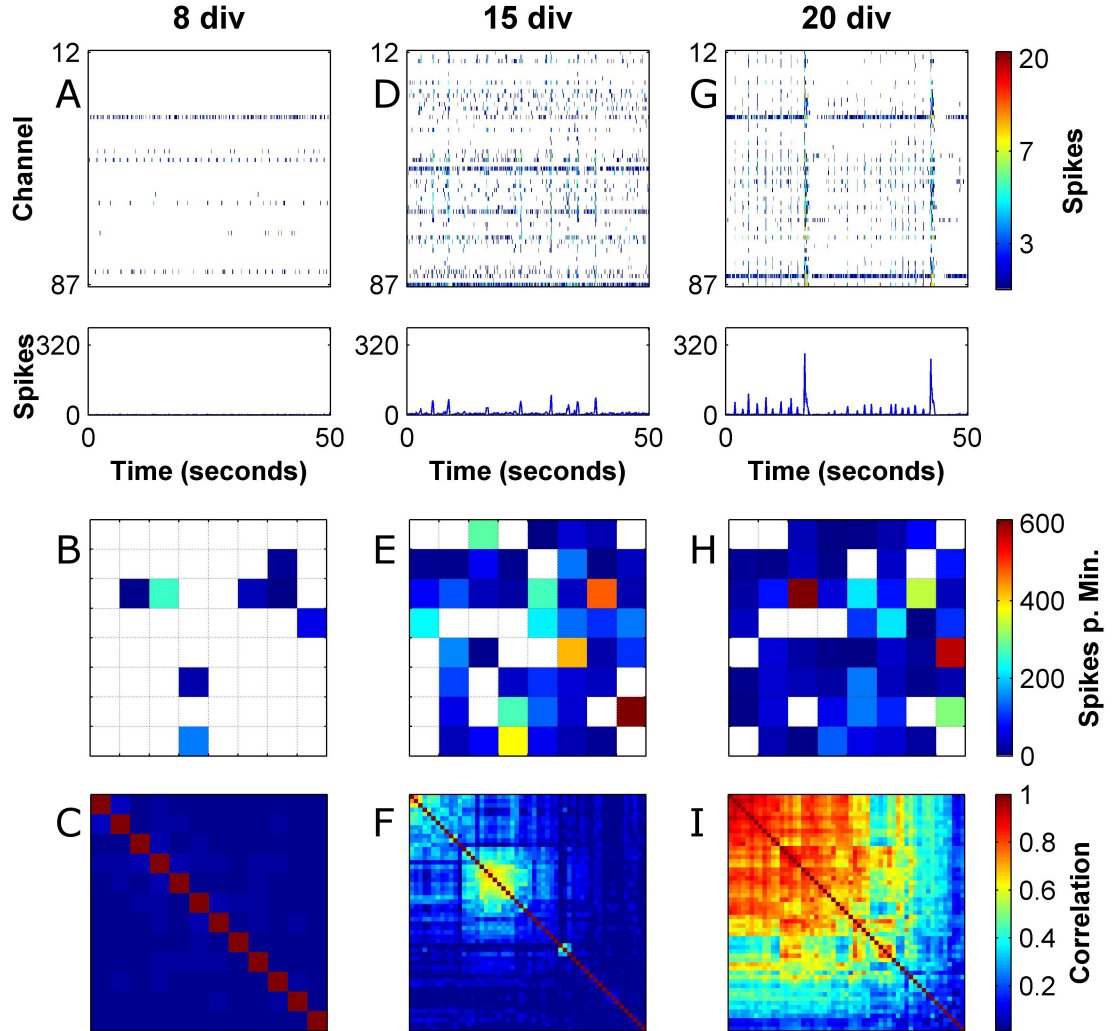


Figure 3.2: Spontaneous activity in mouse culture develops from tonic firing into synchronized bursting events. (A,D,G) Raster plot of spontaneous activity in mouse culture in 3 developmental time points exhibiting the change in the activity structure. Raster plots are presented in 100ms bins. Bottom panels show summation of raster over all channels. (B,E,H) Activity maps showing the spatial organization of activity on the MEA in the same time points. (C,F,I) Dendrogram-sorted correlation matrices showing groupings of channels into correlated blocks.

Virtually no spikes were recorded until approximately 5 days *in vitro*, at which point tonic firing started to emerge in some of the channels. Beyond this point, the proportion of active channels and measured activity increased until reaching a plateau at about 13 days *in vitro* (figure 3.3). The development of synchronization in the cultures is exemplified in Figure 3.2 which shows raster plots at several developmental stages along with the associated mean firing rate maps and dendrogram-ordered cross channel correlation matrices. At 8 days *in vitro* only a small proportion of the channels was tonically active and showed regular spiking (figure 3.2 A). At this point there was very little correlation across the channels suggesting that the measured spike trains aren't driven by synaptic integration but rather controlled through intrinsic neuronal excitability. At 15 days *in vitro* most of the MEA channels exhibited spiking activity (figure 3.2 D). At this point some correlated spiking events (network bursts) began to emerge although most of the the activity was still regular and uncorrelated. These network bursts were not easily discernible in the multi channel raster plot but were evident as large peaks in the summated network activity and as increased correlations between a subset of the channels. To appreciate the significance of the observed correlations, we generated surrogate independent spike rasters where the spikes trains were drawn from an independent Poisson processes with rate parameters as in the original channels (see section 2.5.3). For the data shown in figure 3.2, the maximal observed correlations between two different channels in the surrogate independent spike rasters were 0.05, 0.05 and 0.07 for 8, 15 and 20 days *in vitro*, respectively. These values are negligible compared to the observed values in the correlation matrices for 15 and 20 days *in vitro* and therefore indicate a genuine coupling between the measured neurons. Towards the end of the 3rd week (here 20 days *in vitro*) most of the activity in the cultures was restricted to the network bursts (figures 3.2 G and 3.4 E).

During the early phases of synchronicity (beginning of 3rd week, here 15 days *in vitro*) it was common to observe more than one synchronized cluster of channels in the dendrogram-sorted correlation matrices (figure 3.2 F). Nevertheless, correlations between these clusters continued to develop to the point where the entire culture became a single synchronized unit (end of 3rd week, figure 3.2 I). Previous work showed that applying synaptic blockers at non saturating quantities to fully developed neuronal cultures reveals an underlying modular connectivity pattern through breaking the weaker links between modules while still preserving denser intra-module connections [6]. Our results are compatible with this notion of underlying modularity and show that the modules are formed at the earlier stages of synaptic maturation.

3.2.1 Statistics of activity and synchronicity measures

Figure 3.3 shows activity related statistics over our experimental data set comprising 5 mouse cultures. Long term electrophysiological studies of this type have been facilitated by the introduction of the MEA technology which easily allows sampling of multiple cells

in parallel and repeatedly over long stretches of time. Patch clamp electrophysiology, in contrast, is usually restricted to a few cells at a time and cultures have to be discarded after a single experimental session as it is harder to maintain the cells healthy and sterile. Nevertheless, MEA developmental studies have been almost completely exclusive to cortical cultures made from rat embryos. Thus, with this study, apart from ascertaining that the cultures are healthy, we examine if there are any developmental differences between mouse and the rat based preparations.

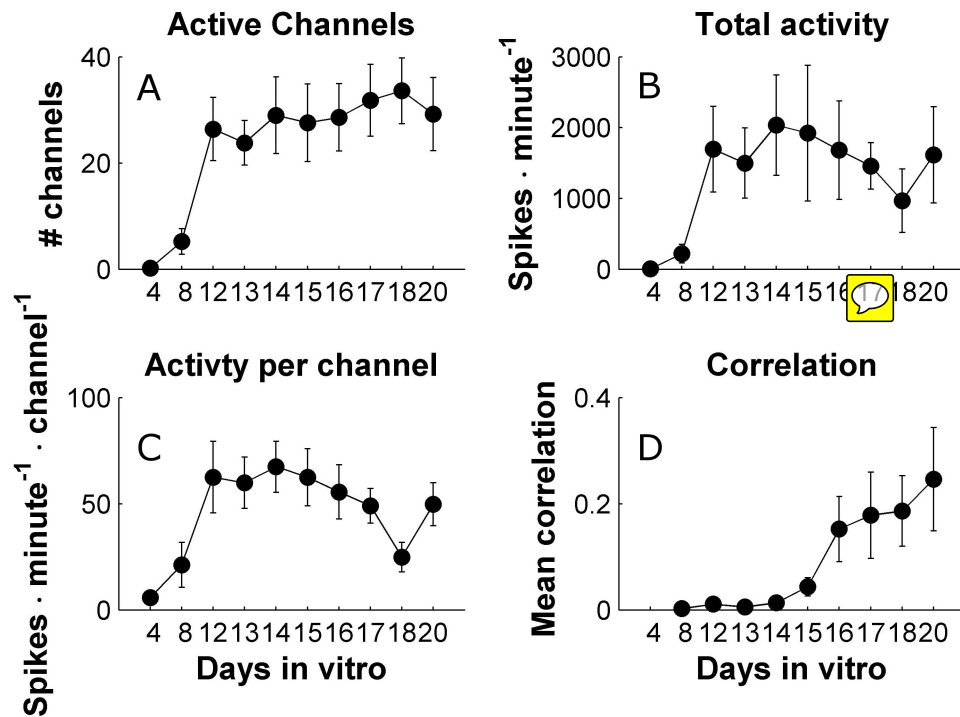


Figure 3.3: Development of synchronicity in mouse cultures lags after activity. (A) Development of the number of active channels as a function of culture age. (B) Development of the total number of spikes recorded on all MEA electrodes. (C) Development of the mean neuron firing rate (average of firing rate over active channels - implied assumption that each electrode records a single neuron). (D) Development of mean correlation. Mean correlation for a recording is the average of the correlation matrix taken without the diagonal. The data is shown as mean and SEM based on n=5 cultures.

The cultures do not become fully active until approximately 2 weeks in culture suggesting that this period of time is required for the seeded progenitor cells to become mature excitable neurons (figure 3.3 A-C). This time frame for activity onset is consistent with rat literature [7, 8, 9] and is generally accepted with regard to culture electrophysiology. After the initial increase, the firing rates (figure 3.3 C) stabilize at around 1Hz and don't exhibit a time dependent trend (1-way ANOVA, p=0.3). The average firing rate per channel is compatible with studies from rat cultures which reported values in the range of 0.4 – 1.5Hz [9, 7, 10, 11]

but the lack of trend is strikingly different as rat cultures are reported to show a marked increase in individual firing rates until 21 days and a decline afterwards [9, 12].

Figure 3.3 D shows the development of correlations in our cultures. The correlation value for a given recording is the mean of the correlation matrix (e.g., figure 3.2 C,F and I) without the diagonal. Evidently, despite the stabilization of the mean unit firing rates at day 13 *in vitro*, significant correlations started to arise only from about 17 days *in vitro*. This suggests that the excitability in the cultures is initially controlled by intrinsic homeostatic mechanisms which are later replaced by synaptic drive. Remarkably, the apparent increase in synaptic efficacy is not accompanied by an increase in spiking activity suggesting that the unit mean firing rate of 1Hz is a controlled quantity which the neurons maintain in the face of a changing network environment around them. Indeed, it has been shown that cultured neurons are capable of rapidly modifying their intrinsic excitability in response to pre-synaptic blockers [11].

To further characterize the spontaneous activity in the cultures we employed a burst detection algorithm as detailed in section 2.5.4 and extracted parameters of burst related measures, shown in figure 3.4. Not surprisingly, the development of bursting activity followed the same pattern as mean correlation and trailed the development of activity by a few days (figure 3.4 A,D compared to figure 3.3 A-C). This separation between measures of activity and of those of synchronicity underlines the utility of the MEA system in recognizing and disentangling biological processes that are linked. Previous rat cultures studies report that regular bursting is apparent already towards the end of the 2nd week *in vitro* [7, 8, 9, 12] whereas in our mouse data this was rare. In these reports the evolution of bursts appeared to go hand in hand with the evolution of activity, both of which peaked at 21 days *in vitro* and declined afterwards. As bursting behaviour in our data is a few days delayed and starts in the middle of the 3rd week *in vitro* it is plausible that a similar trend (but delayed) would be observed had we recorded further into the 4th week.

It should be noted that the peak burst rate value observed (15 minute^{-1}) was much higher than the one reported for rat cultures at the same age of development (5 minute^{-1}) [9]. However, we do not believe that this strong discrepancy lies in the difference between the preparations. Rather, our burst detection algorithm (section 2.5.4) uses an innovative approach for identifying synchronized events. Our method computes surrogate spike rasters with identical firing rates as the original data but without correlations to define the burst detection threshold. The thresholds defined in this way are likely to be tighter than for previous approaches where the thresholds were manually selected based on personal preference of how well they fit the data [8, 13]. Since our thresholds are based on an objective criteria we argue that the observed burst rate indeed reflects synchronized events and that the rate of these is actually greater than previously reported.

Further evidence for delayed synaptic maturation is provided by the burst width and burst size measures. Previous work has established that bursts in naive rat cultures exhibit

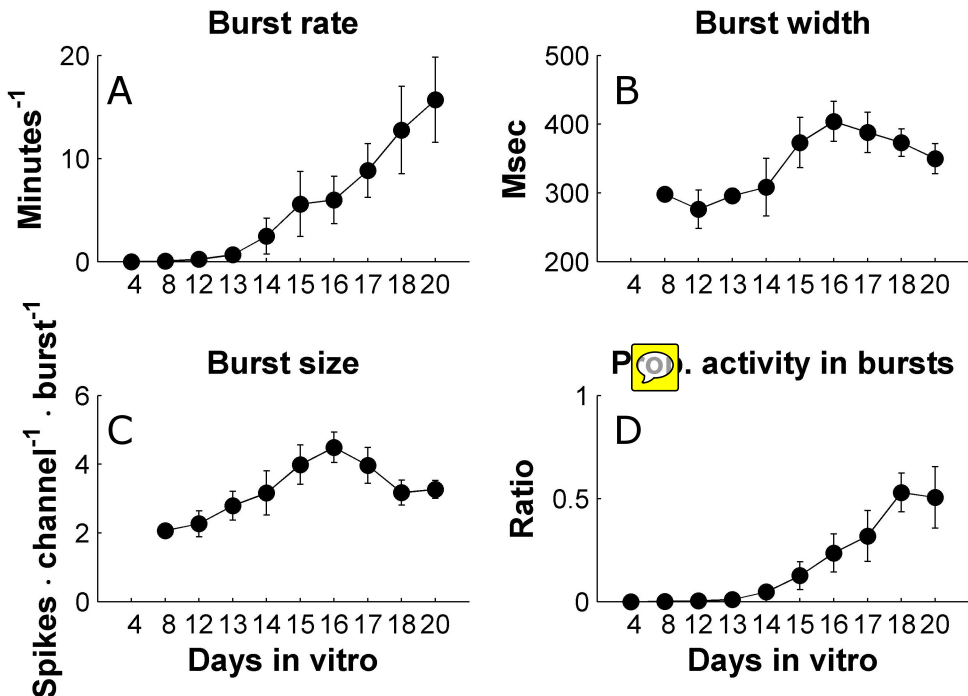


Figure 3.4: **Development of bursting measures in mouse cultures lags behind activity.** (A) Development of burst rate as a function of culture age. (B) Development of burst width. (C) Development of burst size. (D) Development the ratio between the number of spikes observed with in bursting events and the total recorded spikes. Data is shown as mean and SEM based on n=5 cultures.

wide temporal profiles with long tails of spike discharges that could last up to several seconds [9, 14]. Over the 3rd-4th weeks the burst profiles become narrow and exhibit increasingly faster termination until saturating in the end of the 4th week. This change is attributed to the development of the GABAergic neurotransmission which was shown to occur 1-2 weeks in delay as compared to the glutamatergic system [15]. Hence it has been postulated that feedback loops operating through inhibitory interneurons become functional only in the aforementioned time period [7] (also see an *in vivo* correlate in [16]). In the rat data the bursts show maximal width when they first appear (10-14 days *in vitro*). In our data, a similar trend is observed with peaks appearing in the burst size and burst width measures at 17 days *in vitro*, which is approximately the point when bursting activity became appreciable (time effect was found significant through 1-way ANOVA for both burst size and burst width measures with p=0.035 and 0.028, respectively).

Taken together, the results from the spontaneous activity study demonstrate that, on one hand, the development of neurotransmission and synaptic connections in our mouse cultures appears to be delayed between 3 days to one week. On the other hand, irrespective of the delay, the cultures exhibit all the activity features expected from literature, such as,

homeostatic control of excitability, underlying modularity and development of synchronicity and bursting activity which evolve in accordance with the development of the synaptic networks. Nevertheless, as mentioned in the beginning of this section, the mouse cultures posed an added difficulty of a high culturing failure rate which, together with the delayed electrophysiological development raised concerns regarding their utility and ease of use. We therefore decided that, following the study performed in this chapter, rat based preparations would be used for the remainder of the Ph.D work. The next section will outline a brief pilot study to compare our rat based preparations with the mouse based ones and assert that the former shows an electrophysiological profile in par with the literature.

3.2.2 Comparison between mouse and rat cultures

In order to compare the functional development of mouse based and rat based cultures we recorded spontaneous activity from a set of rat cultures, prepared using a protocol identical to the mouse ones. It should be noted that although the reagents, dissociation techniques and growth conditions were indeed identical, there was still a difference originating from the differing tissue source. The rats were delivered from a private animal facility and operated on within our lab space, whereas the mice were bred in a university based animal facility where they were also operated. The cell suspension for the mice culture therefore had to be carried between buildings before plating which could account for an  observed differences. Nevertheless, we believe  this to be unlikely.

Figure 3.5 shows a comparison between rat based and mouse based cultures at the same age *in vitro* for several activity and synchronicity measures introduced earlier. A particularly pronounced difference was observed in the closely related measures of correlation and ratio of intra-burst to total activity both of which showed a significantly higher values in the rat cultures (1-sided unbalanced t-test, $p=0.017$ and 0.039 , respectively). These differences demonstrate that mouse cultures exhibited more uncorrelated activity as compared with their rat counterparts. This reiterates the observation discussed in the previous section that the mouse cultures show delayed synaptic development.

Another observed difference is that the mouse cultures showed a significantly higher average unit firing rate (one sided unbalanced t-test, $p=0.048$). This result could be another manifestation of the rat neurons being more attuned to the synaptic drive from the network but is harder to interpret. In any case, the mean values for both preparations types (1Hz and 0.5Hz for mouse and rat, respectively) are within the literature range ($0.4 - 1.5\text{Hz}$).

Both preparations showed a nearly identical burst rate of about 15 minute^{-1} . The burst rate measure is different to the correlation and activity ratio measures in that it counts synchronized events but is indifferent to activity outside such events. This in contrast to the correlation and intra-burst to total spikes ratio measures which are sensitive to activity both inside and outside the synchronized events. The fact that the reduced synaptic coupling in mouse cultures does not affect the burst rate suggests that this measure is strongly

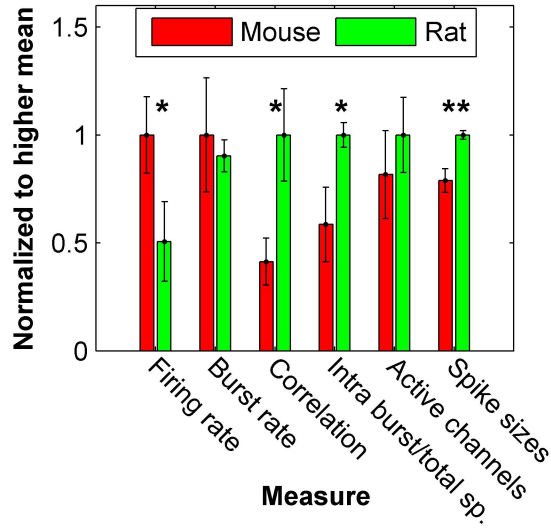


Figure 3.5: **Rat cultures show increased correlation as compared to rat cultures at the same age.** Six measures are considered and are normalized to whatever mean is higher amongst the two compared groups. *, ** indicate statistical significance of the difference between the groups at levels of confidence of 95% and 99%, respectively. Mouse statistics are based on $n=5$ cultures and rat statistics on $n=4$ cultures. Culture ages at the time of recording were selected so that both groups had the same mean age of 19.5 days *in vitro*.

related to the general excitability and not just to the synaptic development.

Finally, the spike sizes measure shows the mean of peak voltage in the recorded extracellular spike waveforms across all mouse and rat recordings (see section 2.5 for example waveforms). Surprisingly, we found a significant reduction in peak voltage for the recording from mouse preparations as compared to the rat preparations. This indicates that the two types of neurons are different in their excitability properties and that, in all likelihood, mouse neurons express a lower density of voltage dependent ion channels.

In summary, the comparison performed confirmed that the mouse cultures are delayed in synaptic maturation as compared to rat cultures and thereby display reduced correlations at the same age *in vitro*. As far as these results can corroborate, our rat based preparations present all the features and developmental time course that have been described in literature and will therefore be selected for the work carried out in the following chapters.

3.3 Evoked activity

An important feature of the MEA technology is the ability to induce generation of action potentials through injection of a current waveform into the extracellular electrodes. This is an important functionality as it provides means to provide input to the network and to control the culture activity. Past work has provided effective stimulation protocols and

showed that short current pulses can induce individual action potentials as well as a network response [17, 18]. This methodology was used to study response properties of single isolated neurons over long periods of time [19] and how several stimulation pulses interact with each other as a function of temporal proximity [20, 21, 22]. This approach was used to model sensory input by providing more complex spatio-temporal stimulation pattern and examining the extent to which the information present in the input signal can be decoded from the culture activity [23, 24]. Interestingly, it was shown that high frequency stimulation can break down the synchronized bursting structure of the culture activity, presumably in analogy to brain structures which exhibit higher frequency content when subjected to a high volume of input during active sensory processing [25].

To demonstrate that our system is able to effectively interface with the culture and provide input, we present data from a stimulation session where 120 test pulses were applied every 5 seconds (see section 2.5.2 for technical details). Data for two distinct stimulation sites  shown. Figure 3.6 A-B shows raster plots of the stimulation responses (at the different sites) averaged over all channels in a 500ms window after the stimulation pulse, as well as a cumulative  PSTH. The PSTH is bimodal with a sharp peak observed within the first 25ms after stimulation and a second, significantly wider and less defined peak which  lasts about 200ms after stimulation. The first peak is considered to represent direct responses, i.e., spikes elicited directly as a result of the stimulation pulse without synaptic mediation. The second peak is thought to be a manifestation of a multi-synaptic reverberating activity in response to the first step of activation. Indeed, it is evident from the response rasters that the first stage of response is significantly more repeatable than the second one which not always present. This is compatible with the above interpretation as direct responses are spikes generated due to a stimulation induced localized depolarization and depend only the specific biophysics and geometry of the neuron so they are expected to occur at a set delay and low jitter. The reverberating response, on the other hand, is a complex phenomena which depends on the network state preceding the stimulus so it stands to reason that it would show large variability or even fail to propagate on occasion. Nevertheless, it should be noted that even the direct responses were far from operating at a 100% success rate, a single neuron reproducibility issue that has been under much debate within neuroscience ci [26, 19].

Comparing between the responses to the two stimulation sites it is evident that they differed in direct responses with stimulations in channel 71 producing a second direct response peak which is also observable as a vertical line in the response rasters. The reverberating response did not show conspicuous differences in shape or latency although it seemed somewhat smaller. Another view on the differences between the two stimulation sites is given in figure 3.6 C-F which show spatially resolved response rasters and response maps for all participating channels, averaged over the stimulations. The spatial response profile appears to be very similar comparing the two stimulation electrodes - each channels showd s similar

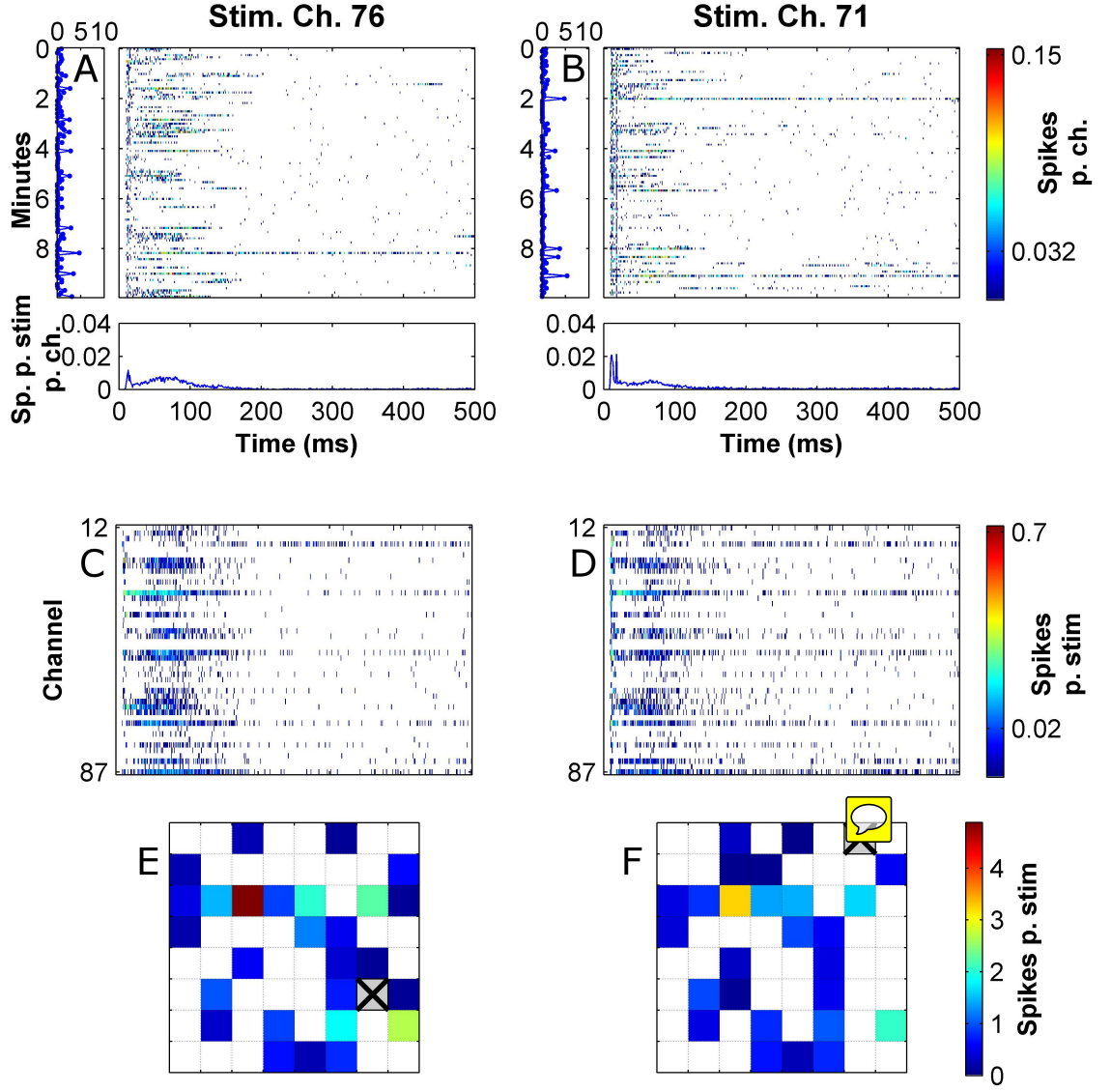


Figure 3.6: Stimulation pulses at different electrodes vary in direct responses but produce a similar reverberative responses. Test stimuli were applied every 5 seconds. (A-B) Main panel: Each line is a response raster for one test stimulus averaged over 510 channels. Left panel shows the sums of the responses shown in the main panel over the post stimulus observation time window (i.e., number of spikes per channel observed in 500 ms period post stimulation). Bottom panel shows the average of the response rasters over all stimuli. This is the PSTH. (C-D) Spatially resolved PSTHs, i.e., each line is a channel PSTH. (E-F) Stimulation response maps showing the sums of the PSTHs in (C-D) in the actual spatial locations. These response maps only show channels with a stimulation response that is significantly higher than background spontaneous activity for that channel (see section 2.5.2 for selection procedure). A,C,E and B,D,F show response data for two stimulation sessions applied to two different electrodes (indicated in E,F) run one after the other in **co**mission on the same culture.

strength and duration of activation. There are some differences in latency but these were relatively unpronounced, at least to the naked eye. Although we did not study this in depth, it was our impression that different stimulation electrodes differ in mainly whether they are able to produce a reverberating response. However, once this response was elicited it seems to be stereotypical, i.e., each culture develops to take on a particular identity which is ~~co~~^{uted} whenever a synchronized burst occurs regardless of the site of induction or if it is spontaneous or evoked. It has been suggested that the lack of sensory input during culture development drives it into a degenerate state of over connectedness which might explain this rigidity. On the other hand, it should be noted that distinct yet overlapping responses to different stimulation sites have been reported [27]. Additionally, decoding of spatial stimulation information from culture data has been successfully demonstrated [28] so this system might nevertheless model genuine neural coding mechanisms from *in vivo*.

3.4 Plasticity induction in the presence of dopamine

Mature neuronal cultures abide to the principles of spike timing dependent plasticity (STDP), demonstrated in a paired pulse paradigm [2]. Modulation of the effective STDP window by dopamine has also been shown [3]. These results have raised the interesting possibility that neuronal cultures grown on multi electrode arrays could be used to study how plasticity operates at the network level. This sparked a substantial body of work to devise paradigms for induction and observation of plasticity using just the extracellular network recordings and stimulations. Initial efforts have focused on brief tetanic stimulations inspired by the original experiments discovering LTP and which used this stimulation protocol [29]. Positive reports employing tetanus based induction have reported either a generalized potentiation in evoked responses which could be observed using simple measures such as summated response over all MEA electrodes [30, 31, 32] or more subtle effect that did not involve global change but rather antagonistic changes to the different channels and required more sophisticated multi-variate analyses to observe [33, 34, 35]. The ~~la~~^{ter} type of plasticity was observed both in evoked responses as well as in spontaneous activity. Indeed that tetanus induces a global potentiation is not surprising given that the original LTP experiments involved potentiation in the LFP measurements which represent large populations of neurons. However, it is known that neuronal systems employ homeostatic mechanisms to keep the general excitation levels constant [36] so such extreme modifications to activity are likely to be unphysiological. In that sense it is interesting that more subtle forms of plasticity are observed in the multi dimensional aspect of the activity. However, it is unclear why similar protocols produce such difference in outcome in different studies and different labs. Later work has shown that low frequency stimulation protocols can also induce changes in spontaneous activity of the subtle type [34, 37]. This result is interesting as natural input during real-life behavioural learning is probably more similar to such low frequency signals than to tetanus. Obviously, behaviour

in general and learning in particular are a closed loop process and this was modeled, to a certain extent, with feedback systems where the stimulation pattern was directly informed by the preceding neuronal activity [38, 39]. These important works showed that the direction and extent of plasticity can be controlled to follow bespoke criteria and therefore established that they are indeed relevant for goal directed learning 

As mentioned above, the quest to find plasticity in neuronal cultures grown in MEAs has produced successes but also contradictory, controversial and negative reports [27, 40]. Here we provide our own contribution to the discussion by applying one of the reported protocols to our mouse  cultures and checking for plasticity. Additionally, as reviewed in section 1.2.1, neuromodulators have been shown to be strongly associated with neuronal plasticity and their presence or absence can strongly affect the direction of change (i.e., potentiation or depression) or even abolish it altogether. Moreover, neuromodulators have been shown to operate in both a tonic and phasic mode, where the phasic discharges are thought to act as a reward signal and whose timings are important for selecting neuronal activity that is relevant for the rewarded behaviour. Since neuromodulators have not been used in conjunction with plasticity and neuronal cultures on MEAs we decided to include a phase within our protocol where dopamine is introduced just for the induction phase and washed away afterwards. This to mimic a phasic mode of dopamine operation and to check if it enables the plasticity.

We elected to use a tetanus based protocol based on [30]. The reasons for selecting this protocol are as follows: Firstly, some of the past plasticity work on MEAs did not include a control to verify that the observed changes are due to the stimulated activity and not an artefact. Although this may seem unscientific it is a consequence of the nature of the system where each sample takes a long time to produce, maintain and measure. As a result, achieving a high n-number for both experiment and control is in some cases impractical. Our protocol works around this by exploiting the fact that neuronal cultures on MEAs can be used continuously for many recordings without compromise so we ran all experimental and control sessions on the same culture consecutively. Secondly, more complicated protocols such as the ones that apply stimulation in feedback from the recorded activity would require a sophisticated drug application system which is not currently available. This protocol  includes a tetanus epoch of just a few minutes which offers a convenient time frame for manual addition and washing away of the drug.

Figure 3.7 shows a schematic of the experiment. The protocol catered for examination of both spontaneous activity and evoked responses. Each measurement epoch comprised a period of 10 minute recording spontaneous activity, followed by 4 x 10 minute periods of recording under 0.2 Hz test stimuli applied at 4 different electrodes, respectively. The electrode identities and amplitudes of test stimuli were selected to produce obvious evoked responses based on a pre-experiment examination. The measurement epochs were separated by 3 induction epoch running an 'associative tetanus' as proposed by [30]. 'Associative tetanus' is a stimulation paradigm designed to induce an association between two stimulated

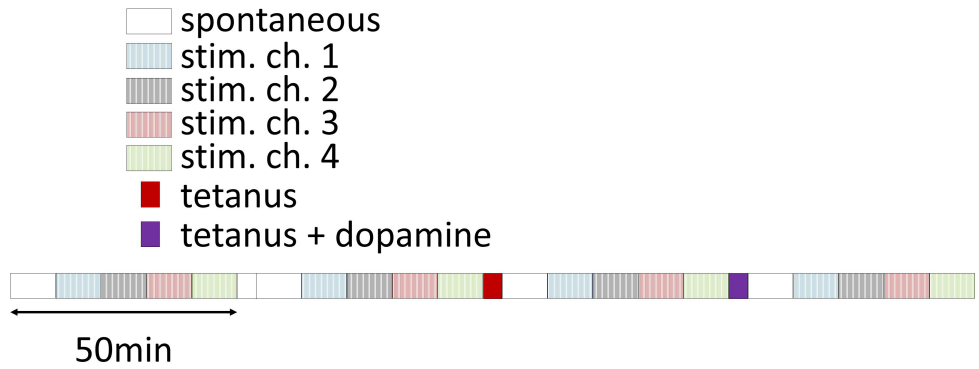


Figure 3.7: Outline of the combined dopamine and tetanus open bath plasticity experiments.

populations. The primary channel produces a tetanus pulse train consisting 50 pulse sets at 0.2Hz each consisting of 50 pulses at 20Hz . The secondary channel produces 50 single pulses at 0.2 Hz in phase with the tetanus pulse sets, i.e., each stimulation pulse in the secondary channel is timed to occur in the middle of a set in the primary channel. The primary and secondary channels were selected randomly out of the 4 stimulation channels used in the measurement epochs. The 3 induction epochs are as follows: (1) a sham (control) 'associative tetanus' executed by the signal generator with pulses of 0mV amplitude. (2) An actual 'associative tetanus' where the amplitudes for the primary and secondary channels are the same as those used in the test stimuli in the same channels during the measurement epochs. (3) An 'associative tetanus' as above where half of the culture media (0.5ml) was first removed for later use and $100\mu\text{M}$ dopamine•HCl was added. After the termination of the tetanus the dopamine containing media was replaced with the portion earlier removed and the final examination epoch was carried through. It should be noted that removal of half of the media during the 3rd induction epoch caused a slight but noticeable increase in the recording noise so the spike detection thresholds in the earlier measurement epochs were matched to the last one to avoid biasing of the results.

3.4.1 Examining changes in response to stimulation

Figure 3.8 shows example stimulation response data for the 4 measurement epochs in one of the tested cultures. Data is presented as explained in section 3.3. Baseline refers to the initial measurement epoch performed prior to any induction epoch. Control refers to the epoch taking place after the sham tetanus and the differences from the preceding epoch reflect spontaneous deviations in the culture activity. Tetanus and tetanus + dopamine are the epochs following the genuine induction phases. The differences between these experimental epochs and their immediate predecessors are compared to the difference between the control and baseline epochs so as to capture the effect of the induction. The baseline, control and tetanus epochs all show a similar PSTH profile and similar channel rasters. However, there

are also some noticeable differences. For example, the latency of the reverberating response seems to increase approximately half way through the control epoch, a change that is carried over to the tetanus epoch. Additionally, the reverberating phase of the control PSTH is smaller than in the baseline and this is observed as reduced intensity in some of the channel rasters. These un-induced changes demonstrate the importance of employing such control epochs to assess how activity features change spontaneously.

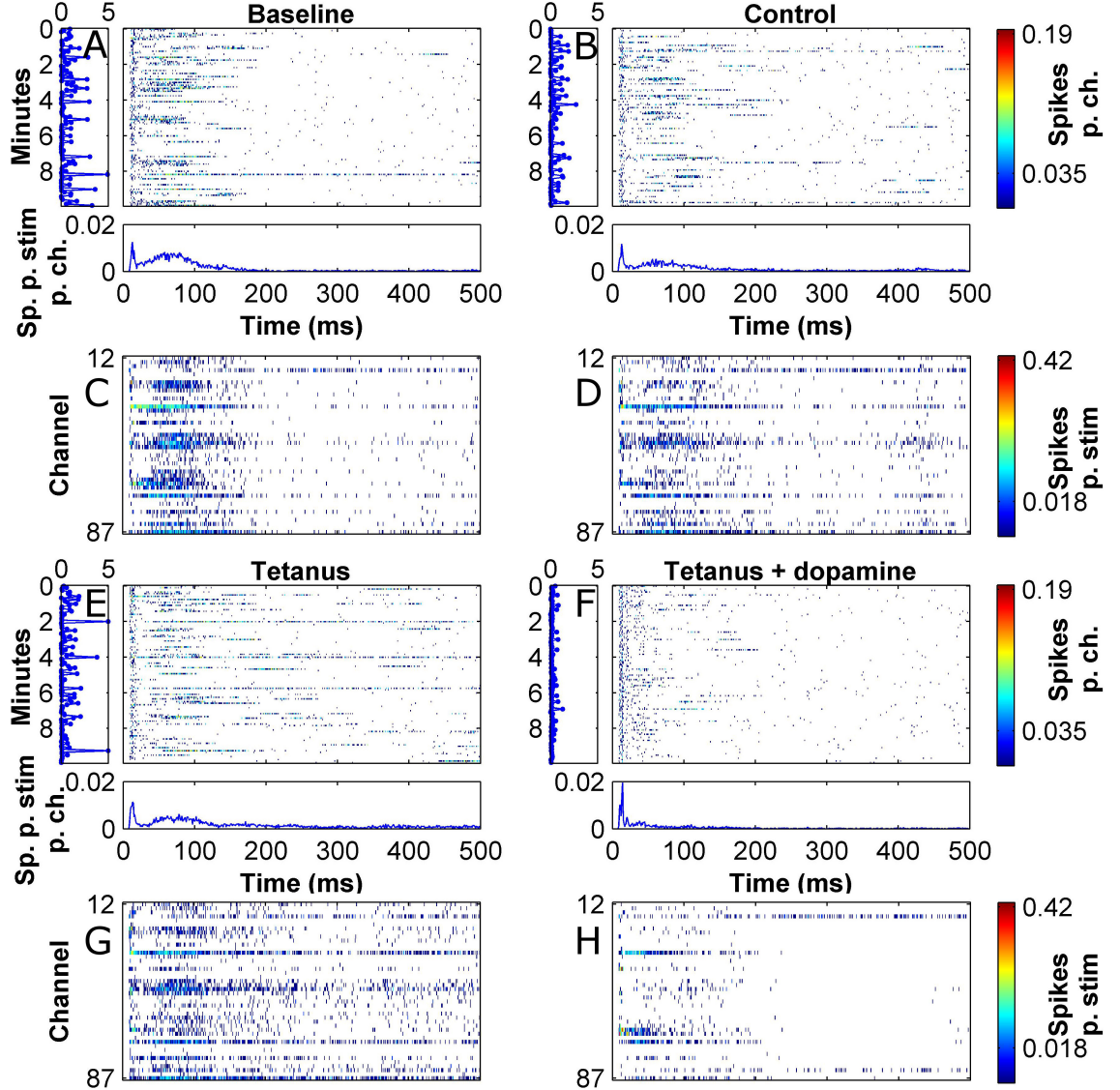


Figure 3.8: Tetanus combined with a dopamine pulse but not tetanus alone induces a depression of evoked responses. (A,B,E,F) Response rasters from the first stimulating electrode of each of the measurement epochs of the induction experiment. These are stimulation resolved (i.e., each line is a response to a single stimulation averaged over all the recording channels). (C,D,G,H) Channel-resolved response rasters of the same stimulation epochs. See caption of figure 3.6 for further details. Note an obvious decrease of evoked responses intensity following the tetanus induction in the presence of dopamine.

The tetanus + dopamine induction resulted in significantly more pronounced modifications to the evoked responses than the preceding inductions. The most obvious difference was the global reduction to the reverberating response in the PSTH. Most of the channels showed a marked decrease in intensity of responses although there were a few that actually increased. Another notable difference is that the direct response had become sharper. This global decrease in response is evident in the response maps in figure 3.9 where the number of responsive channels and their firing rate is markedly smaller after the tetanus + dopamine induction (recall that the response maps show only channels with significantly higher stimulation associated response in comparison with spontaneous activity).

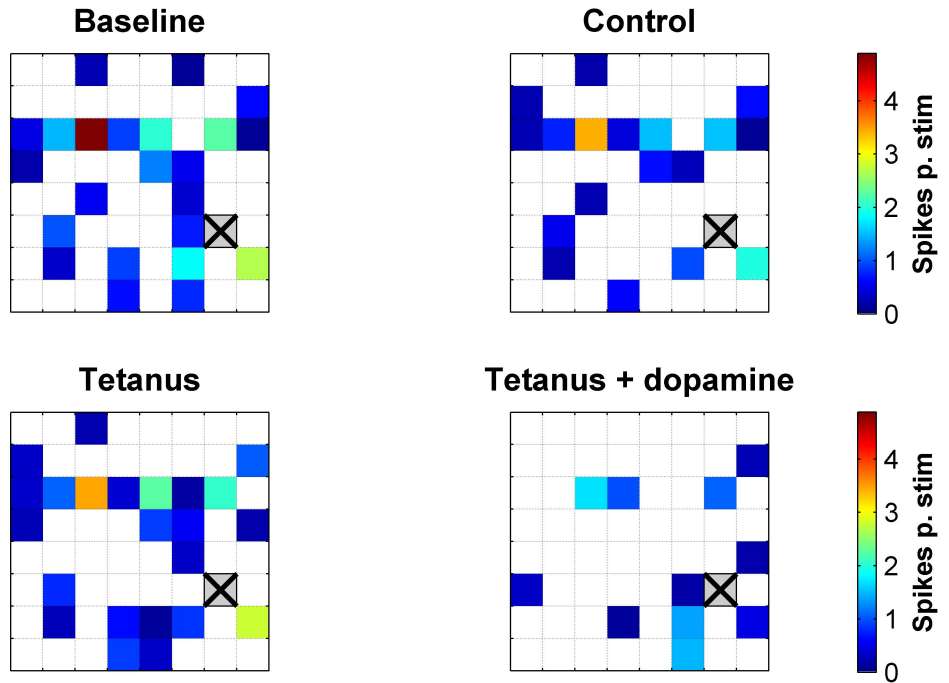


Figure 3.9: Tetanus combined with a dopamine pulse but not tetanus alone induces a reduction in the number of responsive channels. Stimulation response maps of the same data presented in figure 3.8.

Figure 3.10 shows a statistical analysis of the plasticity induction experiments which closely follows the one performed in [30]. In essence, channel responses for each stimulating electrode were compared in a scatter plot of pre induction vs. post induction responses and a linear fit was computed (figure 3.10 A-B). The slope for 'associative tetanus' induction did not show a statistically significant difference from the one for the sham (control) induction (1.01 ± 0.07 vs. 1.07 ± 0.07 , 2-sided t-test, $p=0.5$). The slope for the induction performed under the presence of dopamine was significantly smaller, though (0.66 ± 0.09 , 2-sided t-test, $p=0.004$), indicating a general depression in evoked responses (i.e., across all channels). The potentiation index analysis provided results to the same effect. This analysis

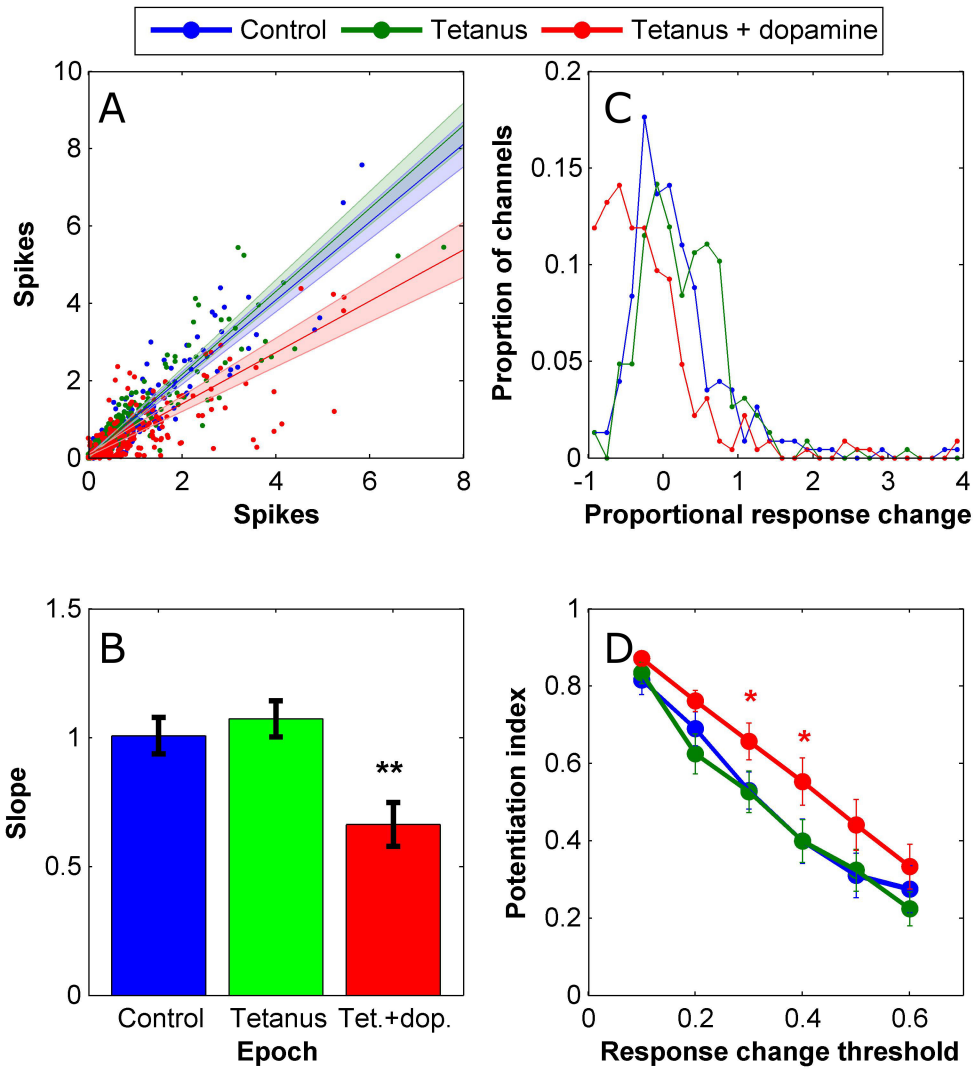


Figure 3.10: **Tetanus combined with a dopamine pulse but not tetanus alone induces a depression of evoked responses.** (A) Scatter plot of pre induction vs. post induction channel responses for the 3 induction steps of our protocol. Data from all tested cultures and from all stimulating electrode are lumped. The analysis, however, considers each of these groups to be an independent data set and fits a line to each. Plotted lines and shaded areas visualize the mean and SEM of these line slopes. Data is based on 4 cultures x 4 stimulating electrodes ($\text{C}_D = 16$). (B) Comparison of fitted slopes from A. (C) Distributions of proportional changes induced in channel responses for the 3 induction steps of our protocol lumped as in A. For computation of potentiation index (PI) such distributions are generated for each data set. For each of these distributions the PI is the proportion of channels exceeding a threshold level of change. Finally, PI is computed for a range of thresholds and averaged over independent data sets ($n=16$ as in A). (D) Mean + SEM of potentiation index as a function of tested levels of change thresholds.

is based on generating distributions of proportional changes to the channel responses before and after the induction (figure 3.10 C). Potentiation index is a measure for comparing these distributions and is defined as the proportion of channels with absolute change exceeding a predefined threshold. By selecting the threshold correctly, a distinction between the distributions based on their width can be generated even if their mean is the same. In other words, this measure is designed to detect more subtle changes to the network activity that may include some of the channels experiencing large but antagonistic changes which cancel out when looking at the mean. In more common terms, one could say this is a variance or a second order measure. Since the appropriate threshold for making the distinction between the distributions is unknown, potentiation index is computed for several thresholds over the entire range of the data. It should be mentioned that the name 'potentiation index' is somewhat of a misnomer as it refers not to potentiation in the sense of strengthening but to absolute change. At any rate, applying this analysis to our plasticity induction data did not reveal any significant differences between the tetanus and control inductions. The tetanus induction in the presence of dopamine, on the other hand, showed a significantly higher potentiation using change thresholds of 0.3 and 0.4 (figure 3.10 D, 1-sided t-test, $p=0.034$ and 0.039, respectively). This, however, is not surprising given that a general depression was observed in the preceding slopes analysis.

3.4.2 Examining changes in functional connectivity

Since the afo^rrmed analyses did not reveal any tetanus-only induced plasticity we decided to try a yet finer probing of the network activity. This is based on the functional connectivity analysis which was reported to capture plasticity in response to tetanus [34]. Mathematical details and examples for computation of functional connectivity are given in section 2.5.5. In essence, the measure is based on locating peaks in the cross correlation function between channel pairs normalized to the number of spikes in the first channel. The size of the peak reflects the probability of recording a spike in the second channel following a spike in the first one at a time captured by the latency of the peak. This computation therefore results in 2 vectors, one holding peak sizes (also termed FC strengths) and the other peak latencies. Finally, differences in functional connectivity between recording epochs is measured as the Euclidian distance between the appropriate vector from the compared epochs. In our analysis we looked only at distances in the FC strengths vector because situations where the functional connectivity is lost completely (i.e., connection strength becomes 0) do not require special treatment. It has been claimed that this measure is more efficacious at detecting plasticity when computed over spontaneous activity [34] so we indeed used the spontaneous activity periods of recording in our protocol for its computation.

Figure 3.11 shows the changes to the functional connectivity over the different experimental protocols (measured as Euclidan distance from the baseline epoch) as well as the mean channel firing rate. The results show that the tetanus induction itself did not generate

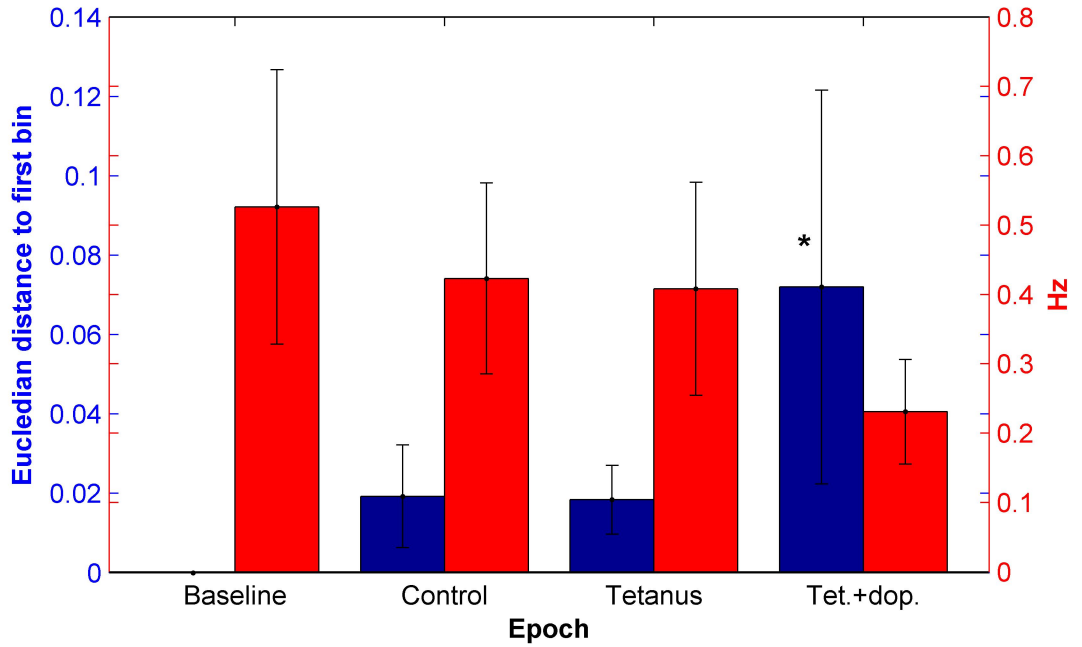


Figure 3.11: **Tetanus combined with a dopamine pulse but not tetanus alone induces a change to functional connectivity as well as a decrease to spontaneous activity.** Blue bars: Euclidean distance of the functional connectivity strength vector from baseline following each induction epoch. Functional connectivity was computed based on the spontaneous activity period in each of the measurement epochs. Functional connectivity computation requires a minimum number of spikes in each of the analyzed channel pairs to generate a meaningful cross correlation function estimation (see section 2.5.5) so only a subset of the possible recording channel pairs normally participate in the analysis. One of the cultures participating the the plasticity induction had to be removed as it had no channel pairs complying with the above criteria. Thus the shown data are based on n=3 cultures with 33, 10 and 179 computable functional connectivity pairs. Red bars: Mean channel firing rates in the same spontaneous activity measurement periods. This data are based on all n=4 participating cultures.

a change to the functional connectivity beyond naturally occurring fluctuations that were already observed after the control induction. A larger change was observed following the tetanus induction in the presence of dopamine which proved to be statistically significant (1-sided t-test, $p=0.026$). However, this change was also accompanied by a strong decrease in the mean channel firing rate which, for this data set, proved to be significant with only 90% confidence (1-sided t-test, $p=0.097$). In light of this change to the averaged culture activity, the observed shift in the functional connectivity measure should be taken with a grain of salt as it was designed to reflect subtle changes to the underlying culture structure in conditions where first order statistics (like mean firing rate) are stable.

3.5 Chapter conclusion

The main purpose of this chapter was to establish the standard neuronal culture on MEAs model system together with the accompanied Matlab analysis and show that the cultures are healthy and exhibit the diverse electrophysiological characteristics which have made them a successful neuroscience model system. Indeed distinct stages of development of network activity were clearly observed. These consisted of initial uncorrelated but widespread firing patterns corresponding to neuronal maturation followed by an increase in correlations and rate of synchronized events which indicate that the synapses are maturing. Further examination of the data revealed evidence for other neurobiological processes that have been described in culture. These included homeostasis of activity rates, existence of strongly intra-connected subnetworks and a gradual temporal narrowing of the synchronized events which has been attributed to a delayed maturation of the GABA neurotransmission system as compared to the glutamatergic one. These processes have not been studied here in depth but are taken as evidence that our cultures are healthy and in par with the literature gold standard.

Another important purpose for the work performed in this chapter is to examine the usability of mouse based cortical culture for MEA studies, as they have been seldom used in this context. We encountered difficulty in getting the mouse cultures to develop well on the MEAs and struggled with sub 50% success rates. In rat cultures, for a seeded culture to not develop well for several weeks was a rarity. Comparing electrophysiological parameters of the two preparations showed that the mouse cultures that did develop had a delayed synaptic maturation as compared to their rat counterparts, manifested in lower correlation values for same age *in vitro* and in synchronized events appearing later than expected from literature. Although the mouse cultures that did survive finally showed all the characteristics that could be expected from this type of preparation, their weakness in development and high failure rate led us to discontinue their use and switch to rat cultures for the following Ph.D chapters.

The final undertaking of this chapter was to explore a protocol for phasic application of dopamine using manual pipetting. We modified a common plasticity protocol to include a step where dopamine is ‘pulsed’ (through manual pipetting and subsequent washing) into the culture during the tetanus induction step. Without any dopamine, we were not able to induce a change in the culture activity, despite reports to the contrary in the paper from which the protocol was adapted. This should not come as a surprise as the literature is controversial in this regard and should just serve as a demonstration that further work is required for these system to serve as a useful model of plasticity. Following a tetanus induction which was performed in the presence of dopamine a significant depression was observed in the evoked responses which measured up to an hour following the induction. The spontaneous activity was also depressed but to a lesser extent. On one hand this could demonstrate a

enabling of LTD by the dopamine. The fact that this effect is present after the dopamine had been removed strengthens the possibility that this is a plasticity effect rather than a result of direct interaction of the cells with the agonist. Indeed a similar experiment had been performed in cortical slices and produced very similar results [41]. On the other hand, it is also known that in neuronal culture the mere action of media replacement drastically reduces activity (this will be made very clear by the results of chapter 5), an effect that could last several hours. Additionally, the presence of dopamine itself is known to have an inhibitory effect in the cortex regardless of plasticity [42, 43] and it is hard to rule out the option that a small concentration of the agonist is still present after the washing step and contributing to the observed effect. Under the constraints of the current bath application methods, it is impossible to run a dopamine pulse without these impinging effects. Indeed we could quantify them by using a set of control experiments but we cannot eliminate them.

To summarize, these dopamine pulsing results are promising in that they suggest a potential for dopamine to enable plastic behaviour in culture. However, this notion wasn't fully proven due to uncertainty about the effects of media replacement and of temporary interaction of dopamine with the neurons. This highlights the need for a precise solution exchange system whereby dopamine can be applied with high spatio-temporal precision and without change to other extracellular ingredients which could interfere with the activity. Such a system would allow interrogation into the fine temporal details of the phasic dopamine and volume transmission processes in general far beyond what was demonstrated in the above-described work. The following chapters in this Ph.D thesis will describe the development and establishment of a microfluidic based rapid solution exchange system where the drug delivery is rapid, precise and decoupled from other changes to the extracellular chemistry.



Chapter 4

Viability of neuronal cultures in microfluidic devices in static conditions and under steady flow

4.1 Introduction

As outlined in section 1.4 the purpose of this Ph.D work is to produce a model for phasic neuromodulator signalling by generating rapid agonist transients onto an entire neuronal culture. This is to be achieved using the interface shifting method in microfluidic devices. Applying this method involves using rapid flow rates at scales of $1 \frac{mm}{s}$ (the rat behind this figure is provided in section 4.2). Previous microfluidics work involving primary neurons used such rapid flow rates but just for short experiments lasting between minutes to 2 hours at most [44, 45, 46, 47]. Studies showing long term neuronal culture development under flow used much reduced flow rates where the convective forces were comparable to diffusion [48, 49, 50, 51]. Thus to avoid the complexity involved in getting neuronal cultures to survive long term under rapid flow we elected to follow an experimental paradigm whereby the cultures were initially grown in microfluidic devices in static conditions. After reaching maturity they were subjected to flow only for the duration of the experimental session. The first part of this chapter is dedicated to development of a protocol for long term culturing of primary rat neurons in microfluidic devices. As reviewed in section 1.3.2, this type of protocol is prevalent in the literature but the configuration of our devices, which were designed with the interface shifting method in mind, required specific adaptations.

An important part of the our experimental design is for the culture to be of restricted size (i.e., a microculture). This is necessary, firstly, because the interface shifting routine

involves having a small proportion of the microfluidic channel area chronically exposed to the agonist, even between transients (see section 1.3.1). Thus to avoid such chronic drug exposure, the culture needs to be located entirely outside the chronically exposed area. Secondly, it is important to note that an agonist pulse in interface shifting method actually takes the form of an agonist wave travelling along the long axis of the channel. This means that, depending on the flow rate and the geometry of the culture, cells at different locations along the channel may experience the drug at different times following the pulse command. In phasic neuromodulator signalling, the agonist molecules are secreted from nerve terminals that innervate the entire volume of the target tissue. Consequently, a neuromodulator pulse involves an approximately synchronous increase of agonist concentration over the entire innervated tissue followed by a decrease in concentration as the agonist molecules get locally re-uptaken [52]. It is important to note that, due to inhomogeneities in the spatial distribution of the innervating neuromodulatory fibers, different parts of the tissue still exhibit some delays in exposure to the agonist depending on their proximity to neuromodulatory synapse clusters. Nevertheless, these delays are small compared to the time scales of the global pulse [52, 53]. Because of the functional importance of timing in the neuromodulator signalling, it is essential that the microfluidic model does not exhibit increased delays in arrival of the agonist to different parts of the culture as compared to the *in vivo* tissue. To achieve the right timings, the flow speed and culture size need to be selected so that the drug traversal time across the culture matches the delays in the modeled tissue. The ability to control the culture size is crucial and the second part of this chapter will describe a method for generating microcultures which harbour small specific areas of the channel by utilizing microwells. The viability of these microcultures will be analyzed to establish their usability.

A final important topic that will be covered in this chapter is that of neuronal viability under rapid flow. Primary neurons are considered to be highly sensitive to shear stresses. Since this system is developed with long term plasticity in mind it is important to make sure that the culture is kept viable and functional for at least several hours under the applied shear stresses. It is also important to take into account that a functional neuronal tissue employs a large number of intrinsic volume transmission processes which comprise controlled secretion and uptake of active substances into the ECM (reviewed in section 1.2). These substances include neurotransmitters, hormones, neurotrophic and growth factors and are generally termed conditioning factors. Rapid flow is likely to interrupt these processes by changing the concentrations of the conditioning factors or their spatial distributions. Since microfluidic flow has been scarcely used with primary neuronal cultures the flow rate limits have not been established and it is currently unclear what is the impact of each of the above-mentioned factors, shear stress and conditioning removal, on the culture viability. To characterize the effect of these factors we performed a viability assay under flow with a range of flow rates and media conditioning levels. In the tested range, we found a strong correlation between conditioning and viability but no shear effect. We established a protocol for media

conditioning which, when used for flow, maintains the culture above the 90% viability mark for over 5 hours. Chapter 5 will further address the question of functionality and will describe a characterization of the network activity under flow.

4.2 Long term neuronal cultures in microfluidic devices

4.2.1 Development of protocol

This section outlines the development of a protocol for long term culturing of primary hippocampal neurons in microfluidic devices. Long term culturing of cortical and hippocampal neurons has been established for over 30 years [54, 55, 56]. Recently, there has been an emerging use of microfluidic devices to culture neurons with increased control over the topology  and to access specific neuronal compartments [57, 58, 59]. Nevertheless, neuronal cultures are infamous for their sensitivity to subtleties in the preparation technique and the materials that come in contact with the media or the cells and often require specific adaptations for the specific lab / application [60, 49]. The  are discussed next.

Figure 4.1 shows the dimensions of the devices used in this study. The dimensions were selected so that, given the volumetric flow rates allowed by our flow system, a flow speed would be produced that is compatible with the desired agonist exposure times. Thus the main channel width was 1.5mm and the height was $65\mu\text{m}$ giving a cross section of $\approx 0.1\mu\text{m}^2$. Using a flow rate of 100nl/s gives an averaged flow speed of 1mm/s . Assuming that the long dimension of the culture would be less than a millimeter and that the culture would be positioned less than a millimeter from the agonist port then the agonist should reach the culture within a second and clear it a second later, which is the correct order of magnitude for neuromodulator phasic signalling [53]. Obviously this is just a back of the envelope calculation which does not take into account complexities in fluid dynamics and delays inherent to the flow switching system and its purpose is to provide a relevant geometry. A more rigorous examination of pulsing time scales will be performed in chapter 6 where the final microculture pulsing system is described.

The devices were bonded to glass cover slips using plasma bonding (see section 2.2 for details and more illustration of the assembled devices), oven sterilized, and then subjected to PLL surface treatment as detailed in section 2.3.

Due to the need to interface with a flow system, the microfluidic devices used in this work were made with biopsy punched ports of $\approx 0.8\text{mm}$ diameter which allow connection to the flow tubing by simple pressure fitting. This design contrasts with standard neuroscience oriented microfluidic devices where the ports are typically of 8mm diameter [57]. In these standard devices the seeding proceeds through pipetting of the cell solution into the ports and allowing the cells to flow through the channel (flow is enabled by controlling for a differential media height across the inlet and outlet ports). In the case of these standard devices, the

ports function as de facto reservoirs by holding a significant volume of media ($400\mu L$ each) and therefore protect the device  from dehydration and serve as a source of nutrients. Due to the smaller port size in our devices, plating was performed by injecting the cells into the inlet port using a gel loading tip. The volume of injection was selected to be larger than the internal volume of the device so as to fully flood it with cells. The devices used here had an internal volume smaller than $1\mu L$ (figure 4.1) and the injection volume was $2\mu L$. After completion of the injection the cells were left suspended in the channel volume and were allowed to settle down in the incubator. The lack of flow following the cell injection made this protocol more consistent than the flow based seeding in standard devices. In those cases too strong of a flow ends up in having most of the cells flow through the device without settling and therefore in inconsistent seeding densities. On the other hand, a down side to our design is that due to their smaller diameter, the ports in our devices only hold about $2.5\mu L$ of media each and therefore cannot effectively fulfill the role of media reservoirs.

The following subsections will outline the major steps taken during the development of the protocol to circumvent the issues encountered along the way. The development of the protocol did not include an in depth scientific investigation to prove all the observed effects and interactions as doing so would have taken a long time and would have been counter productive with respect to the global project. The information is therefore not statistically complete  and is presented in the form of examples which are meant to provide an intuitive and heuristic guide for scientists who would want to employ these techniques in the future.

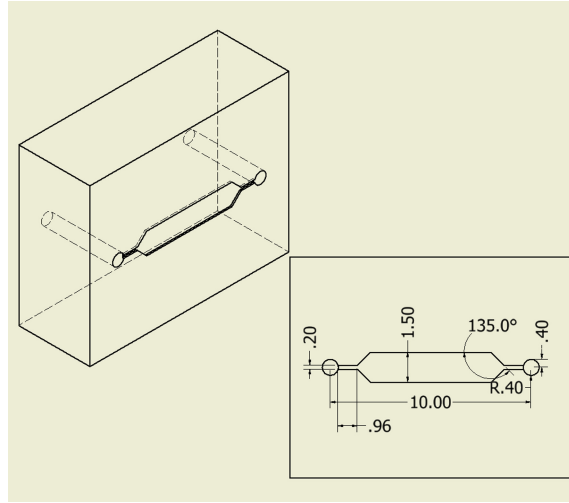


Figure 4.1: Schematics of the standard single layer microfluidic devices. All measurements listed in mm. Standard single layer microfluidic channels used in this section comprised both 2-port and 3-port (y-shaped) configuration. Only the 2-port configuration is presented here for simplicity. 

4.2.1.1 Evaporation and surface chemistry considerations

The initial incubation configuration explored was to apply a $200\mu L$ drop of media to the top of the PDMS surface to act as a media reservoir from which nutrients are exchanged and to preserve the aquatic environment. To minimize evaporation, the devices were further kept in a closed petri dish next to a dish with $1mL$ I_V. The petri dish was kept in a humidified CO₂ incubator (Figure 4.2 A). The initial configuration also incorporated a 30 minute incubation with PLL solution as surface preparation. Cultures seeded in this configuration did not develop long term. The cells were initially healthy and adhered to the surface but the adhesion was non-uniform and by 5 days *in vitro* the cultures degenerated completely (figure 4.2 C-D). The main issue associated with this device configuration was that evaporation from the media on top of the devices was causing a rapid increase in the media osmolarity at a rate intolerable to the cells. We quantified this effect by measuring the osmolarity (Osmomat 030 by Gonotec) of the media on top such devices after an overnight incubation. We found that the osmolarity drifted by $126 \pm 97mOsm$ overnight, implying an evaporation rate of $49 \pm 20\frac{\mu L}{day}$.

We tried to circumvent the evaporation issue by changing the drop on top of the devices every day (as opposed to twice weekly) and assessed the effectiveness by following the osmolarity of 4 devices for several days following the plating. Figure 4.2 B shows that the osmolarity in this case was stable but still very high (typical osmotic strength values for cell culture media is $\approx 300mOsm$ and the osmolarity of our Neurobasal growth media is $225mOsm$). A better solution was provided by switching to a maintenance routine where the devices were fully immersed in $2.5 - 3mL$ of culture media for the duration of the culture development (figure 4.3). Full details of this routine are provided in section 2.4. The volumes of media applied to each sample in this approach are comparable to what is used in standard cell culture samples so media could be changed just twice a week without incurring excessive osmotic drifts. After 3 weeks of culturing in this approach, media osmolarity never drifted more than $30mOsm$. Beyond this, the initial patchiness in adhesion led us to suspect that 30 minutes of PLL incubation, which is adequate for standard open surfaces, might be insufficient in the case of microfluidic devices where the extreme surface to volume ratio might cause an increased flux of PLL molecules into the PDMS and reduce the effective concentration available for the glass surface. Consequently, we also modified the protocol to an overnight PLL incubation. With this modified protocol we were able to sustain neuronal cultures for long term (figure 4.4) but still not ideally, as will be described in the next section.

4.2.1.2 Considerations of factor circulation

Figure 4.4 A-B shows microscope images of two sides of an example device 12 days after seeding during which it was maintained using the modified protocol as described above. The

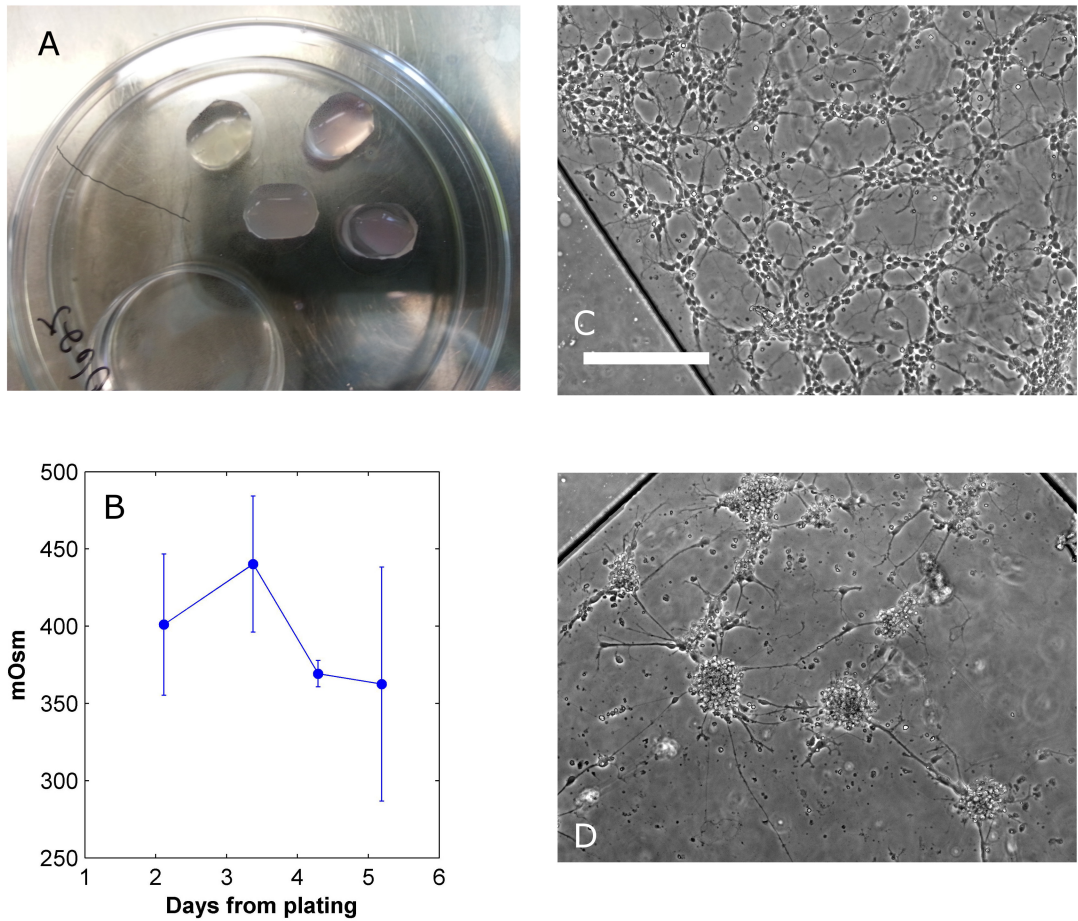


Figure 4.2: The ‘drop on top’ configuration results in excessive osmotic drifts and degeneration of the cultures. (A) Top view of a group of devices illustrating the ‘drop on top’ approach. (B) Osmolarity measurements taken from the drops on top of the devices in A during a maintenance protocol where the drop on top was changed every day. (C-D) Images of a culture growing in the ‘drop on top’ configuration and where the drop was changed only twice weekly. Images are at 2 and 5 days *in vitro*, respectively. Scale bar is $200\mu\text{m}$ long and is consistent for both images C and D.

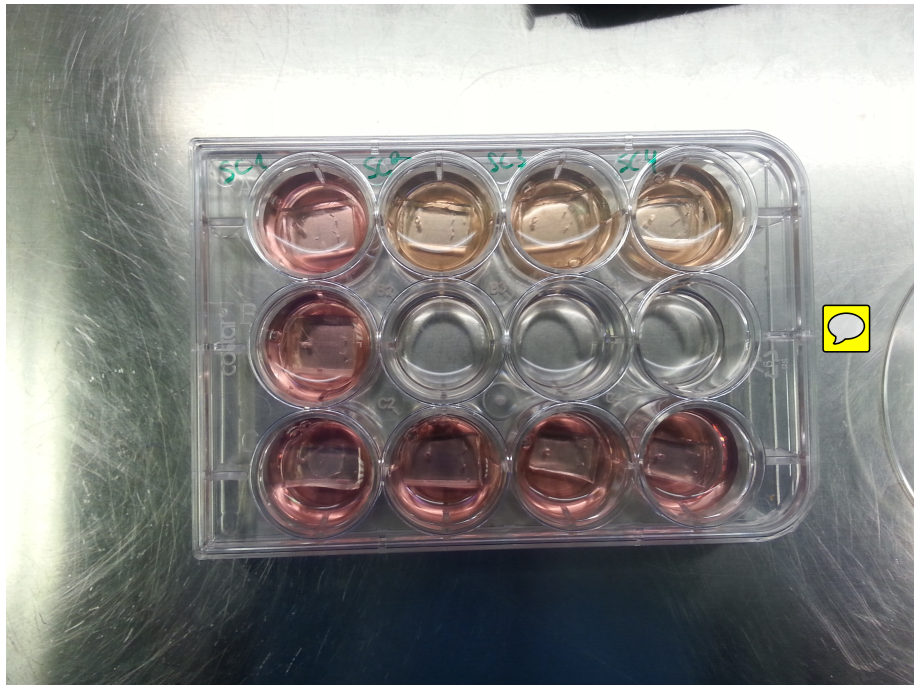


Figure 4.3: **The immersion configuration.** In this configuration, the devices were immersed in 12-wells with $2.5 - 3ml$ media each to prevent excessive osmotic drifts. This configuration required immersion 24 hours prior to seeding to release air trapped in the PDMS.

part of the culture residing in the vicinity of the seeding port did not develop properly and was mostly degenerate. Remarkably, the part of the very same culture residing on the side opposite to the seeding port was able to develop properly and maintain a healthy appearance for several weeks. A hint as to the mechanism operating behind the above phenomena comes from devices where one of the ports was punched to be twice as big (figure 4.4 C-D). In this case the cells were seeded from one of the ports opposite to the large port. In these large port devices the whole culture developed healthily without any significant spatial differences. Another clue was provided by our exploration of devices with a larger architecture where the height of the channel was $1mm$ and its internal volume $\approx 20\mu L$. The density of the plating solution for these devices was calculated so that the plated area density would be as in the small devices, $2600 \frac{cells}{mm^2}$. Nevertheless, culture grown in these larger devices never exhibited any sign of such spatially arranged degeneration and typically developed well for several weeks (results not shown). We argued that the most likely explanation for the above observations is that the configuration of small devices and small ports does not provide adequate circulation to remove metabolic by-products and provide fresh nutrients to all parts of the culture. The fact that the degeneration occurred in proximity to the seeding port could be explained either by the port being blocked by lumps of cells or by a existence of a gradient of cell density along the channel. In both cases there would be a large unmet circulatory demand around the seeding port. In the case of the large port or the large devices,

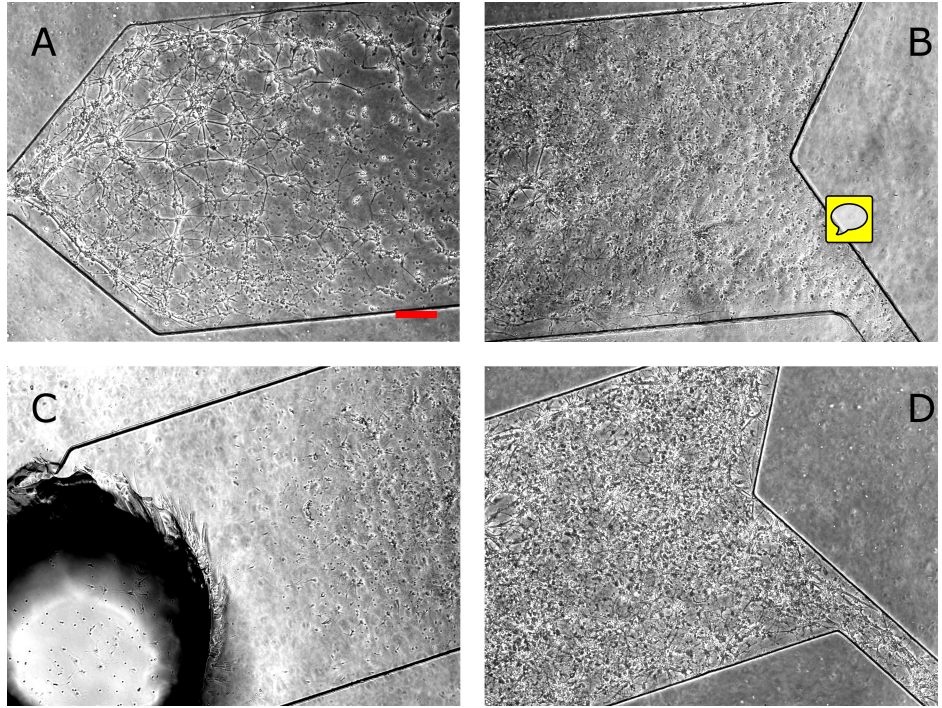


Figure 4.4: A circulation bottleneck can emerge in microfluidic devices. (A-B) Images of a culture growing in 3-port microfluidic devices where all the ports are 0.8mm in diameter. The images show the culture condition in the seeding port side and in the other side, respectively. (C-D) Images of a culture growing in 3-port microfluidic devices where one of the ports is twice as big (1.5mm). Images show culture condition in both sides of the device as before. Images were taken at 12 days *in vitro*. Seeding solution density was of $40 \times 10^6 \frac{\text{cells}}{\text{ml}}$ which is equivalent to $2600 \frac{\text{cells}}{\text{mm}^2}$ assuming homogenous distribution of the cells. Devices were maintained as described in section 2.4. Scale bar is $200\mu\text{m}$ long and is consistent across all images.

a stronger diffusive coupling between the culture and the external bulk media is enabled so in those cases circulation was not an issue. Since the configuration of small devices and small ports was required to properly interface with the flow tubing and to reach the required flow speeds we experimented with reduced plating densities in hope that these will have reduced circulatory demands. Indeed we found that by decreasing the plating density 6 fold (giving an area density of $\approx 450 \frac{\text{cells}}{\text{mm}^2}$) the spatially arranged degeneration phenomenon disappeared.

The observations described in this section demonstrate how microfluidic technology can impose conditions that are not normally met in standard preparations. The area density of $2600 \frac{\text{cells}}{\text{mm}^2}$ seeded in the earlier versions of the protocol is high but still commonly used for many applications involving neuronal culture. In those cases the culture is in immediate contact with a large volume of bulk media which readily supplies nutrients and removes by-products via diffusion. In our microfluidic devices, the internal volume of media is 3 orders of magnitude reduced ($\approx 1\mu\text{L}$) and it is only in this extreme configuration that circulation

becomes an issue. This situation is similar to cases where non-vascularized 3D cultures develop a necrotic core due to the lack of oxygen and nutrient penetration.

4.2.1.3 Alternative bonding methods

Plasma bonding is a lengthy process that needs to be applied to each sample separately and therefore is not well suited for producing large quantities of devices. Additionally, it is not practical for more complex devices involving several layers as having to apply plasma bonding methodology to each layer separately makes the production of every single device very tedious. Consequently, we experimented with alternative bonding approaches that have been recently suggested for assembly of microfluidic devices [61, 62]. Complete protocols and illustrations are provided in section 2.2.

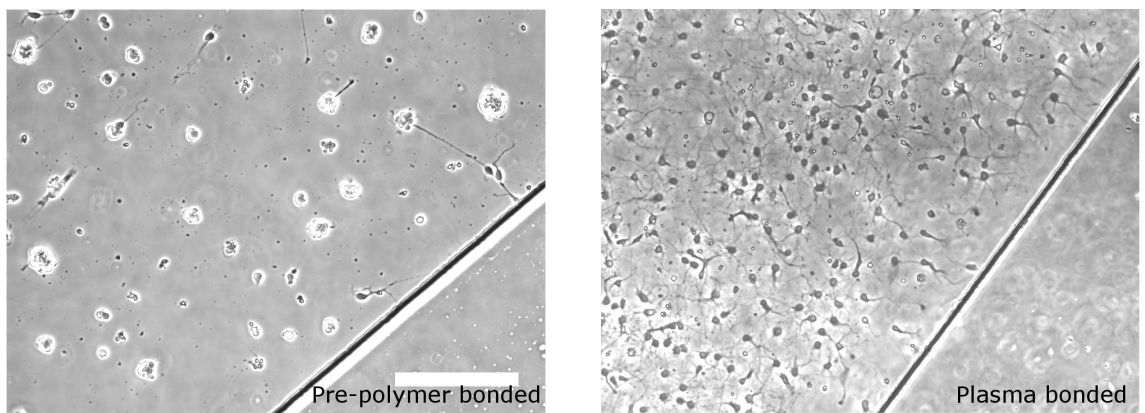


Figure 4.5: Contamination associated with pre-polymer bonding renders the surface unsuitable for neuronal adhesion. Images comparing a culture growing in pre-polymer bonded devices to one growing in plasma bonded devices. The images were taken at 5 days *in vitro*. Following bonding, the devices were subjected to identical surface preparation, seeding (density $7 \times 10^6 \frac{\text{cell}}{\text{mm}^2}$)^{cell} and maintenance protocols (see sections 2.3 and 2.4). Scale bar is $200\mu\text{m}$ long and is consistent across both images.

The first approach attempted was to use the PDMS polymerization catalyst as an intermediate layer between the glass and PDMS bulk. The PDMS is dipped in catalyst solution, placed on top of the glass substrate and left to cure. This apparently induces further polymerization as well as partial covalent binding with the glass and results in a bond strength comparable or greater than plasma bonding [61]. We were able to achieve adequate bonding using this method but unfortunately the internal device surface proved to be completely inadequate for neuronal growth (figure 4.5. Interestingly, such a problem was not presented for other cell types such as astrocytes and HEK cells (data not shown)). This issue serves as another demonstration of the specific demands that are presented by neuronal culture. It is known that PDMS, when in contact with a surface, can contaminate the exposed areas around the point of contact through ‘leaching’ of PDMS oligomers or curing agent molecules. Indeed it has been shown that PDMS sometime acts as a source of contamination interfering

with neuronal growth inside microfluidic devices [49]. The lack of adhesion reported here for the pre-polymer bound devices is probably an extreme manifestation of exactly these contamination processes.

A different bonding alternative explored was that of using double sided silicone transfer tape [62]. In this case channel features are not engraved into the PDMS through soft-lithography but simply cut out of the tape which is consequently joined with the glass surface. A square PDMS bulk with punched ports is joined to the top side of the tape to complete the body of the device. Since this method does not disrupt the surface coating of the non taped parts of the glass and can be performed in a sterile hood it opens the door for a new surface treatment approach. With tape based assembly the device can be taped to a pre-treated glass (surface-then-bond) whereas previously, with plasma bonding, the surface coating chemicals had to be introduced and incubated in the assembled device (bond-then-surface). This shift in paradigm allows to utilize the device geometry to control which parts of the treated surface will be exposed and available for culture adhesion and therefore offers an easy way of controlling its shape and size. This concept will be critical for the establishment of the microculture geometry in chapter 6.

Figure 4.6 compares cultures grown in plasma bonded devices to ones grown in tape based and using the surface treatment paradigms appropriately as discussed above. The cultures are indistinguishable and appear to develop identically over the 12 days of inspection. This shows that the silicone tape is safe for use with neuronal culture and does not leach significant amount of toxins onto the surface or media. This tape based assembly approach will be cardinal for the multilayered devices described in chapters 5 and 6.

4.2.1.4 Extraction of PDMS

PDMS extraction is the last topic described with regards to the development of the basic protocol. As was apparent from the results of section 4.2.1.3, traces of curing agent or short oligomer chains can be harmful to neuronal cultures grown in the presence of PDMS. Indeed, even though the maintenance protocol achieved in section 4.2.1.2 did generally sustain neuronal cultures for at a couple of weeks *in vitro*, there were occasions where the cultures did not develop adequately. We reasoned that PDMS leaching might play a role in that inconsistency and therefore decided to try and employ a protocol for extraction of toxic species out of the cured devices. The protocol follows the suggestion from [49] and is detailed in section 2.1. Figure 4.7 compares cultures grown in standard devices to those grown in extracted devices from the same plating and using the same maintenance protocol. In this plating, the cultures in standard devices seemed to fasciculate early on and completely degenerated by 12 days *in vitro* ($n=5$). In the extracted devices ($n=10$) there was no sign of such degeneration. It should be noted that the extraction process involves immersing the devices in highly toxic solvents such as pentane and xylenes. When these are not properly oven-baked out of the devices a highly violent toxic effect is generated with the cells dying

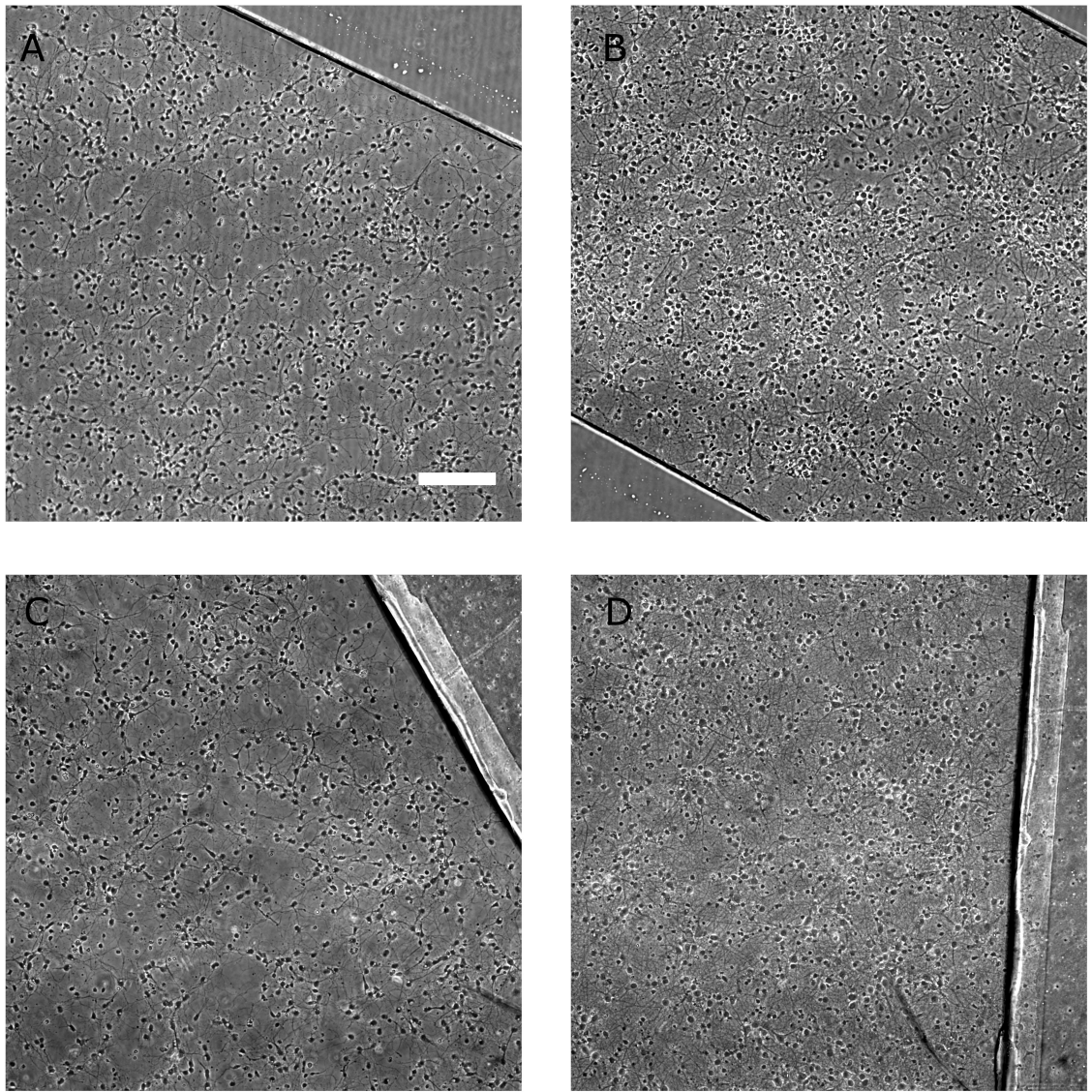


Figure 4.6: Tape based device architecture is fully compatible with neuronal culture. (A-B) Cultures growing in plasma bonded devices at ages 5 and 12 days *in vitro*, respectively. (C-D) Cultures growing in tape based devices at different stages of development as above. Plasma bonded devices were subjected to ‘bond-then-surface’ surface preparation approach whereas tape based devices were subjected to ‘surface-then-bond’ (see section 2.3). Both devices were seeded and maintained as described in section 2.4. Seeding density was $7 \times 10^6 \frac{\text{cells}}{\text{ml}}$. Scale bar is $200\mu\text{m}$ long and is consistent across all images.

immediately upon seeding (figure 4.7 C). Faulty development in non-extracted devices was not always observed and could be attributed to a specific PDMS mixing batch or to interactions with other factors. Nevertheless, to maximize the consistency of the preparations we added PDMS extraction to the standard protocol.

To summarize, we have developed a protocol for long term growth of neuronal culture in planar (1-layer) microfluidic devices. We reviewed what we consider to be the important

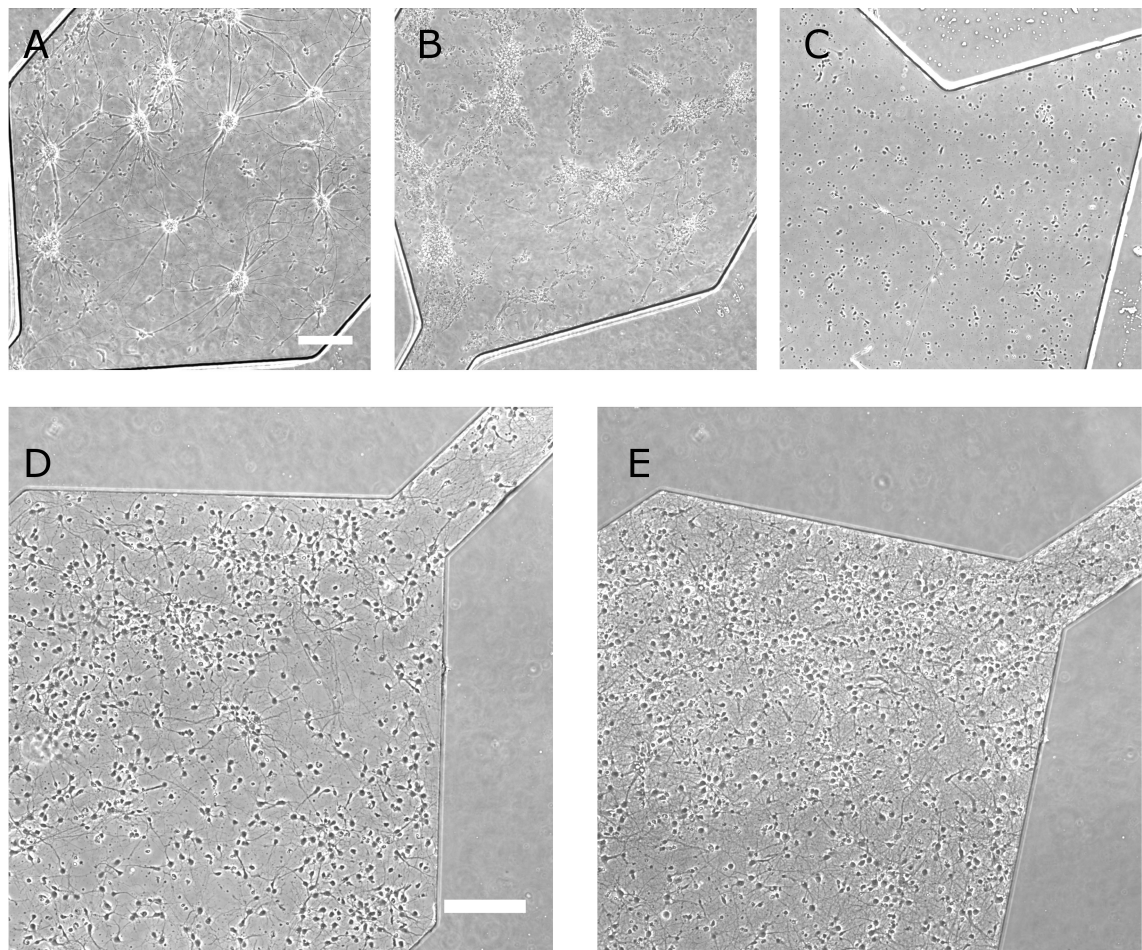


Figure 4.7: Non extracted PDMS devices can leach out chemicals that are harmful to neuronal growth. (A-B) Neuronal culture exhibiting adhesion and development issues that are thought to arise from PDMS leaching. Same culture is shown at ages 5 and 12 days *in vitro*, respectively. (C) Culture seeded in a device made from extracted PDMS which was not baked long enough for removal of noxious extraction chemicals. Image was taken at 2 days *in vitro*. (D-E) Cultures grown in extracted PDMS devices at 5 and 12 days *in vitro*, respectively. These images represent the typical cultures achieved for the final protocol incorporating all the principles discussed in this section. All devices were plasma bonded (section 2.1), subjected to ‘bond-then-surface’ surface preparation (section 2.3), seeded at a density of $7 \times 10^6 \frac{\text{cells}}{\text{ml}}$ and maintained according to section 2.4. Scale bar is $200\mu\text{m}$ long and is consistent across all images.

factors in the development of such protocols, namely, osmolarity, circulation of nutrients and oxygen, ease of assembly and leaching of chemicals from the construction materials (usually PDMS). Full details of the final protocol are provided in section 2.4. This protocol is the basis for all the subsequent device types used in this Ph.D thesis. All of them will use the same preparation and maintenance routines and will differ only in the seeding density and volume which require adaptation to the specific device and culture geometry.

4.2.2 Growing microcultures in plasma bonded devices

As explained in section 4.1, controlling the physical extent of the culture is necessary in order to apply the interface shifting method in a way that produces physiologically relevant concentration pulses. Here we describe confinement of the cultures into microwells of a desired size. To add microwells to our device geometry, we produced a PDMS sheet with rectangular holes via thin film spinning on a silicon/SU-8 mold comprising pillars in the shape of the required microwells (see section 2.1). To assemble the devices, the PDMS sheet was placed on a glass coverslip forming a reversible hydrophobic bond. The PDMS bulk with the engraved channel (as in figure 4.1) was then plasma bonded to the PDMS sheet while being manually aligned to position the microwell within the channel borders (figure 4.8). The devices were seeded at density of $20 \times 10^6 \frac{\text{cells}}{\text{ml}}$ and volume of $2\mu\text{L}$. The seeding filled the entire device volume with cells which settled arbitrarily on the exposed PDMS or inside the microwells. After the initial seeding the devices were inspected under the microscope to check if there is adequate inhabitation of the microwells and subjected to flushing and re-seeding as necessary. As shown in figure 2.1.2, an undesirable side effect of the way the PDMS sheet was manufactured is that the microwells are produced with an elevated ridge around them. The ridge caused a directing of the cells around the microwells rather than into them which was the main reason why flushing and re-seeding was necessary at times. After obtaining adequate microwell inhabitation, the devices were left in the incubator for 2-3 hours for initial adhesion of the cells, then media was pulled through with a 1ml syringe. This pulling had a differential effect on the cells depending on their location, i.e., most of the cells on the PDMS surface were ripped off and removed by the pulling whereas the cells in the wells tended to stay put as they were protected from the shear. In this way, isolated neuronal microcultures were generated and they were maintained as described in section 2.4.

Section 4.2.2 highlighted how, due to the small internal volume and narrow ports, our microfluidic devices can limit nutrient and oxygen circulation to the extent that necrosis is induced. In the case of the microcultures, however, the opposite extremity of factor circulation seemed to present itself. Initial attempts to grow microcultures under the  afore-mentioned maintenance protocol resulted in the cells showing an initially good adhesion but failing to show any subsequent development and degenerating altogether by 5 days *in vitro* (figure 4.9). This degeneration was similar in time scales to the one caused by the osmotic drift but seemed to be more aggressive as the cells did very little even in the direction of initial sprouting of neurites. This type of degeneration is known to occur in small / low density cultures even in standard preparations (i.e., open surfaces, not microfluidic devices) [60] where it is presumed that the neurons are not able to generate a sufficient concentration of conditioning factors around them to sustain their development. The typical solution in this situation is to grow the cultures in proximity to a large pure astrocyte culture which shares the same media and secretes the required conditioning factors. This auxiliary astrocyte culture is sometimes termed support culture. We followed this approach by adding two

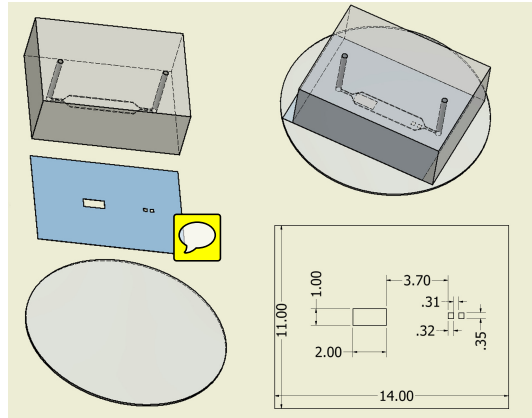


Figure 4.8: Schematics of the 2-layered microfluidic devices with microwells. The three components (PDMS bulk with an engraved microchannel, PDMS sheet and coverslip glass) of the device are shown separately and after bonding to illustrate how the the microwells are aligned to be within the channel boundaries. Dimensions of PDMS sheet are also presented in mm units. In this case, the microwells were of size $350 \times 320\mu\text{m}^2$. Dimensions of microchannel are as in figure 4.1.

levels of support culture. One was harboured in a large well situated within the device several millimeters away from the microcultures (see figure 4.8). A second one was a large culture plated outside the devices on the bare cover slip glass around the PDMS bulk. We found that the presence of these support cultures indeed prevented the afore-mentioned degeneration (figure 4.10) and that both of them together were required for best results (data not shown). We did not attempt growing pure astrocyte cultures for this as regular cortical cultures (which contain astrocytes) seemed sufficient to produce a beneficial effect.

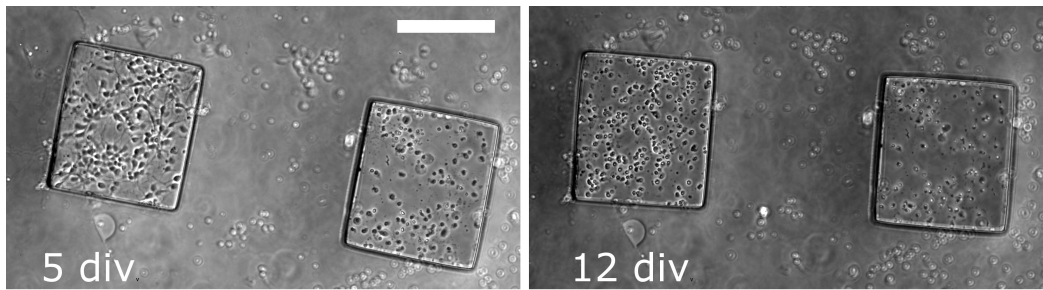


Figure 4.9: Neuronal microcultures do not develop without a support culture. Representative images of microcultures developing without seeding a support culture outside the device. The microwells were of size $300 \times 270\mu\text{m}^2$. Scale bar is $200\mu\text{m}$ long and is consistent across both images.

Since such microcultures are not a standard neuroscience model preparation in and it is unknown what is the smallest size they can be made while still developing properly, we decided to conduct a quantitative examination of their viability. To that end, we designed devices with 3 different microwell sizes and followed their development over 12 days *in*

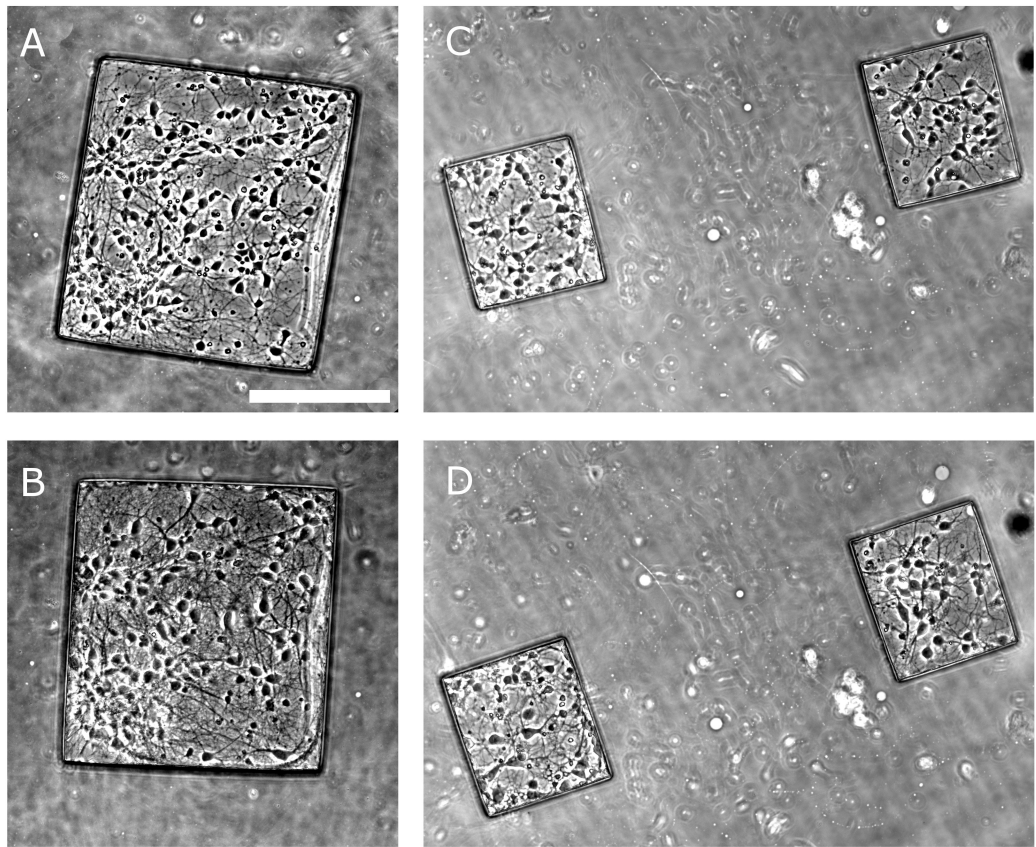


Figure 4.10: Development of neuronal microcultures. (A-B) Images of a neuronal microculture growing in a microwell of size $400 \times 370\mu m^2$ at 5 and 12 days *in vitro*. (C-D) Images of two neuronal microcultures at developmental stages as above in microwells of size $220 \times 190\mu m^2$. Microcultures were seeded at a density of $20 \times 10^6 \frac{cells}{ml}$, flushed and maintained as described in section 2.4. Scale bar is $200\mu m$ long and is consistent across all images.

in vitro. We counted the number of healthy cells in bright field images taken at 1, 5, 12 days *in vitro* and calculated the proportion of cells dying between consecutive counting time points. This data are presented in figure 4.11 as a function of the density of cells in the well at the preceding time point and grouped by well size. This is compared to the same statistic computed in the same way for images of the standard cultures from section 4.2.1 referred to here as macrocultures. It is evident from figure 4.11 A that, regardless of microwell size, the microculture death rates are strongly and negatively correlated with their density. This was corroborated with a linear regression analysis giving a statistically significant linear correlation (F-test, $p = 2 \times 10^{-4}$). The macrocultures did not show such a density associated death rate (F-test, $p = 0.26$) but the macroculture densities were much less variable so the analyzed density range was smaller. The averaged death rates of the macro- and microcultures are compared in figure 4.11 B. Microcultures of all 3 sizes exhibited a significantly higher death rate than the macrocultures (unbalanced t-test, $p =$

2×10^{-5} , 0.0012, 0.0027 for well edge sizes 200, 300, 400 μm , respectively).

Since microculture densities appeared to be a key factor in their long term viability we also performed a similar comparison with the microculture data restricted just to densities higher than $1500 \frac{\text{cells}}{\text{mm}^2}$. This density threshold was selected because the data beyond it did not show a density dependent trend which meant that the beneficial effects were saturated. Indeed the death rates at such high density microcultures were reduced and the large 400 μm ones exhibited death rates indistinguishable from those in macrocultures (unbalanced t-test, $p=0.23$). Smaller high density microcultures of sizes 200 and 300 μm still showed a significantly larger death rate (unbalanced t-test, $p=0.0012$ and 0.0012, respectively).

The above data are consistent with the notion that neuronal cultures need to generate an environment of conditioning factors around the cells to support their own development. Since this environment comprises secreted factors its buildup would strongly depend on the density and the size of the culture. Indeed the effect of both of these parameters is evident in the data shown here and a practical heuristic emerges that microcultures larger than $400 \times 400 \mu\text{m}^2$ and denser than $1500 \frac{\text{cell}}{\text{mm}^2}$ have a potential of developing as well as macrocultures.

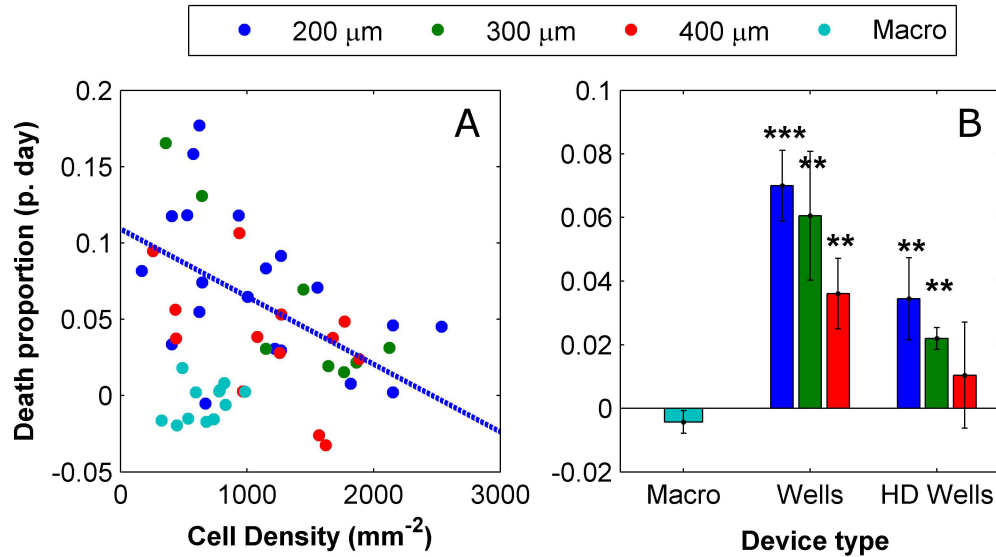


Figure 4.11: The viability of the microcultures is correlated with their density and size. (A) Scatter plot of the proportion of dead cells observed in the microcultures and macrocultures between consecutive counting time points as a function of microculture density. Each point represents a comparison between counts at 2 consecutive time points. Cells were counted at 1, 5 and 12 days *in vitro*. Death proportion is normalized to the number of days between the counts. Data is color coded according to microwell size or if it is a macroculture. (B) Comparison of mean proportional death rates between all the microcultures or microcultures with density higher than $1500 \frac{\text{cells}}{\text{mm}^2}$ and macrocultures. The data is based on 44 microcultures and 9 macrocultures from 4 different platings.

We would like to conclude this section by making a note about the quality of isolation of the microcultures. Since the devices considered here were assembled using plasma bonding, the surface treatment had to follow the ‘bind-then-surface’ approach. This means that the assembled devices were filled and incubated with surface coating solution (PLL) so all exposed internal surfaces were actually chemically prepared for cell adhesion. This means that cells from within the wells were free to send  neurites out onto the PDMS surface and even to migrate there. Additionally, the flushing procedure applied after the seeding was imperfect and sometimes left a substantial amount of cells on the PDMS sheet surface. This lack of restriction meant that after two weeks of growth the microcultures had significant innervation from neurons outside of the well (figure 4.12). Axons seemed to traverse the entire distance between the the microwells and the large support well which was located 3.7mm away. This lack of isolation defeats the purpose for which the microwells were designed. This issue is solved in chapter 6 where tape based design allows a ‘surface-then-bond’ approach whereby only the well bottom is chemically prepared for cell adhesion.

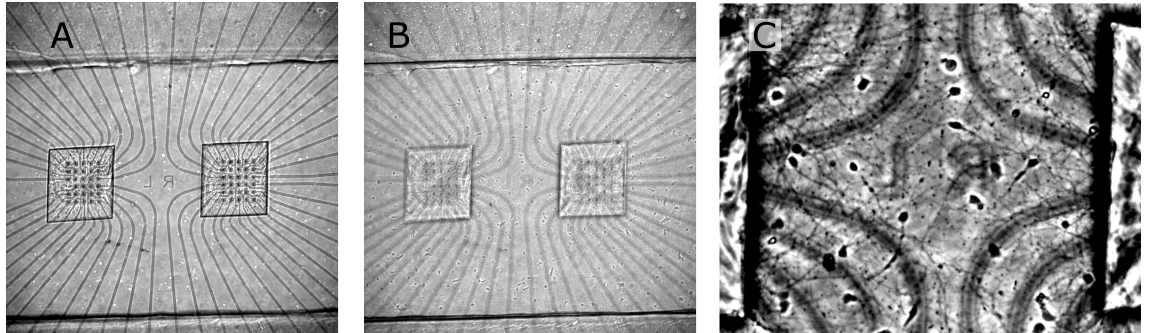


Figure 4.12: Microcultures are not well restricted to the microwell area with bond-then-surface approach. (A) Image of microcultures growing on top of commercial microelectrode arrays at 12 days *in vitro*. (B) Image of the same view field as in A focused on the top surface of the PDMS sheet. This image reveals the substantial inhabitation of the top surface by cells and neurites. (C) A zoom into the area between the microwells in B to highlight the presence of neurons and neurites outside the microwells. Microwells are of sizes $300 \times 270\mu m^2(L \times W)$ for scale reference.

4.3 Viability of neuronal cultures under steady microfluidic flow

4.3.1 Pilot flow study

The operation of the system  concern involves subjecting the neurons to flow rates in the order of millimeter per second. Thus, in this section as well as in chapter 5, we address the question of how well the cultures perform under flow. Primary neurons are considered to

be highly sensitive to shear stresses so we suspected that subjecting them to flow might be non-trivial and that there might be a limit to how high a flow rate they can bare. Since the interaction of primary neurons with flow is completely uncharted we conducted preliminary experiments where cultures at various ages were subjected to steady flow with growth media while being continuously monitored via time lapse imaging. The flow apparatus used for these experiments is described in section 2.8. These experiments seemed to develop in a stereotypical pattern: shortly after initiation of flow, the cells started losing the surface adhesion which was manifested by obvious fasciculation. In younger cultures where not too much ECM tissue had been built it could be observed that the fasciculation was accompanied by a retraction of processes (figure 4.13). By 20 hours, most of the cells appeared to degenerate. In older cultures rich in ECM this degeneration also involved complete detachment of the tissue, which was left floating inside the device volume.

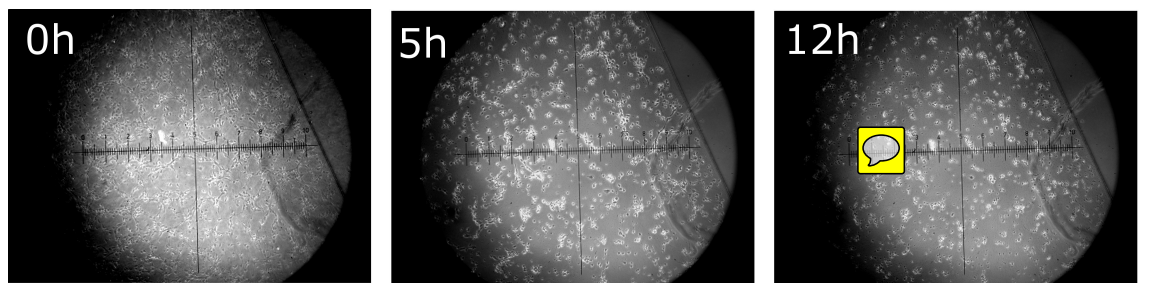


Figure 4.13: Neuronal cultures exposed to steady flow lose their surface adhesion, retract their processes and degenerate after several hours. Time lapse of a neuronal culture grown in the standard 1-layer microfluidic devices (section 4.2.1) placed under flow at 1 day *in vitro*. The flow rate was $1 \frac{nl}{s}$. Scale units: $\approx 100\mu m$

Initial experiments were conducted with the devices placed openly in the ambient environment while only plugged into a custom made heater system where heating resistors were brought into contact with the glass and the PDMS bulk and were controlled to $37^\circ C$ [63]. However, we had concerns as to how well this system controls the internal device temperature given that media at room temperature is pumped in. Additionally, maintenance of media CO₂ levels was based on connecting the pressure control system to a 5% CO₂ / 95% air gas supply. This configuration assured that the media in the flow reservoirs were fully CO₂ saturated but there was still a concern that as it travels through the tubes in the ambient air some CO₂ content could escape. To alleviate these issues we built a custom made compact environmental chamber whose internal environment was controlled to $37^\circ C$ and 5% CO₂ (figure 2.8.1). The flow tubes were introduced into the environmental chamber through a small side hole before connecting to the devices. The tube configuration was purposefully selected such that the total tubing volume outside the environmental chamber was 3 times less than that of the internal tubing ($\approx 16\mu L$ vs. $\approx 60\mu L$). This meant that, while travelling from the reservoir to the device, the media spent triple the time inside the

chamber environment than in the ambient one so any CO₂ lost outside would necessarily have been reabsorbed. We also calculated that the residence time inside the chamber is at least 10 minutes which is more than enough to heat the media to 37°C given the micrometer scale of the tubing (this was verified with an inline flow thermocouple, PH-01, Multi Channel Systems). Nevertheless, the employment of the chamber did little to change the outcome of the flow experiments leading us to conclude that the basic physiological parameters of temperature and media CO₂ saturation did not play a major role in the degeneration.

Since conditioning factors are known to exert a protective effect on neuronal culture [60, 64] we explored the option of using conditioned media, i.e., media taken from a different culture for flow. We found that this had a pronounced effect on the cultures' tolerance in the sense that there was an initial flow period where the cultures' appearance did not seem to change. Additionally, even though fasciculation and degeneration still occurred, they developed much later, typically more than 10 hours into the flow session. Another interesting observation was that the rapid degeneration observed with fresh media flow seemed to occur regardless of the flow rate and presented itself even when the tubes were connected but the flow was set to 0°C. These observations suggested that, when using conditioned media, a time window could be present where the culture is functional and useful experiments may be performed. They were also surprising in that the flow rate, i.e., shear, appeared to play a smaller than expected role in the adverse effects of flow. We therefore decided to conduct a systematic study to quantitatively assess the effect of conditioning and shear on the viability under flow and to establish what is the practical experimentation time window. Description of this study follows.

4.3.2 Quantitative viability analysis

Analyzing how media conditioning affects viability under flow requires an analytic measure of conditioning. Since conditioning involves a continuous secretion of factors into the bulk media, it seemed plausible that, a conditioning measure would be proportional to the length of time which the media was in contact with the cells. We produced conditioned by growing cortical rat cultures of prescribed densities in T-25 flasks with prescribed media volumes and without changing of the media. The precise protocol and the conditioning scale are provided in section 2.7. Roughly, every 3.5 days of incubation in the flasks *in vitro* are equivalent to 1 conditioning units.

We ran a large set of steady flow experiments on macrocultures growing in standard 1-layer devices. The experiments were conducted in a range of conditioning levels and flow rates. To provide a quantitative measure of viability these flow experiments also included a propidium iodide assay (protocol and example in section 2.8). In brief, propidium iodide was added to the flow medium so it was present around the cells for the length of the experiment. Intact plasma membranes of healthy cells are impermeable to fluorescent DNA-binding molecule. However, when cells die their nuclear material becomes exposed and

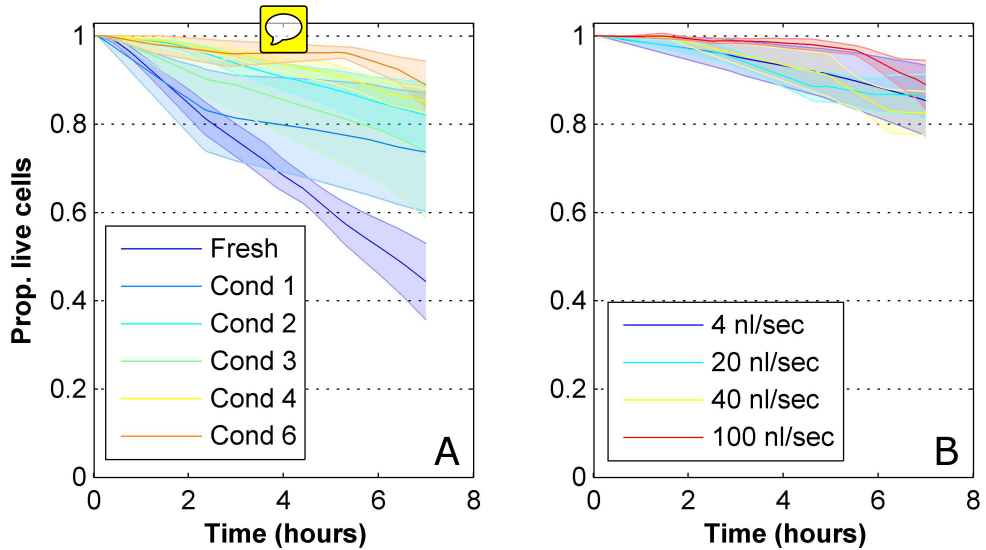


Figure 4.14: Using conditioned media for flow can significantly prolong the culture viability regardless of the flow rate. (A) Averaged viability curves for flow with media of increasing conditioning levels. Every curve averages data from several flow experiments where a propidium iodide assay was used to quantitatively assess the number of dead cells over time (full description is given in full in section 2.8). Example for such individual flow curves can be seen figure 4.15. The flow rate for all experiments was $40 \frac{nl}{s}$. Shaded areas depict the SEM. (B) Averaged viability curves as in A but where the flow rates are varied whereas the conditioning level is fixed at 4. The data is based on 36 experiments from 9 platings. Every curve except for Cond 6 in panel A is the average of at least 3 experiments from 2 different platings. Cond 6 is based on 2 experiments from one plating.

readily serve as a seed for propidium aggregation and therefore appears as a dot in fluorescent microscopy. These dots are counted to provide a quantitative measure of how many cells have died since the initiation of the flow. During a flow experiment fluorescent images were taken every 1-2 hours to generate a curve of the deterioration in viability. Figure 4.14 shows averaged viability curves for a range of conditioning levels where the flow rate is fixed and for a range of flow rates where the conditioning level is fixed. The observations made in the previous section are clearly manifested in these curves: increasing of the conditioning levels is negatively correlated with the death rates whereas increase in flow rates within the tested range is not.

To facilitate the statistical analysis we grouped the conditioning scale into 3 groups: Fresh media (same as before), intermediately conditioned (grouping conditioning levels 1 and 2) and highly conditioned (grouping levels 3-6). Figure 4.15 shows the averaged viability curves generated with new grouping as well as a control curve made without connecting the cultures to the flow system at all (static). The figure also shows a breakdown of the averaged curves into the constituent individual ones per experiment. Since the individual curves did not

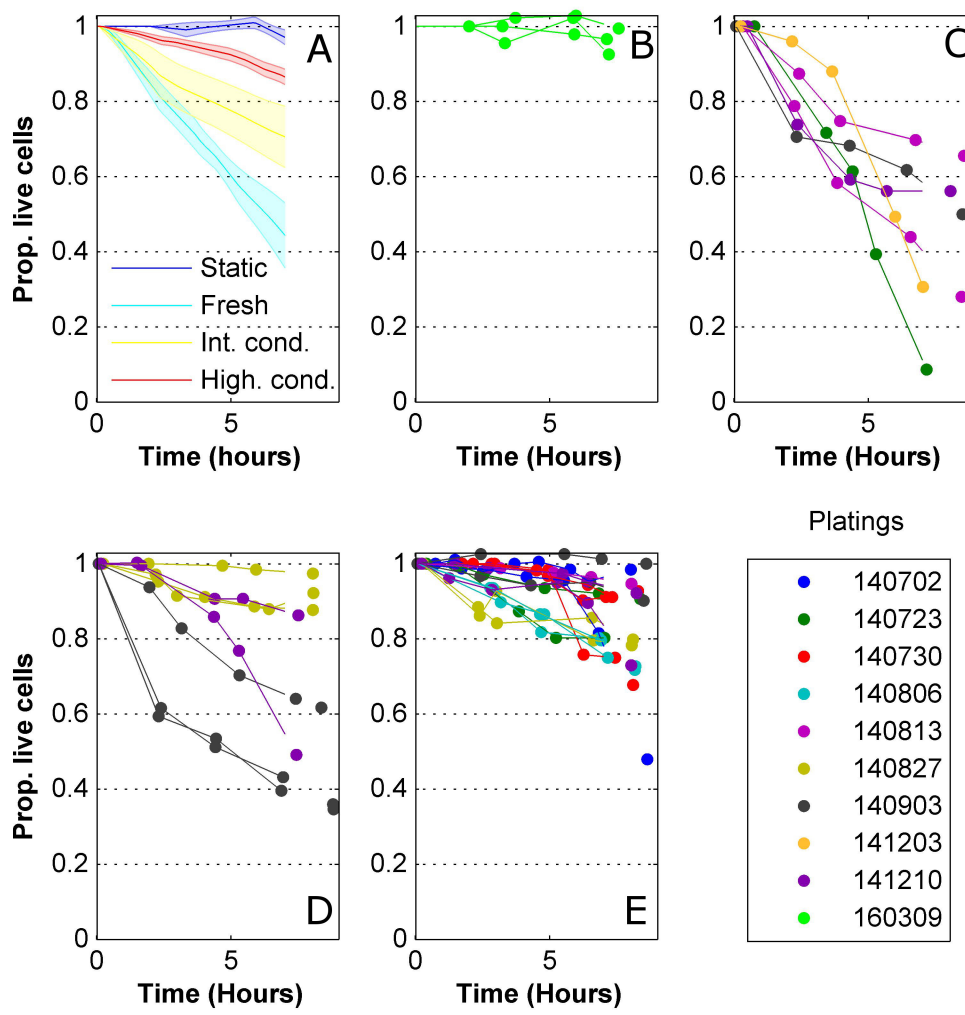


Figure 4.15: **Individual viability curves do not exhibit any common temporal features so their average is linear.** (A) Averaged viability curves for increasing conditioning levels as in figure 4.14 A but with a grouping applied to get improved separation (grouping specified in the text). The flow rate for all experiments was $40 \frac{nl}{s}$. An additional control curve is included where the devices were not connected to the flow system. (B-E) Individual viability curves from the experiments that were averaged in A. Each dot represents a fluorescent image where the number of dead cells were counted. The order of the panels B-E matches the order of the averaged curves as listed in the legend of panel A. Individual curves are color coded according to the date of plating of the given culture.

exhibit any conspicuous common time dependent features and as the averaged curves were strikingly linear we reasoned that a fixed death rate model (linear) would be a plausible a description of this data. In accordance with this notion, the statistical analysis was based on fitting a line to the viability time series of each experiment with a forced intercept at

(time=0, viability=1). The statistical testing was then performed on the fitted slopes and is discussed next.

Figure 4.16 shows a comparison of the fitted death rate slopes for various flow conditions. The conditioning levels of the flow media were shown to have a significant effect on the death rate (Figure 4.16 A, 1-way ANOVA, $p = 1.5 \times 10^{-5}$). However, flow under all conditioning levels still resulted in death rates significantly higher than control (unbalanced t-tests, $p = 2.1 \times 10^{-4}$, 0.049 and 0.021 for fresh media, intermediately conditioned and highly conditioned respectively). Thus we were not able to find a conditioning regime where the cultures were viable for long term under flow. To get an idea as to how much using conditioned media can extend the experimentation time, we calculated how long at least 90% of the cells will be alive, given the established death rates. This provided times of 1.3, 2.5 and 5.6 hours respectively for the 3 conditioning levels at hand. Given that highly conditioned media was used, changing the flow rate did not produce a significant difference (Figure 4.16 B, 1-way ANOVA, $p = 0.91$). The main experiments above were performed with PEEK tubing. We also tested if changing the tubing material would affect the viability under flow. We found that stainless steel tubing gave the same results as the PEEK for flow with highly conditioned media. PTFE tubing, however, was surprisingly associated with a significantly higher rate of degeneration (Figure 4.16 C, unbalanced t-tests, $p = 0.95$ and 7.5×10^{-11} for stainless steel and PTFE tubing, respectively). Thus, The beneficial effect of conditioning seems to be absent when using PTFE. This could suggest that our PTFE tubing absorbs valuable conditioning factors or that it introduces contaminants into the media during flow. We did not further interrogate this non-trivial effect but it is important to make a note of how the tubing selection can affect these types of experiments. Finally, since all the conditioned media in this study was used straight from the culture flask we wanted to check whether it could be stored for later use as that would greatly simplify the experimental design. Consequentially, we extracted highly conditioned media, kept it frozen at -80°C for several weeks and then heated it back up to 37°C prior to using it for flow. We found that the frozen media did not preserve the beneficial effects of the conditioning and resulted in significantly faster death rates as compared to the media used directly from the flasks (4.16 D, unbalanced t-test, $p = 0.0073$). Interestingly, the performance of the frozen media was statistically the same as that of the intermediately conditioned media (unbalanced t-test, $p = 0.59$) so the benefits of conditioning were still partially present. It is likely that some of the conditioning factors degrade over time and are sensitive to freezing and thawing (e.g., large protein molecules) hence the above results.

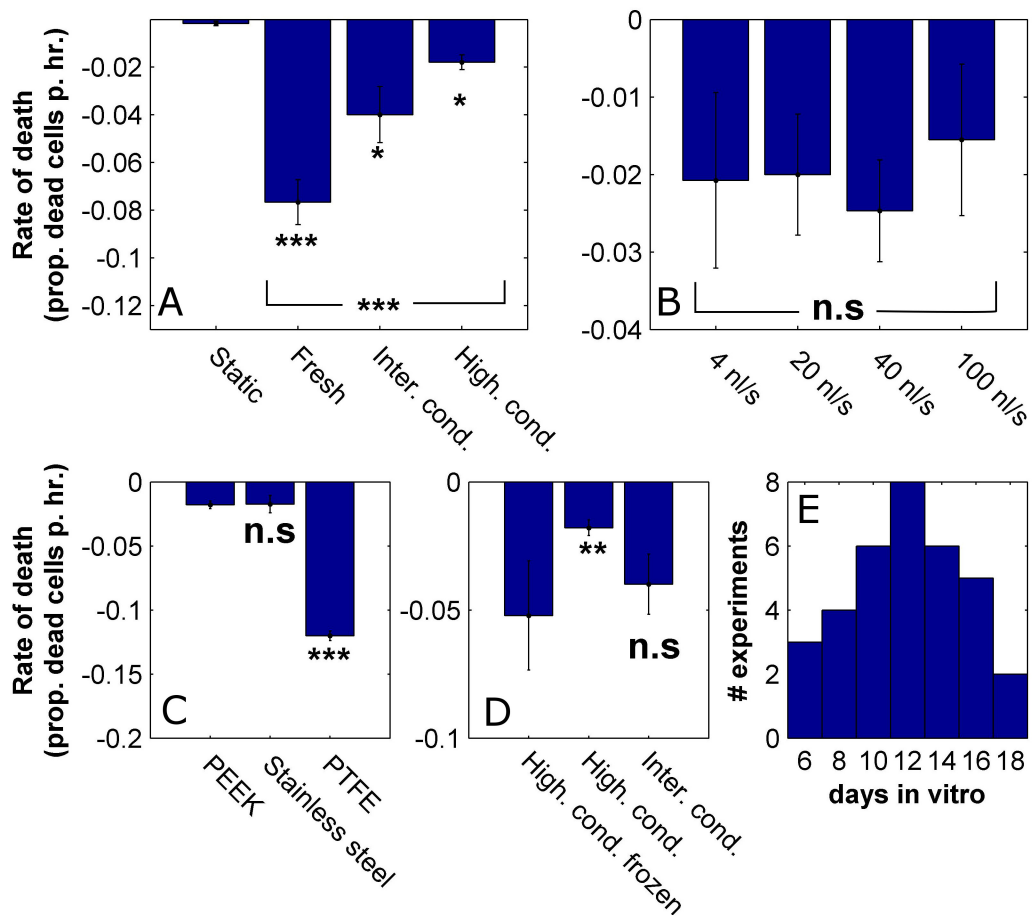


Figure 4.16: Death rates under steady flow depend on media conditioning levels and on the type of flow tubes but not on flow rates in the tested range. (A) Comparison between the measured death rates under steady flow for increasing media conditioning levels and for control devices. Experiments were identical in all other parameters (flow rate $40 \frac{nl}{s}$ and PEEK tubing). **(B)** Comparison between the measured death rates under steady flow for increasing flow rates (all highly conditioned media, PEEK). **(C)** Comparison between the measured death rates under steady flow for different tube types (all highly conditioned media, $40 \frac{nl}{s}$). **(D)** Comparison between the measured death rates for conditioned media that was frozen and re-thawed and conditioned media that was directly used ($40 \frac{nl}{s}$, PEEK). **(E)** Distribution of the ages of the cultures used in this study. The data is based on 49 experiments from 9 platings. Every bar is based on data from at least 3 experiments from 2 different platings except for the static data in panel A and the PTFE data in panel C which are each based on 3 experiments from one plating. Asterisks that group several bars indicate statistical significance of an ANOVA test. Asterisks next to individual bars indicate statistical significance of a t-test between the leftmost condition and the condition at hand. *, **, ***, n.s indicate statistical significance at a level of confidence of 95%, 99%, 99.9% or <95%, respectively.

4.4 Chapter conclusion

In this chapter, we demonstrated a capacity for growing rat macrocultures (standard size) and microcultures in microfluidic devices. The observations made in sections 4.2.1.2 and 4.2.2 highlight the challenges that exists in the design of microfluidic devices for neuronal culture in finding a ‘goldilocks’ circulation regime. On one hand, enough nutrients and oxygen need to be allowed into the device to meet the requirements of the culture and, on the other hand, conditioning factors must be prevented from ‘escaping’ as they are required for sustaining the development. The precise design is strongly dependent on the size and density of the culture as these inform its oxygen and nutrient requirements and also the secretion rate of conditioning factors.

In the second part of this chapter we used a viability assay to quantitatively observe the cultures’ health under flow. We found that using highly conditioned media can sustain the viability of the culture for several hours under flow and therefore consider it a promising approach for establishment of the system. Interestingly, the shear rate induced by the flow did not correlate with the viability which suggests that the deleterious effects are mediated solely by removal of conditioning factors and not at all by physical shear. Nevertheless, this is not the only possible interpretation for these results. A related study testing the viability of neuronal culture under a range of flow rates reported a shear threshold associated with culture degeneration [65]. This study found that a compound isolated from brain tissue named Galanin protects the cultures from the shear so, when it is introduced into the flow media, an effective increase in the degeneration threshold is observed. A possible interpretation of our results could therefore be that the conditioned media contains factors similar to Galanin that protect the cells from the shear and therefore effectively increase the flow rate threshold to a level exceeding the tested range. The study presented here cannot unambiguously distinguish the above-described narratives. This issue will be further addressed in the next chapter where electrophysiological measurements under flow will be presented and shed light on the mechanisms by which flow interacts with the culture.



Chapter 5

Activity under steady microfluidic flow

5.1 Introduction

In the previous chapter, we found that when using conditioned media for flow the cultures' viability may be extended so as to allow conducting of useful experiments. The viability assay used, however, is a crude measure of neuronal functionality and indicates that a cell has died only at late stages of apoptosis / necrosis, after the plasma membrane had been breached. This Ph.D work is concerned with how volume transmission interacts with network activity and plasticity so electrophysiological measurements are the relevant measure of functionality. In this chapter, we used multi electrode array electrophysiology to monitor the network activity of the culture as it was subjected to steady microfluidic flow at various flow rates and media formulations. We also explored using a semi-permeable membrane to de-couple the flow from the cells. The media formulation described in the previous chapter as 'highly conditioned' was found in preliminary experiments to be inadequate for electrophysiology under flow as it gave rise to inconsistent results and generally to silencing of most of the activity. Thus, the experiments in this chapter are predominantly based on using conditioned media taken from the same culture dish (i.e., media which the particular tested culture grew in, termed 'self media') and this approach was the one that finally gave usable behaviour. Nevertheless, how flowing with media from other culture dishes affects the activity was also explored.

We found a strong flow rate dependent effect whereby for slow flow rates the network dynamics were preserved. For faster flow rates, a disruption to the network activity was observed consisting a partial silencing of the active MEA channels and a loss of synchronization and of the response to electrical stimulation. This disruption was present even when a semi-permeable membrane was used to de-couple the cells from the flow. Such a membrane was shown to reduce the shear underneath to negligible levels [66] so this observation strongly

suggests that the cause of the effect is a disturbance to the chemistry around the cells. An improvement in the stability of activity was provided by the use of media from older cultures but this was still inconsistent. Finally, we found that typical synchronized network dynamics were preserved in older cultures (aged over 20 days *in vitro*) under fast flow but this was still strongly dependent on the source of the media (self media vs. media from younger culture). We argue that these results indicate an interaction between the flow and intrinsic volume transmission signalling in the tissue and propose that microfluidic flow could potentially be used as a novel assay to study these poorly understood processes. Furthermore, these results highlight the important factors that need to be addressed when designing microfluidic based drug delivery systems to neuronal tissue and the implications for device design are discussed. Most importantly, This study provides a protocol where network activity is preserved under rapid flow and is therefore the basis for the final microculture pulsing system presented in chapter 6.

5.2 Neuronal cultures in cross flow devices on MEAs

Figure 5.1 shows the devices used for the experiments conducted in this chapter. In contrast to the devices used for the viability study in chapter 4, these devices comprised multiple layers so as to allow the inclusion of the semi-permeable membrane (Whatman cyclopore, 100nm pore size, cat. no. 7060-4701). Thus they comprised a flow and cell layers which were joined either to each other or to the membrane from each side, depending on the experiment. Because of the perpendicular arrangement of the flow channel in relation to the cell channel the devices were tagged ‘cross flow’. Since assembly of such multi layered devices through plasma bonding is problematic and since plasma bonding of PDMS to the commercial MEAs could damage the surface and is not practical for re-use, we opted to use the tape technology (section 4.2.1.3). Thus prior to device placement, the MEA surfaces were treated with PEI (section 2.3). In parallel, the device layers were cut out of the 125 μ m silicone transfer tape and aligned using a custom made alignment tool (essentially comprising two pegs holding the layers in place through alignment ports). The assembled devices were oven sterilized and joined with the MEA surfaces, after these have been washed and dried from the PEI solution. The devices were manually aligned to the MEAs in such a way that the intersection area between the flow and cell channels was on top of the central electrode pads area. Since self media is extracted directly from the tested sample we increased the volume of growth media to 4ml per sample to make sure that enough supply would be available for the flow session. We used custom made glass cylinders which were glued to the MEA following the attachment of the devices to hold the media (figure 6.1).

To seed the cross flow devices, the flow channel ports were blocked so as to prevent seeding solution from being diverted through the flow channel. The seeding volume was 3 μ L which is enough to fully saturate the cell layer ($\approx 2\mu$ L). The seeding density was $7 \times 10^6 \frac{\text{cells}}{\text{ml}}$

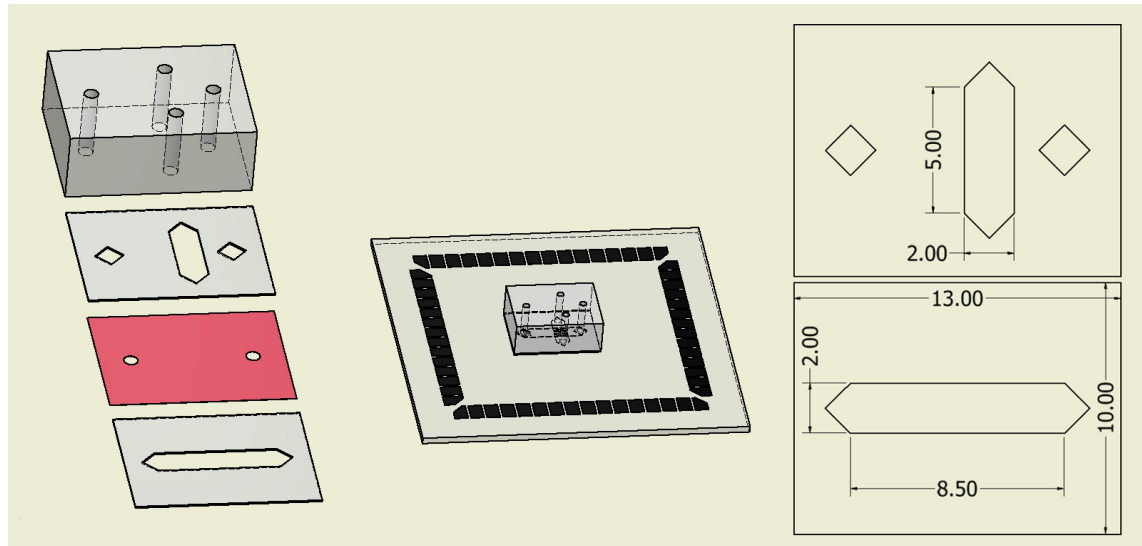


Figure 5.1: **Illustration of the cross flow devices.** Illustrations showing the constituent layers of the device laid out as well as assembled and joined to an MEA. The semi-permeable membrane is optional and shown in red. The dimensions of the flow and cell layers are also shown in millimeter units. Further details about the device fabrication are found in the text.

which was calibrated to achieve an area density of $\approx 1000 \frac{\text{cells}}{\text{mm}^2}$ in the central electrode pads area. Cultures seeded in such devices typically developed well for over a month. This contrasted with the standard 1-layered devices introduced in section 4.2.1 where many of the cultures did not develop past the end of the 3rd week. This could be attributed to the increased volume of the cross flow devices which would be associated with improved nutrient and by product circulation or to the switch to PEI surface treatment which is considered better for neuronal adhesion. Maintenance of the seeded devices was as described in 2.4 and completely follows the protocol achieved in section 4.2.1.

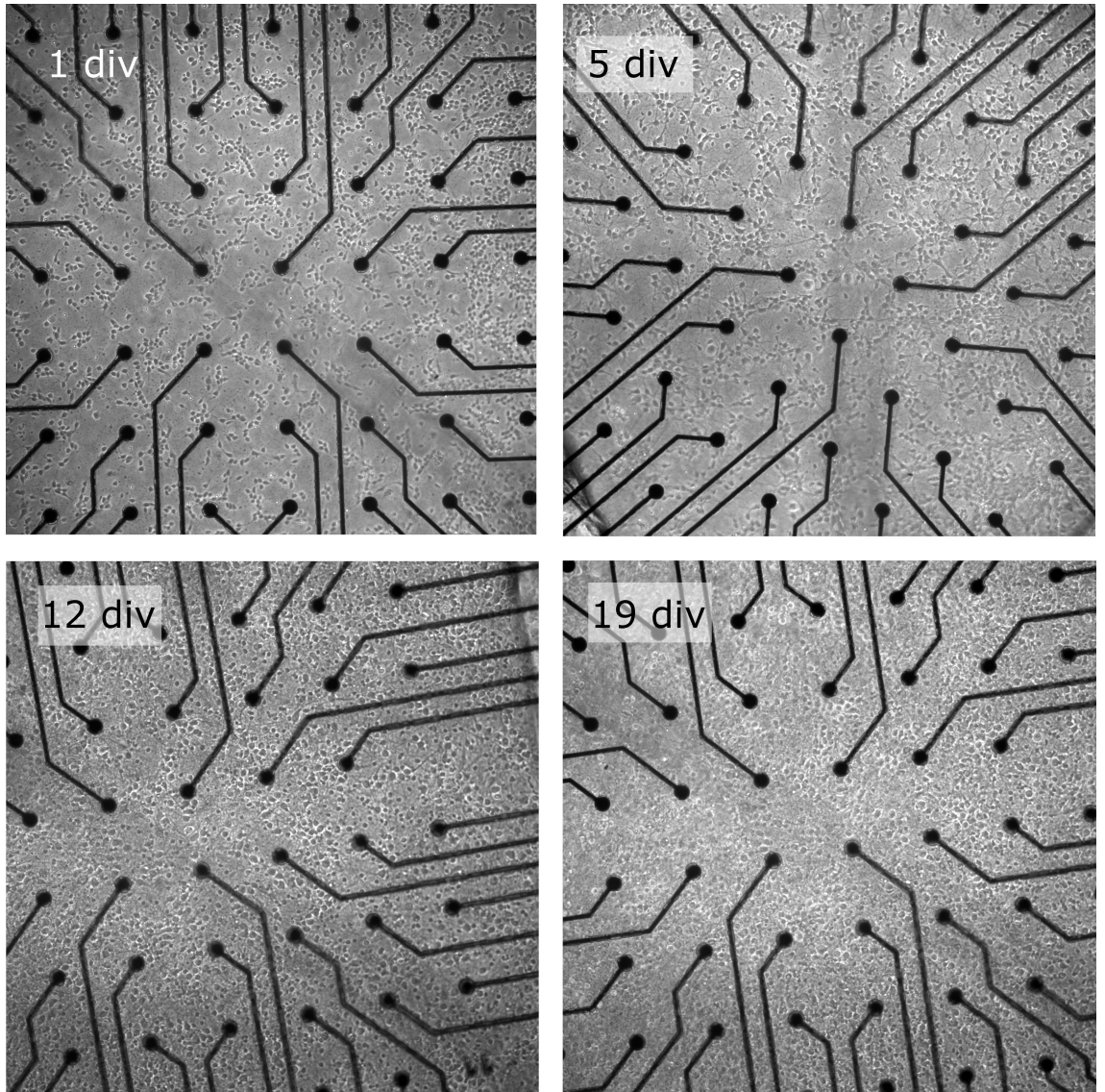


Figure 5.2: Neuronal cultures develop well in cross flow devices for over 3 weeks *in vitro*. Images of neuronal culture growing in the cross flow devices at several developmental time points. The images were taken in the area of intersection between the flow and cell channels. The electrodes are spaced 200 μm apart for length reference.

5.3 Activity under flow for young cultures

The first set of experiments were performed on cultures at ages 12-15 days *in vitro* which were termed ‘young’ cultures. This age range is similar to the one used for the viability study in section 4.3 so the results shown here probably best reflect the state of the cultures in that study. The recordings in this chapter were all performed in the presence of electrical stimulation in the form of a single test pulse delivered to a single MEA electrode every 5 seconds. The stimulating electrode and the pulse voltage amplitude were selected before the experiment so that an observable network response would be elicited by the stimulation. The reason for using stimulations is twofold: firstly, spontaneous activity is known to be inherently volatile as it probably depends on stochastic processes of intrinsic excitability and synaptic noise. Since the aim of these experiments is to identify conditions where the activity is stable we were concerned that variability associated with spontaneous activity would be confused with the destabilizing effects of flow. Thus, we argued that electrical stimulation which is more deterministic than spontaneous activity might be a more adequate basis for assessing the stability under flow. Secondly, the ability of neuronal ensembles to respond to stimulation underlies their facility for representing and transforming external information. We therefore found it is important to include a criteria where the response to stimulation would be maintained under flow.

The extracellular recordings and data analysis pipeline as well as the stimulation protocol are specified in section 2.5 and have been further described in sections 3.2 and 3.3. All the experiments described in this chapter were initiated with a 30-60 minute period of baseline recording before the sample was plugged into the flow system. When self media was used, it was withdrawn from the sample and flushed through the system after the baseline recording.

5.3.1 Effect of flow rate

We found a strong flow rate dependent effect on the activity which is exemplified in figure 5.3 which shows baseline as well as slow and fast flow data for a young culture. In the baseline recording, the culture exhibited typical synchronized bursting dynamics which are typical for rat cultures of this age (sections 3.2 and 3.2.2). These synchronized dynamics were manifested in vertical lines in the raster plots and with high values of correlation throughout the correlation matrix. Additionally, the culture responded to test stimulation pulses with a network reverberation, although these sometimes failed to appear. Immediately upon initiation of the fast flow, these synchronized dynamics broke down with the neurons initially switching to a fast tonic firing and then gradually becoming silent. The tonic firing was manifested in a dramatic reduction in the correlation values. Additionally, the stimulation response was all but completely abolished with the activity not occurring preferentially after the stimulation but tonically spread in the observed time window (figure 5.3 B). Remarkably, even the direct responses (low latency, low jitter responses appearing as straight lines in the

response rasters) were abolished under flow which suggests that the basic biophysics of the neurons had been compromised. Under slow flow, there was no sign of these dramatic perturbations to the activity. Indeed, it is evident that the slow flow induced some changes to the activity but overall the synchronized bursting dynamics and the stimulation responses were maintained and the structure of the correlation matrix was preserved.

To make sure that the phenomena reported above were indeed consistent we ran several such experiments with slow and fast flow rates and show the statistics in figure 5.4. The results are presented through 3 measures: global firing rate (i.e., total number of spikes recorded over all electrodes), mean correlation (i.e., the mean of the correlation matrix without the diagonal elements) and stimulation response ratio which is explained next. Stimulation response ratio refers to the ratio between the total spike count (over all electrodes) in a $200ms$ window just following the stimulation and a window of the same size 2 seconds later. The reason for this definition is that a measure that counts only the spikes following the stimulation is very sensitive to the background spontaneous activity. Thus we employed a second window at a distance from the stimulation under the assumption that its spike count is attributed solely to spontaneous activity. The ratio measure therefore represents the relative increase in firing rate due to the stimulation relative to the ongoing spontaneous activity. As some of the conditions used here caused large changes in intensity and temporal distribution of the spontaneous activity, using a simple stimulation response measure would have been meaningless. The firing rate and stimulation response ratios are further normalized to the baseline values of these measures (i.e., from the baseline recording period prior to connection of the tubes). Measures for control cultures were normalized to the mean value over the first hours of recording.

The above-mentioned activity measures are shown in a brief 40 minute window following flow initiation (figure 5.4 A-C) to observe the immediate consequences and also for an extended period of over 3 hours (figure 5.4 D-E) to assess the longer term behaviour. The short term window was also used for statistical testing. Cultures placed under fast flow with self media showed a rapid reduction in firing rates and synchronicity and their response to stimulation was immediately abolished (difference from control was verified through 2-way ANOVA with $p = 0.005$, 5×10^{-10} and 3×10^{-9} , respectively. P values shown are the lower between the group and the interaction effect). Cultures under fast flow were not able to recover their activity and all the measures tended to zero in the long run. Cultures placed under slow flow did not show a significant difference in firing rate or in stimulation response and had just a marginal decrease in correlation (2-way ANOVA, $p = 0.61$, 0.20 and 0.04 , respectively). It is evident from the long term plots for the firing rate and correlation that there was a high degree of variability associated with the initiation of slow flow (connecting the tubes probably causes a sudden flush of media internally in the device). However, over time the cultures were able to adapt to the conditions and the variability subsided. In the case of the response to stimulation, a dramatic increase was observed from about the 3rd

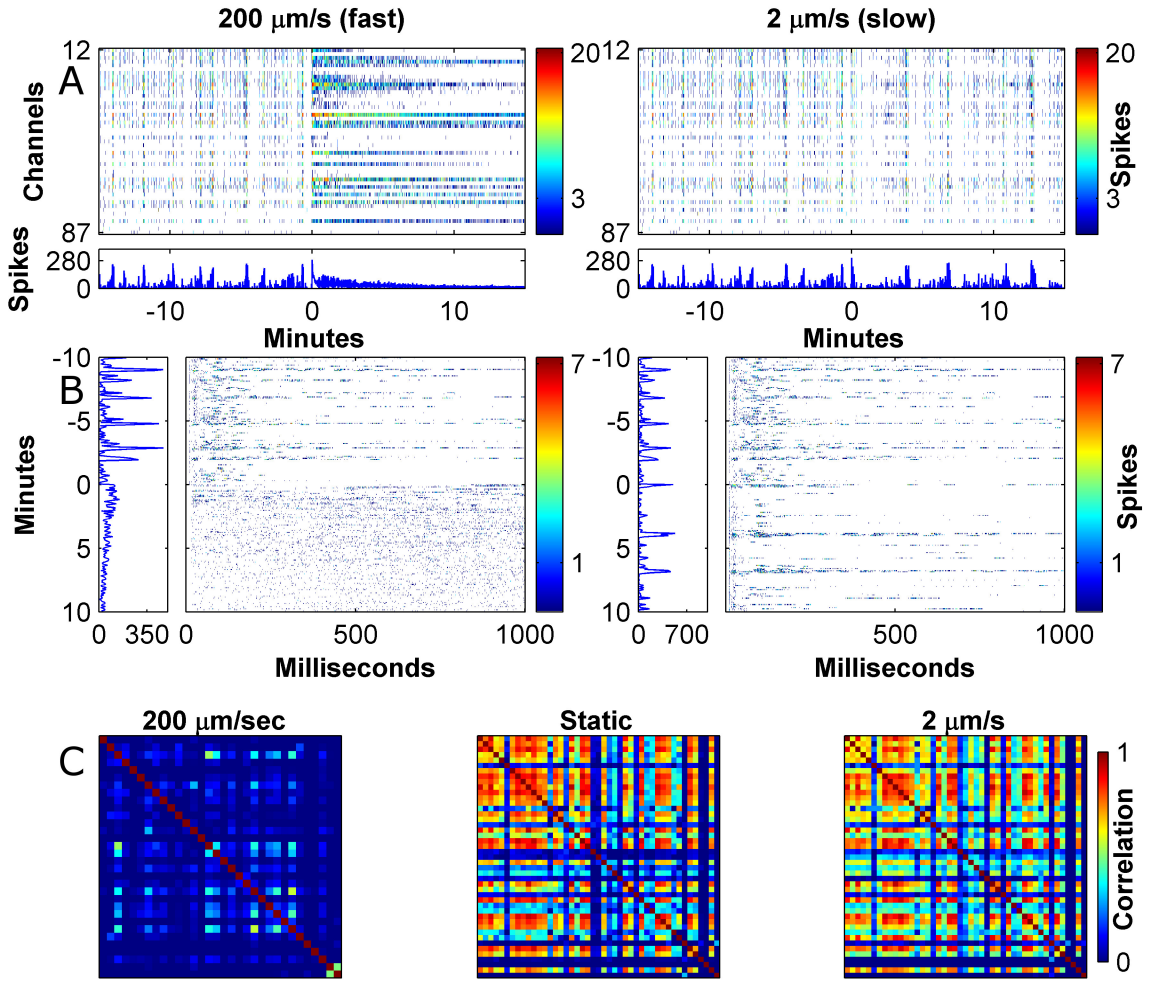


Figure 5.3: Young cultures placed under flow with self media suffer a flow rate dependent disruption to the activity. (A) Network raster plots showing the activity of the culture before (negative times) and just after (positive times) initiation of slow and fast flow (left and right panels, respectively). Note the immediate switch to a tonic and desynchronized regime in the case of the fast flow (B) The culture's network responses to stimulation before and just after initiation of slow and fast flow. Note the immediate loss of the temporally localized stimulation response in the case of fast flow (C) Correlation matrices representing the culture's activity in static conditions and under flow. All matrices are based on 10 minute activity samples. In the case of flow the samples were taken 15 minutes into the flow session. To obtain the shown data, the culture was initially recorded for 30 minutes in baseline conditions following which the flow tubes were connected and 20 minutes of slow flow were recorded. The flow was then increased to the fast rate and remainder of the session was recorded in this setting. This experimental sequence was an exception which was made to observe different flow rates applied to the same culture. In the typical case (figure 5.4) slow and fast flow regimes were conducted in separate experimental sessions.

hour of the flow session. This later effect shows that even the slow flow induces changes and instability to the culture over time. However, the mechanism behind this non-trivial effect is probably different from those operating immediately at the onset of flow and was not investigated further in this work.

5.3.2 The semi-permeable membrane approach for shear reduction

The results in the previous section reveal a flow rate threshold which cannot be exceeded if the culture is to maintain a stable network activity. Unfortunately, using direct flow at the permissive rate is incompatible with the rapid drug delivery which is the concern of this work and which requires flow speeds in the order of $1\frac{mm}{s}$ (see section 4.2.1). Thus we decided to explore an approach of decoupling the flow from the cells by means of a semi-permeable membrane. In this approach high flow rates would be maintained over the membrane to allow rapid drug delivery to the cell area above the membrane. The next step of the delivery would then be carried out via diffusion / slow convection through the membrane. Since the membrane can be positioned in close proximity to the cells the second delivery can potentially be made as quick as necessary. After all it is known that neurons use diffusion over short distances for inter-cell signalling which can be extremely fast (e.g., synapses). For example, if a $10\mu m$ membrane was to be positioned $5\mu m$ above the cells giving a total of $15\mu m$ drug travel distance then, by using the estimated diffusion time relation $t \approx \frac{x^2}{4D}$ with $D = 400\frac{\mu m^2}{s}$ (typical diffusion coefficient value for a neurotransmitter sized molecule [63]), the drug delivery time would be $\approx 140ms$ which is easily compatible with the total required drug pulse time scales. In the case of the devices used here the height of the cell compartment is dictated by the thickness of the tape $\approx 100\mu m$ so the distance is far greater than that required for rapid delivery. However, the aim here is to test the applicability of the approach and the correct distances can be implemented as needed in drug pulsing devices. Indeed this approach has been implemented before for shear free agonist gradient generation to cultured neurons [45, 66]. In that study an analytical estimate was developed for the maximal flow speeds which could be experienced by the cells underneath the membrane as a function of the flow speed over the membrane, of the membrane properties and of the device geometry. Applying this estimate to our devices provides a flow speed of $20\frac{nm}{s}$ in the cell compartment at most for the highest possible flow speed over the membrane. This estimate is 2 orders of magnitude lower than even the slow flow rate that was shown to be permissive of proper electrophysiological function in section 5.3.1 so this approach holds a potential to sustain the network function.

Young cultures growing in membrane devices were subjected fast flow under the same protocol as in the previous section (figure 5.5 shows images of a culture stained following one such experiment). The results are compared to the fast flow on the non-membrane devices in figure 5.6. Remarkably, the introduction of the membrane did nothing to change the effect of the fast flow on the culture activity with all observed measures crashing with a very

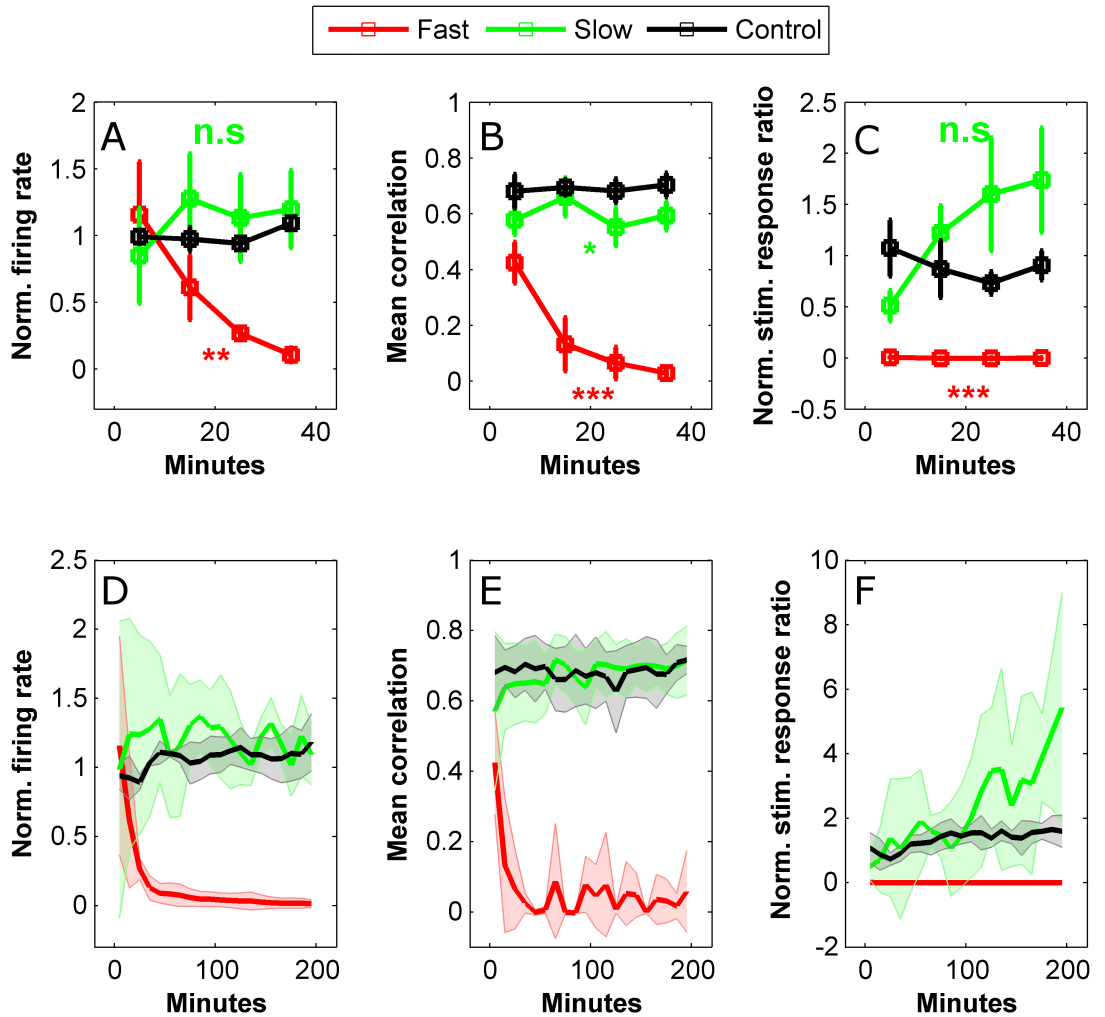


Figure 5.4: **Young cultures placed under flow with self media suffer a flow rate dependent disruption to the activity which does not recover over time.** (A-C) Averaged measures of firing rate, mean correlation and stimulation response ratio in a 40 minute interval immediately after initiation of flow for 2 different flow rates and for recordings in static conditions (color coded). The measures are calculated in 10 minute bins. Error bars indicate SEM. A detailed definition of the measures can be found in the text. Time course of the 3 measures for the 2 flow rates is compared to control by means of a 2-way ANOVA. The statistical significance is determined by the lowest of the p values for group and interaction effects and is indicated by *, **, ***, n.s which refer to confidence levels of 95%, 99%, 99.9% or <95%, respectively. (E-F) Same measures as in A-C in an extended observation period of 200 minutes. All 3 measures crash immediately with fast, but not slow, flow onset. Shaded area represent the standard deviation of the measures. Firing rate and stimulation response ratio measures are normalized to their averaged value in the baseline recording prior to flow (or to the first hour in the case of the control). Data are based on n=4, 5 and 3 experiments for the fast flow, slow flow and control conditions, respectively.

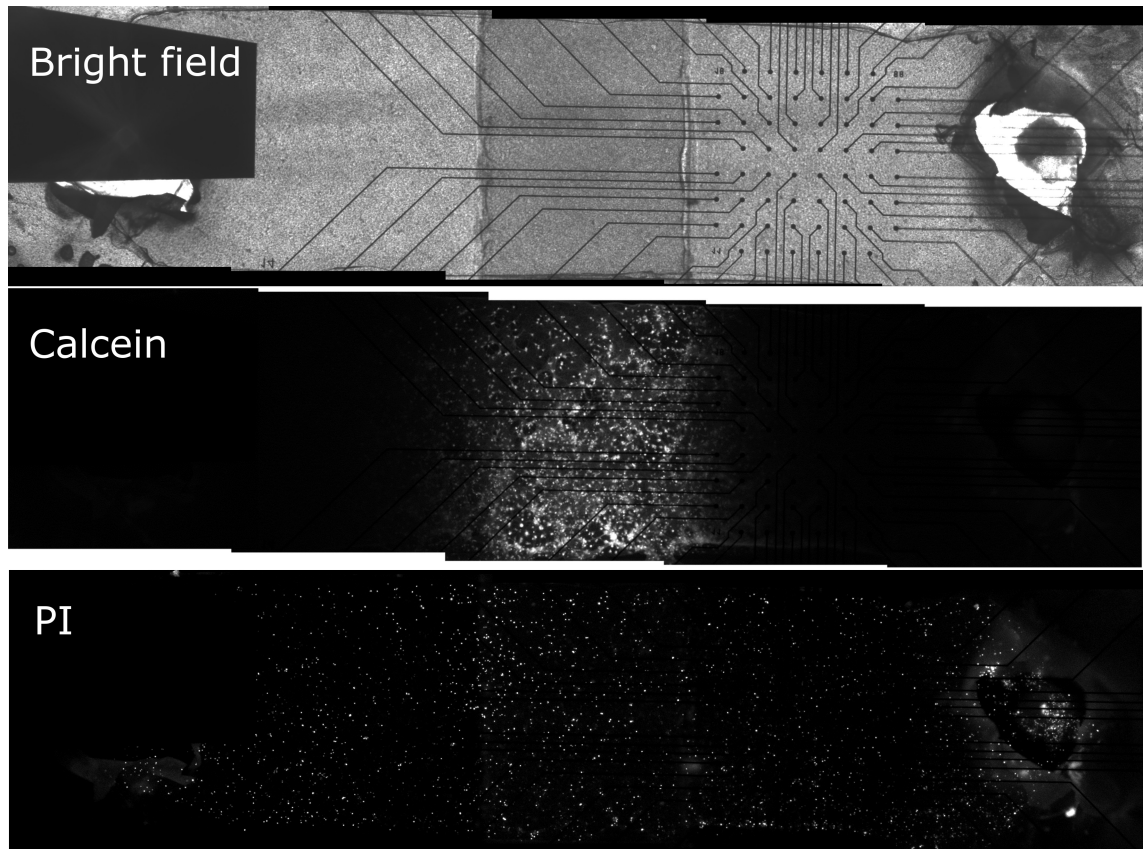


Figure 5.5: Dead live stained Neuronal culture in a semi-permeable membrane device. Polycarbonate membrane is not optically clear so cells are hard to distinguish in bright field image. The culture had been under flow with propidium iodide (dead cell stain, see sections 2.8 and 4.3.2) for 8 hours so the stain had diffused through the membrane opening to the extents of the culture channel. The live cell stain, Calcein-AM, had been introduced into the flow line only for the final 30 minutes of the flow session so that staining is present only immediately underneath the membrane opening. In this case the recording pads were not positioned directly under the membrane opening but rather shifted to one side.

similar time course to that of the non membrane devices.

We also include here the data from a single experiment where the MEA central area which contains the recording pads was not located directly underneath the membrane but was shifted to be entirely inside the non exposed area (figure 5.5). Since this was only a single experiment it cannot be included in a rigorous hypothesis testing analysis so it shown only in the long term plots for impression. This experiment did not include electrical stimulation. The recorded activity and the synchronicity in this case maintained a stable level for the full extent of the flow session. The level of synchronicity was markedly low compared to control but nevertheless stable. These data demonstrate that culture regions which are not placed directly underneath the membrane opening are able to maintain stable

electrophysiological function. This experiment provides a positive control for the type of coupling that the culture can have with a flow environment while still sustaining its activity.

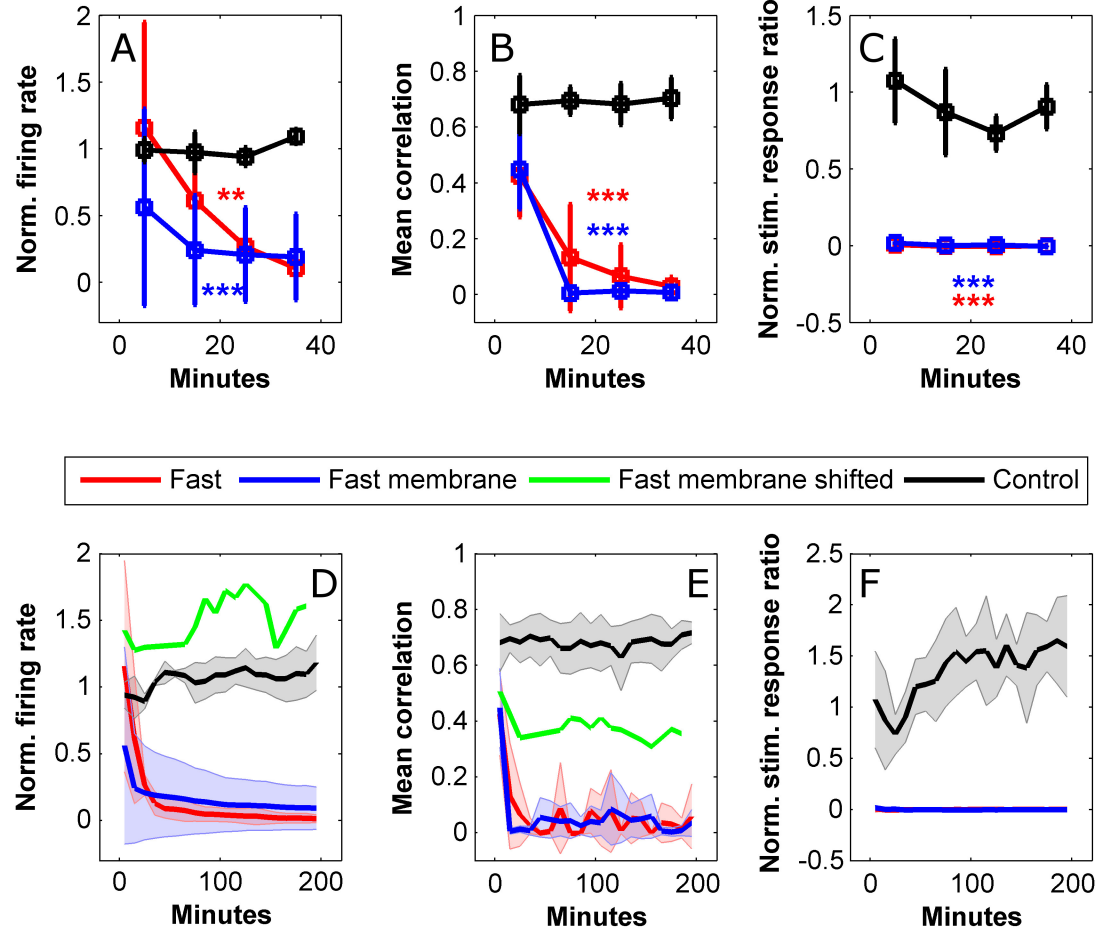


Figure 5.6: Introduction of a semi permeable to decouple the cells from the flow does improve the activity disruption under fast flow. Measures are as in figure 5.4 which also contains further information about the data presentation. Note the flow over the membrane (i.e., with $\approx 100\mu m$ distance imposed between the flow interface and the culture) generates exactly the same effect as direct flow. Data are based on $n=4, 3, 3, 1$ experiments for conditions of fast flow, fast flow with membrane, control and membrane with shifted recording, respectively.

5.3.3 Considerations of diffusive flux

The above showed that despite the presence of the membrane the disturbance to the network activity remained as it was before. At first glance, this is surprising because one would expect

that the decrease in convective flux due to the presence of the membrane would assist in both in diminishing the shear stress and in maintaining a stable chemical environment under the membrane. Thus it could be expected that regardless of the cause of the disturbance, shear stress or convective flux, the membrane should afford protection. However, this intuition does not take into account the diffusive flux which becomes dominant for short distances. Thus, in what follows, we compare the diffusive flux present in the case of the membrane experiments to the convective flux induced by the slow flow.

Considering a certain conditioning factor species which is produced by the culture and normally present at a concentration $C \frac{\text{moles}}{\mu\text{L}}$. Then in the case of direct flow through the channel this species would be carried away by the flow and removed at a flux:

$$J_{conv} = QC = 1 \times 10^{-3} C \frac{\text{moles}}{\text{s}},$$

where $Q = 1 \times 10^{-3} \frac{\mu\text{L}}{\text{s}}$ is the volumetric flow rate for the slow flow.

In the case of the membrane experiments, we assume that the aforementioned conditioning species is not present in the flow media so its concentration over the membrane is null. We further assume a linear concentration gradient for the species between the cells and the top of the membrane. Then, according to Fick's law the diffusive flux density between the membrane from the cells across the gap and through the membrane is:

$$j_{diff} = D \cdot \frac{C}{h} = 4 \times 10^{-3} C \frac{\text{moles}}{\text{s} \cdot \text{mm}^2},$$

where $D = 4 \times 10^{-4} \frac{\text{mm}^2}{\text{s}}$ is the diffusion coefficient for neurotransmitter sized molecules and $h = 0.1\text{mm}$ is the height of the cell compartments. To get the total flux through the membrane we multiply the flux density by the area of the membrane opening $A = 4\text{mm}^2$:

$$J_{diff} = j_{diff} \cdot A = 1.6 \times 10^{-2} C \frac{\text{moles}}{\text{s}}.$$

Thus the total diffusive flux of the considered conditioning species through the membrane is actually more than an order of magnitude **higher** than its convective flux during the slow flow experiments. It should be noted that the above calculations include only diffusive flux for the membrane scenario and therefore subliminally assume that the membrane is an ideal diffusive barrier. However, in the case of a real membrane (which is never ideal) the removal flux would be yet more extreme. Another heuristic which emerges from these calculations is that the diffusive flux is inversely proportional to the height of the cell compartment (i.e., the distance between the neurons and chemical sink). In order to equalize the factor removal flux to that of slow flow scenario the membrane needs to be located about $1 - 1.5\text{mm}$ away from the cells. This would explain why standard perfusion systems, which exchange media only from the top surface of the culture bath do not exhibit issues with the network activity as seen here. This heuristic fits well with the results from the experiment where the recorded portion of the culture was shifted relative to the membrane opening. In that experiment the recorded cells were positioned at distances between $400 - 2000\mu\text{m}$ from the membrane which

means they were only partially in the ‘safe’ region. Indeed the stable synchronized network activity in that experiment persisted but the effect of the flow was still evident through a decrease in synchronization level compared to the control.

The diffusive flux considerations discussed here give rise to an important heuristic: drug delivery through a diffusive barrier designed to introduce a certain agonist at a given rate would inevitably remove agonists of a similar size at the same rate unless they are also present in the delivery media. The results of the membrane experiments, therefore strongly suggest that the self media used for flow does not fully reflect the chemical environment in the internal volume of the devices, even though it was extracted from the same culture dish. In the next section we provide evidence that, in the case of older cultures, this discrepancy is reduced thus providing means to achieve stable activity under rapid flow.

5.4 Activity under flow for old cultures

In this section we describe a set of experiments measuring the activity of cultures aged 20-23 days *in vitro* placed under fast flow with various media formulations. Section 5.3.1 described how, when young cultures were placed under fast flow with self media, the network activity was immediately abolished. Remarkably, when an identical experiment was performed on old cultures, the synchronized network dynamics persisted under flow with little interruption, namely with the spontaneous activity proceeding in the form of synchronized bursts, with high values in the correlation matrix and with stable responses to stimulation (figure 5.7). Nevertheless, the initiation of flow was still evident in some subtle yet distinctive changes to the activity structure. Specifically, some of the channels exhibited tonic discharges in discord with the bursts. This can be seen directly in the raster plots (figure 5.7 A, right panel) and also in the correlation matrices which, despite generally maintaining their structure, contained some channels whose correlation values were reduced under flow (figure 5.7 C, compare middle and right panels). Additionally, the stimulation responses intensified and became somewhat longer (figure 5.7 B, right panel).

The stability of activity under flow was consistent over several old cultures from several platings as is shown in figure 5.8 which compares the 3 activity measures introduced in the previous section for young and old cultures under flow as well as for control (static) cultures of the same age groups. The firing rate and synchronicity measures for old cultures are indistinguishable from their controls (2-way ANOVA, $p = 0.084$ and 0.35 , respectively. P-values given are the minimum between the group and interaction effects). The reported lengthening of the stimulation response was manifested as a significant two-fold increase in the stimulation response ratio as compared to controls (2-way ANOVA, $p = 2.7 \times 10^{-5}$) but the response was stable throughout the observation period.

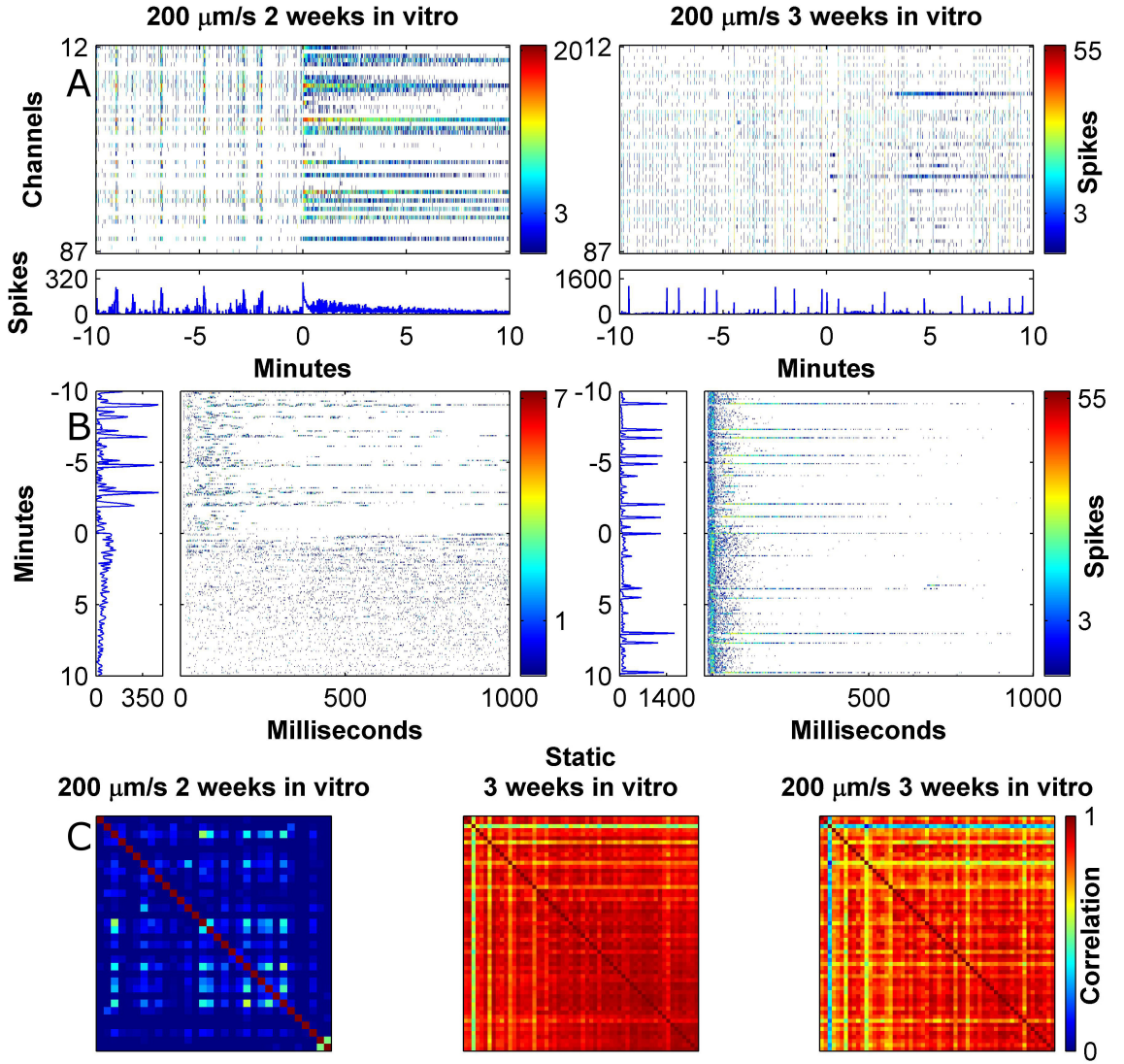


Figure 5.7: **Old cultures under fast flow maintain a stable network activity.** Data presented as in figure 5.3 only in this case two different cultures (young and old) are compared rather than flow rates on the same culture. In this case the activity and stimulation responses are maintained under fast flow with only small modulations. The correlation matrix for static conditions shows the data from the old culture before it was subjected to flow.

5.4.1 The effect of the media source

It is quite evident from figure 5.7 that young and old cultures are conspicuously different in their response to stimulation. In both cases the responses are bi-modal in strength, i.e., usually take the form of a short network reverberation of $\approx 200ms$ but occasionally produce a long response of a second or more. However, in the case of old cultures the short reverberations are stronger and more consistent as compared to young ones. As mentioned in section 3.2.1, although synapse density peaks at the end of the 2nd week *in vitro* [67], there is evidence that other synapse related processes such as pruning and changes to the GABA

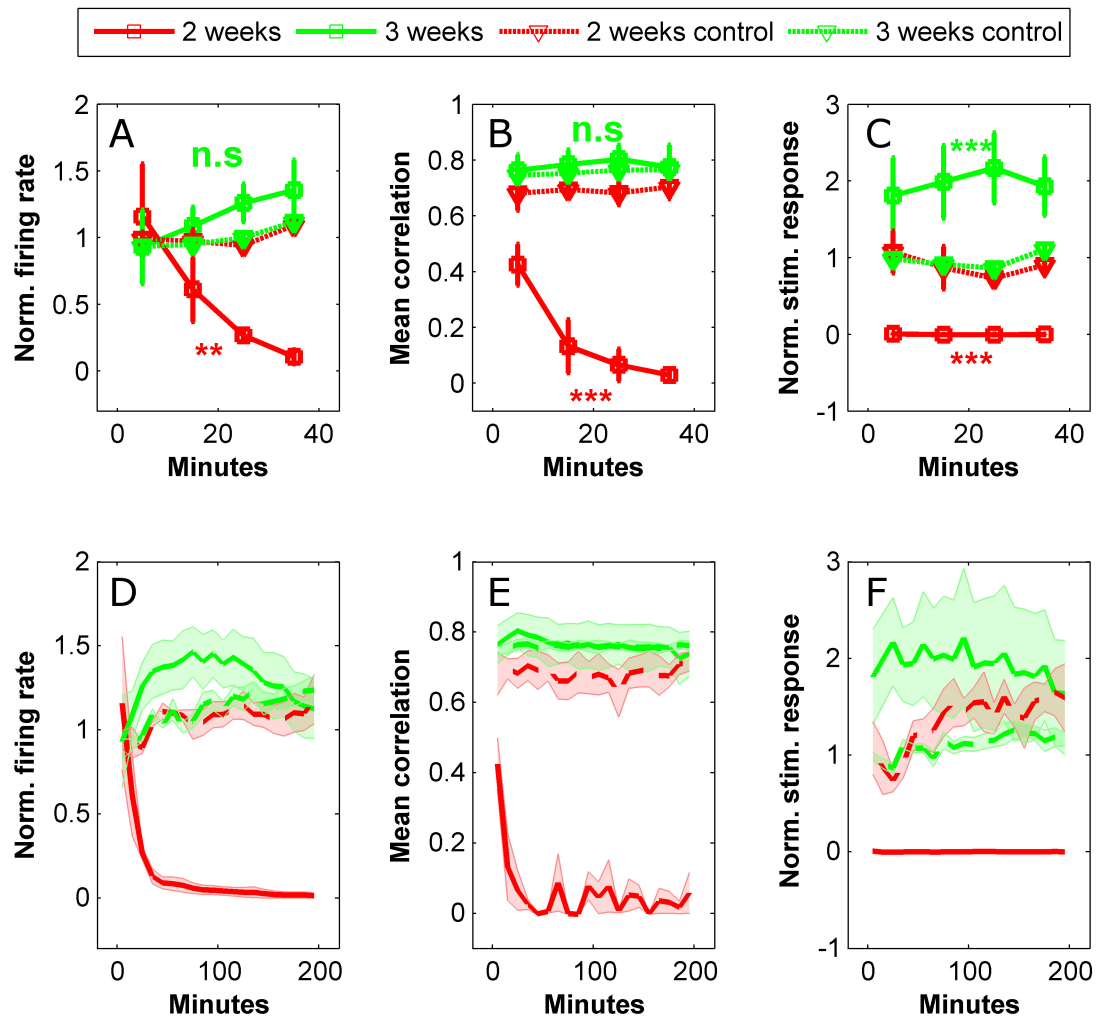


Figure 5.8: **Old cultures under fast flow maintain a stable network activity for and extended period of time.** Measures are as in figure 5.4 which also contains further information about the data presentation. Data are based on n=4, 4, 3, 5 experiments for conditions of fast flow young, fast flow old, young control and old control, respectively.

system still significantly affect the network dynamics at later stages (3rd and 4th weeks). The observed increase in the reliability of reverberative response to stimulation might be another manifestation of these later maturation processes although their exact nature is not completely understood. In the present context, it is possible that these age-related changes to the network structure render it more robust to environmental perturbations and therefore could explain why activity is maintained under flow with only minor perturbations. Another age related process which may have to do with the results is ECM formation. It is known that the ECM content in neuronal culture increases over the the 3rd and 4th weeks and that its presence facilitates synaptic function by preventing spill over [12]. It is possible

that increased ECM content in the old cultures serves as a protective barrier which allows them to sustain the network activity under flow. The results of the membrane experiments in section 5.3.2 suggested that the self media lacks important conditioning factors which consequently get removed by the flow causing the activity disruption. It is therefore possible that the developed ECM help to sustain a localized chemical environment by tethering important conditioning factors even if they are not present in the flow media. It is also possible that the more developed synapse formation renders the activity more stable and makes the culture insensitive to perturbation in the environment chemistry. We wanted to test if indeed old cultures are characterized by a reduced sensitivity to the culture media as this information could inform future flow applications. We therefore conducted two more sets of flow experiments. In the first one we used media from young cultures for flow. In the second one we used self media again but performed the experiments 1-3 days following a media change whereby 25% of the culture's media was replaced with fresh media (the previous self media experiments in section 5.4 were performed 6-9 days following a media change).

Figure 5.9 shows the results of flow with the two media types described above. Interestingly, flow with media taken from a young culture (blue curves) resulted in a dramatic disruption to the activity of a similar nature to the one observed in the young cultures, namely that all 3 measures rapidly crashed. However, there were also some obvious differences: Firstly, the total firing rate initially jumped 4-fold and despite dipping rapidly it stayed elevated compared to the control for the first 40 minutes (2-way ANOVA, $p = 5.0 \times 10^{-5}$). In fact, the firing rate decreased to a level lower than control only after about 100 minutes and was never abolished completely. Secondly, the correlation levels were significantly reduced as compared to control immediately with flow onset (2-way ANOVA, $p = 1.0 \times 10^{-12}$) but deteriorated more gradually compared to the young cultures (compare to figure 5.6) and were never completely abolished. Finally, the response to stimulation initially persisted (2-way ANOVA on the first 40 minutes did not reveal a significant difference from control, $p = 0.90$ for group effect and 0.28 for interaction effect). However, after 40 minutes the response was already significantly below control (unbalanced t-test on the final sample of panel C, $p = 0.0038$). This time course of loss of the response to stimulation was slower than in the young cultures where the stimulation response was abolished virtually immediately with the onset of flow.

Figure 5.9 also demonstrates that the mere action of changing the media can significantly affect the the culture's response to flow with this media (red curves). In a 40 minute window after flow initiation this was mainly evident in increase in firing rate as compared to control (2-way ANOVA, $p = 6.5 \times 10^{-6}$) whereas the synchronicity was reduced only with a 90% level of confidence (2-way ANOVA $p = 0.054$ for group effect). The stimulation response was significantly stronger than control ($p = 7.3 \times 10^{-4}$) but an increase with the same level of confidence was found for the original flow experiment with self media on old cultures. The

long term trends show a less stable behaviour under flow with recently changed media in all 3 measures. Nevertheless, the effects of the media change were quite subtle and these culture generally seemed to maintain basic network function under flow and considered useful for experimentation.

The results provided in this section show that, even in the old cultures, the formulation of the media used for flow is crucial for sustaining a stable network activity. Indeed, as we noted, the old cultures performed better as compared to the young ones but this improvement was marginal given the overall trend. Thus older cultures exhibit a strong sensitivity to the contents of the flow media despite their increased ECM contents and mature synaptic configuration.

5.4.2 How old conditioned media performs on young cultures

The results of the previous section suggest that media drawn from old cultures contains chemical species that enable stable network function under flow and that these species are absent in media from young cultures. This led us to ask whether these enabling features of old media are specifically linked to old cultures or are they more universal and would facilitate stable network function under flow for young cultures as well. To answer this question, we conducted a final set of experiments where media taken from old cultures was used for flow on young cultures. Figure 5.10 shows the results of these studies using the same measures used before. Interestingly, old media did in fact improve the performance of young cultures. These cultures generally did not exhibit the high rate tonic firing that characterized cultures under flow with young media (not shown) and indeed the firing rate in the first 40 minutes was not significantly different from control (2-way ANOVA, $p = 0.5$ for group effect). The mean correlation did dip significantly (2-way ANOVA, $p = 0.0016$) but was initially stable. The stimulation response was also stable but interestingly was significantly **lower** than the control (2-way ANOVA, $p = 0.0027$) rather than higher which was the case when the same media was used with old cultures. Nevertheless the longer term performance was unstable as most of the cultures gradually became silenced in the extended period of observation (figure 5.10 D-F). Additionally, it should be noted that these averaged measures are somewhat misleading as the individual measurements in this case were highly variable as could be understood from the thickness of the shaded areas in the extended period panels. Out of 5 cultures measured, 2 had their activity abolished and 3 lost their stimulation response almost immediately. On the other hand, the 2 other culture performed very well under flow. These results demonstrate that the beneficial effects which old conditioned media has on old culture are partially carried over to young cultures. Some of the cultures sustain a stable network activity but only for a short while and in highly variable fashion. These results are not surprising as one might expect that the flow media chemistry needs to match the specific identity and developmental stage of the observed culture.

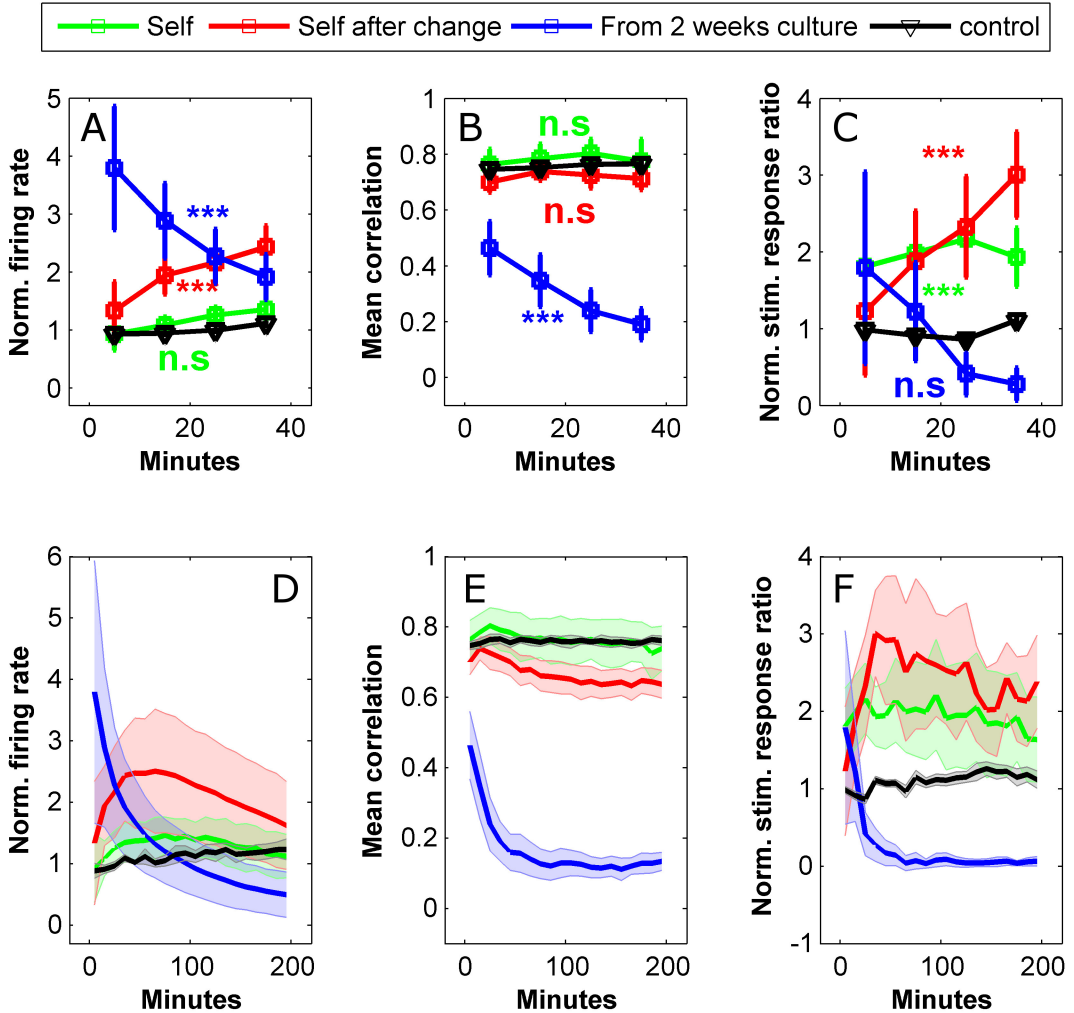


Figure 5.9: **The type of media used for flow strongly modulates the activity of the cultures and can cause the activity can crash.** Measures are as in figure 5.4 which also contains further information about the data presentation. Data are based on $n=4$, 4, 4, 5 experiments for self media, media from young cultures, changed media and control respectively.

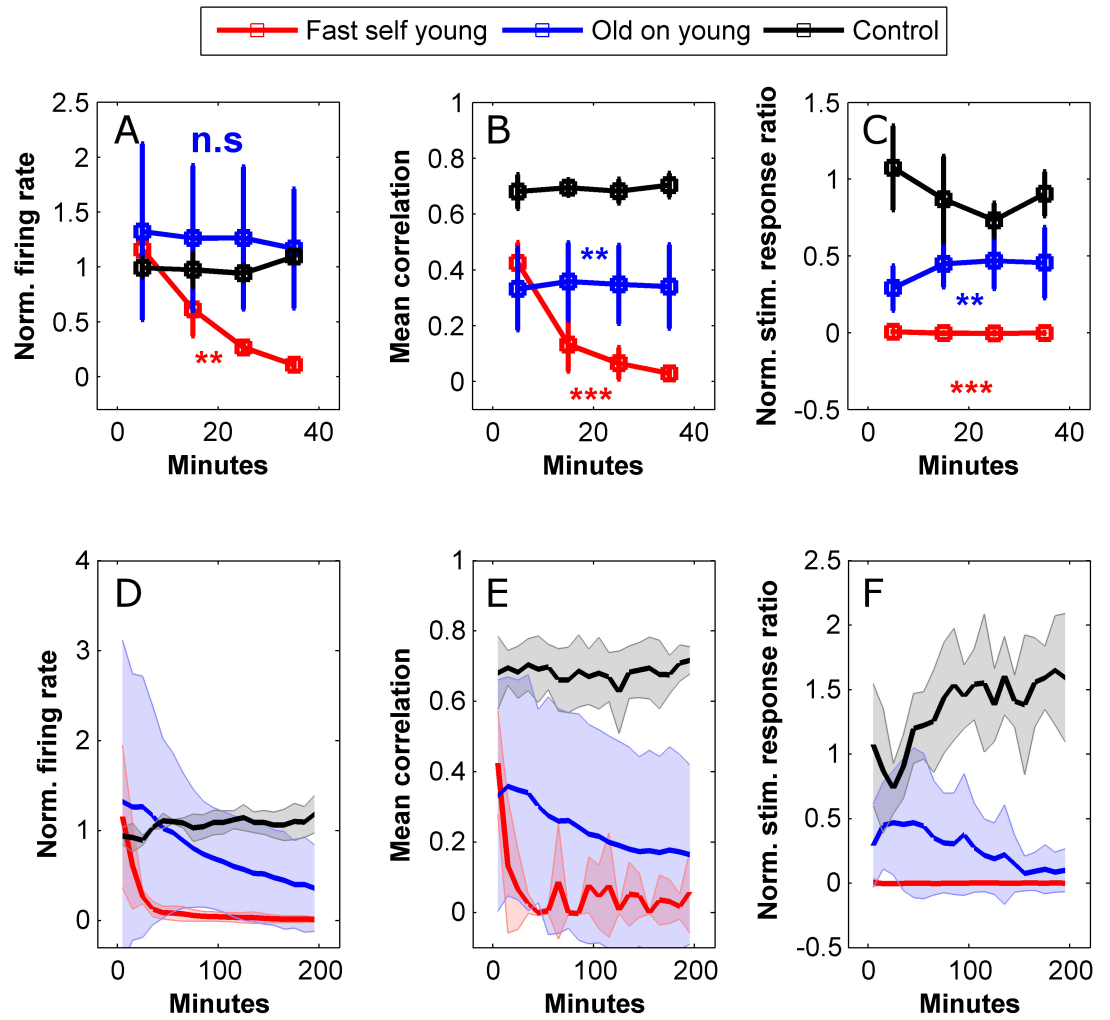


Figure 5.10: **Old media improves the performance of young cultures under flow**
 Measures are as in figure 5.4 which also contains further information about the data presentation. Data are based on $n=4, 5, 3$ experiments for self media, media from old cultures and control respectively.

5.5 Interpretation of the activity under flow results

In the previous chapter we have reported that conditioned media can sustain neuronal viability under flow. However, the nature of interaction between the media and culture and cause of the degeneration remained unclear. In this chapter, we extended the flow experiments to observe the network action potential activity under flow and gained valuable insight as to how flow bears on the culture tissue. Previous flow microfluidic work focused on the need of mitigating shear [45, 46] which neuronal tissue is exposed to and attributed the positive effects of the chemistry of the flow media on the viability to ‘shear protection’ by molecules secreted specifically for that purpose [65]. In this work we observed a strong disruption to the network activity under fast flow. Indeed this could be attributed to shear activating stretch receptors or simply tearing up the cellular membranes and eliciting an inflammatory response. However, using a semi-permeable membrane shown to reduce the shear to negligible levels [66] did not result in any improvement whatsoever. Furthermore, the membrane results were consistent with an assumption that a neuromodulator sized chemical species ($D = 400 \frac{\mu\text{m}^2}{\text{s}}$ [63]) is being diffusively removed through the membrane opening. Calculation based on this scenario predicted that cells located at a distance of $1 - 1.5\text{mm}$ from the diffusive sink would be ‘safe’ from the removal. Indeed the shifted recording experiment showed that a culture area partially located in the safe distance maintained its activity with only minor modulation. Had we performed the calculations with diffusive coefficients of ions ($D = 4000 \frac{\mu\text{m}^2}{\text{s}}$) or small proteins ($D = 40 \frac{\mu\text{m}^2}{\text{s}}$) then we would have expected either a disruption to occur over the entire culture area of the device or no disruption at all, respectively. However, these predictions are in disagreement with the results thus pointing specifically to neurotransmitter sized molecules as the culprits. Given the obvious importance of neurotransmitters to neuronal activity we argue that the immediate activity effects observed here are best explained by action of neurotransmitters on their respective receptor ion channels and that other explanations involving shear should be rejected on the basis of an Occam’s Razor reasoning. The results shown in this chapter do not rule out the possibility that shear contributes to other long term effects but they definitely demonstrate a that a disruption to neuronal signalling is a strong part of the effect of flow which needs to be taken into account.

In section 5.4 we showed that the activity in old cultures was maintained under fast flow with self media although these cultures were very sensitive to changes in the media chemistry (for example, their activity was disrupted in similar fashion to what was observed in young cultures, when media from such young cultures was used for flow). This result suggests that self media in old culture is chemically more matched with the micro-environment around the cells than in young cultures. Nevertheless, as the self media is in direct contact with the culture one would expect chemicals secreted by the cells to quickly diffuse to the bulk, especially in the case of small neurotransmitter molecules, so it may seem surprising that a strong gradient would develop between them. However, as mentioned in section 3.2.1,

the period of development occurring between the young (beginning of 3rd week) and old age (beginning of 4th week) time frames is characterized by fast changes to the neurotransmission systems. HPLC measurements of the glutamate and GABA contents of neuronal culture media show that the levels of both these major neurotransmitters rise over the first month *in vitro* and saturate only at around day 35 [15]. In particular, the GABA levels do not rise monotonically but remain low for the first 3 weeks and then jump sharply to reach the final saturated levels. This sharp rise in the media GABA content might correlate with the induction of the astrocytic GABA [68] or maturation of late interneurons [16]. Additionally, some reports claim that synaptogenesis in culture extends into the forth week which might also explain the increase in neurotransmitter production during the preceding period [69, 70]. Although the exact nature and timing of these maturation processes has not been completely clarified, there is ample evidence that the tonic neurotransmitter levels strongly depend on the culture age. In our devices, a large support culture comprising 250k cells is seeded on the outside (compared to 14k inside) and this external culture is probably the main source for diffusible factors in the bulk media. A possible explanation for the mismatch of the self media in young cultures could therefore be that the external support cultures were at a considerably different developmental stage as compared to the internal cultures and so the self media was not well matched to the latter. Indeed it has been shown that cultures grown in microfluidic devices develop faster than standard ones, possibly due to localized buildup of conditioning factors [71]. In the case of older devices, which are one week more developed, both the internal and external cultures may have entered a saturation in development so they were more similar. Another possible explanation for the self media mismatch is that during periods of accelerated development the rate of changes to the local neurotransmitter environment exceeds the rate of diffusion so that the bulk media is ‘lagging behind’ in accumulating the chemicals from the microenvironment. After all, even though neurotransmitters are small molecules they would take about 17 hours to diffuse through a media reservoir of height 10mm (note that the bulk media volume per sample was bigger in the cross flow devices to allow enough supply for the flow session).

The afore-mentioned delay in development of some GABAergic elements of the neurotransmission system raises the possibility that it is indeed GABA that is lacking in the flow media. Indeed it has been shown that the action of tonic extrasynaptic GABA exerts inhibition that is several times **stronger** than that of the fast synaptic one [72, 73] which could explain how drastic the effects of flow are. Some specific features in the response to flow provide further indication that an inhibitory transmitter is involved. Namely, when young media was used on old cultures the response was an immediate 4 fold increase in the spiking activity followed by a gradual decay, possibly due to depletion of resources. This could be interpreted as a release from strong inhibition. On the other hand, when old media was used on young cultures the stimulation response immediately decreased and the activity became silenced after a while. This could be explained by the young cultures being accus-

tomed to lower levels of tonic inhibitor compared to the old cultures and hence becoming silent when exposed to media from the latter. Indeed GABA is recognized as the major inhibitory neurotransmitter operating in the CNS and its extrasynaptic function has been receiving growing interest [73, 68, 74]. Nevertheless, the activity patterns observed under fast flow with young conditioned media are inconsistent with results from application of GABA antagonists [12, 75]. These studies did not report a decrease in synchronization but rather an increase in burst frequency and burst length so removal of GABA alone is probably not enough to explain the observed disturbance. Intrinsic volume transmission comprises an assortment of other signals including the major excitatory neurotransmitter glutamate [76] as well as ATP, NO and various neuropeptides [77, 78]. Thus the observed disturbance cannot be attributed to any specific species and is more likely a holistic effect associated with perturbations to all the intrinsic volume transmission processes at varying degrees. We believe that our results warrant an in depth investigation into the source of the disruption as it could entail a novel signalling species. Such an investigation could proceed by applying a cocktail of receptor blockers matching the known volume transmission signals to see if the effects of flow may be induced in this manner.

Even when the media is matched the flow could still affect more than just the extrasynaptic tonic concentrations of signalling molecules. This is explained next. The accepted paradigm is that neurotransmission proceeds in two distinct compartments, intra- and extrasynaptic. The most recognized neurotransmission action is the fast synaptic one where vesicle release on the presynaptic side causes an extremely rapid (time constant $< 1ms$) phasic increase in the neurotransmitter content in the synaptic cleft. The time course of these phasic signals is mainly determined by outwards diffusion to the extrasynaptic space [79]. Although the phasic dynamics are the hallmark of synaptic function it has also been established that there is an appreciable tonic concentration of neurotransmitters in the synaptic cleft which is enough for a continuous activation of postsynaptic receptors [80]. The source of this tonic transmitter level is most probably simply diffusion from the extrasynaptic space. In contrast to the intrasynaptic compartment where only neurotransmitters are known to operate, the extrasynaptic compartment contains a mixture of neurotransmitters and neuromodulators operating through both ionotropic and metabotropic receptors. In recent years, more focus has been given to the extrasynaptic species which were shown to have a strong effect on network dynamics and therefore a computational importance [81, 82, 83, 84, 76]. Such extrasynaptic neurotransmitters and neuromodulators are usually referred to as the 'tonic environment'. However, this terminology could be misleading by giving the impression that this environment is completely static whereas in fact it is temporally varying (i.e., it has phasic aspects) or else it would not be able to modulate the network activity. Since this intrinsic volume transmission is based on discrete secretion events from specific cells it stands to reason that it will have a spatial organization as well (this was shown for the case of adenosine in [81]). Thus, to summarize,

both intra- and extra-synaptic compartments contain signals with tonic and phasic components and they are not completely segregated but rather coupled via diffusion (e.g., synaptic spill over contributes to the phasic extrasynaptic signals and changes to extrasynaptic concentrations of non-synaptic origins can influence the tonic activation of the synapses).

Out of the signalling modes mentioned above, The phasic synaptic one the least likely to be affected by the flow because the neurotransmitter pulses are extremely quick and the concentrations are dependent on release from vesicles which are located intracellularly. Nevertheless there is a concern that if rapid convective flow is channeled through the synaptic cleft then it could wash away the neurotransmitter molecules as they are released and therefore to significantly modify the temporal profile of activation. To check if this could indeed be of concern we compared the diffusive flux out of a synapse with the expected convective flux due to flow assuming that the synapse is indeed open and that the flow is directed perpendicularly to the transmission line as depicted in figure 5.11. The calculations are as follows: assuming a parabolic flow profile (using the laminar flow between parallel plates approximation because channel height \ll channel width [85]) the flow velocity around the synapses is

$$u = u_{avg} \left(1 - \frac{y^2}{h^2}\right) \approx 15 \frac{\mu m}{s}$$

where $u_{avg} = 200 \frac{\mu m}{s}$ is the average flow velocity, $h = 50 \mu m$ is half the channel height and $y = 48 \mu m$ is the location of the synapses relative to the horizontal center of the channel, i.e., $2 \mu m$ from the surface. The diffusive flux out of the synapse is

$$J_{diff} = D \frac{c - b}{d} (4A) \approx 32(c - b) \frac{moles}{s}$$

where $D = 400 \frac{\mu m^2}{s}$ is the diffusion coefficient for a neurotransmitter sized molecule in free media, c and b are the intra- and extra-synaptic neurotransmitter concentrations, respectively in $\frac{moles}{\mu m^3}$, $d = 0.2 \mu m$ is the diffusion distance and $A = 0.2 \times 0.02 = 0.004 \mu m^2$ is the area of one external face of the synaptic cleft (taking the cleft gap to be $0.02 \mu m$ and cleft width to be $0.2 \mu m$) ($4A$ is then the entire face area available for diffusion). The total convective flux is

$$J_{conv} = J_{flowout} - J_{flowin} = Auc - Aub = Au(c - b) = 0.06(c - b) \frac{moles}{s}.$$

Thus, somewhat unintuitively and owing to its nano-scale dimensions, the outwards flux out of the cleft due to diffusion (which is the main determinant of the temporal concentration

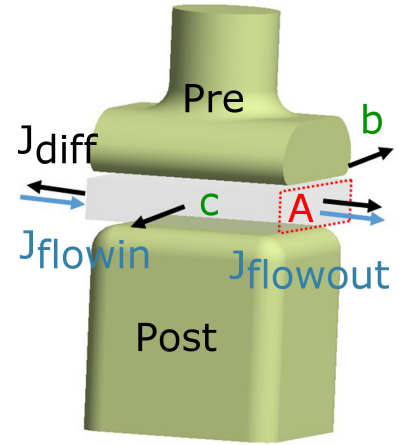


Figure 5.11: Illustration of the synaptic cleft geometry and symbols used to compare the convective and diffusive flux in the case where the flow runs directly through the synapse.

profile during synaptic activation [79]) is 3 orders of magnitude larger than the that due to convection even if the cleft is completely open to the flow. In reality, the synapses are usually enveloped in neuronal and astrocytic membranes which are unlikely to allow any degree of flow through. Thus we would expect phasic synaptic dynamics to be maintained even under much faster flow rates or shallow device geometries (i.e., where the flow velocity at the boundaries would be higher). However, the same cannot be said about the phasic extrasynaptic signalling which is much slower and operates over much larger space scales and about tonic synaptic concentrations. Thus, fast flow, beyond the obvious effect of changing the basal extrasynaptic species concentrations, could have generated the observed disruptions by indirectly changing the tonic receptor activation within the synapses and also by disturbing the phasic (and spatially organized) aspects of the intrinsic volume transmission.

Despite recent research into the diversity of volume transmission mechanisms, the fundamental paradigm is still that the functional identity of the network is stored in its synaptic connections and that extrasynaptic processes play only a supporting role. Given this view it is surprising that the effects of flow, when the media was not matched, were so profound and seemed to drive the network outside its functional regime (inability to maintain any level of activity and abolishment of the stimulation response). Thus these results serve as a reminder of the importance of intrinsic volume transmission processes and promote the view that the fast synaptic currents in fact only modulate the neuronal activity on top of a much stronger signal that is carried by the former. In these cases the functional properties of the circuit were not restored even after a few hours under flow. This demonstrates that the neurons lack other homeostatic mechanisms (e.g., intrinsic or synaptic) that can operate within hours to restore the activity. An accepted paradigm in contemporary neuroscience is that neuronal activity is governed by a balance between excitation and inhibition. These results raise the possibility that this balance is strongly dependent on volume transmission processes rather than on synaptic ones. On the other hand, we have argued that the experiments with old cultures and self media represent a scenario where the extracellular concentrations were roughly maintained because the flow media was matched to the local microenvironment. In this case, it likely that the fast flow, which was in direct contact with the culture, perturbed the fine spatial details of the volume transmission signalling and, to a certain extent, forced it to be truly tonic, i.e. temporally constant without an ability to respond in feedback from the neuronal activity. In this scenario, the fundamental functional identity of the circuit was maintained in the sense that the activity measures that we used as well as the structure of the correlation matrix were roughly maintained (figures 5.8 and 5.7). This supports the original view that intrinsic volume transmission only holds a supporting role with regards to network function. Nevertheless, these latter experiments still exhibited a doubling in the intensity of the network stimulation response and an increase in its length. This could point to an interruption in feedback mechanisms operating through phasic volume transmission to control neuronal excitation. Such mechanisms were observed for GABA [86], adenosine

[81] and ATP [87]. This could suggest that indeed some of the network activity stabilization mechanisms which operate via phasic volume transmission have been compromised by the flow.

5.6 Chapter conclusion

We have argued that the fast microfluidic flow operates as a 'concentration clamp' because it delivers chemical species faster than the culture can uptake or metabolize. This claim has not been fully tested here and doing so might require use of biosensors to directly measure some of the extrasynaptic species. Nevertheless, if this is indeed the case, we propose that, apart from the obvious rapid agonist delivery application, rapid microfluidic flow offers a novel way of holding extrasynaptic concentrations of signalling molecules at set levels. Since neuroactive chemical like neurotransmitters and neuromodulators are directly controlled by the tissue, applying them to the bath is ineffective so the study of their function is classically performed via pharmacology to block the associated receptors. However, this approach ignores potential indirect effects of the presence of these agonists, e.g., elevated extrasynaptic glutamate may operate both through extrasynaptic metabotropic receptors as well as through tonic activation of excitatory synapses. Thus it would be beneficial to be able to control the extracellular concentration of the chemicals to check for remaining effects beyond the obvious receptor blockade. Indeed direct control over extracellular concentration is made possible through enzymatic degradation or chelating agents (e.g., [88]) but that approach is less accurate and depends on availability of specific pharmacology. Thus the so called concentration clamp offers a method of holding an entire tissue at a specific concentration. Additionally, by applying the rapid agonist delivery approach, one could artificially generate volume transmission pulses of specific agonists while keeping others at a constant level. This would require adaptation of the microfluidic geometry and application paradigm to the required time scales but offers a novel way of studying intrinsic volume transmission processes in neural tissue.

Finally, The control experiments presented in this chapter and in section 4.3.2 suggested that the imposed 'concentration clamp' is the main culprit in the observed effects of flow, both in terms of activity as well as viability. Because of the strong action of diffusion at short distances the only way to restore volume transmission processes that are perturbed by the flow is to increase the distance to the flow interface. This may have implications on the level of functionality and viability that may be achieved while preserving the time scales of the drug delivery.

Nevertheless, we have identified conditions where the network activity is adequately maintained under fast flow. The flow protocol described in this chapter will be the basis for the final phasic neuromodulatory signalling system described in the next (and final) chapter.

Bibliography

- [1] N. Caporale and Y. Dan, “Spike timing-dependent plasticity: a hebbian learning rule,” *Annu. Rev. Neurosci.*, vol. 31, pp. 25–46, 2008.
- [2] G.-q. Bi and M.-m. Poo, “Synaptic modifications in cultured hippocampal neurons: dependence on spike timing, synaptic strength, and postsynaptic cell type,” *The Journal of neuroscience*, vol. 18, no. 24, pp. 10464–10472, 1998.
- [3] J.-C. Zhang, P.-M. Lau, and G.-Q. Bi, “Gain in sensitivity and loss in temporal contrast of stdp by dopaminergic modulation at hippocampal synapses,” *Proceedings of the National Academy of Sciences*, vol. 106, no. 31, pp. 13028–13033, 2009.
- [4] D. Eytan, A. Minerbi, N. Ziv, and S. Marom, “Dopamine-induced dispersion of correlations between action potentials in networks of cortical neurons,” *Journal of neurophysiology*, vol. 92, no. 3, pp. 1817–1824, 2004.
- [5] N. Herzog, M. Shein-Idelson, and Y. Hanein, “Optical validation of in vitro extracellular neuronal recordings,” *Journal of neural engineering*, vol. 8, no. 5, p. 056008, 2011.
- [6] I. Breskin, J. Soriano, E. Moses, and T. Tlusty, “Percolation in living neural networks,” *Physical review letters*, vol. 97, no. 18, p. 188102, 2006.
- [7] J. van Pelt, P. S. Wolters, M. A. Corner, W. L. Rutten, and G. J. Ramakers, “Long-term characterization of firing dynamics of spontaneous bursts in cultured neural networks,” *IEEE Transactions on Biomedical Engineering*, vol. 51, no. 11, pp. 2051–2062, 2004.
- [8] D. A. Wagenaar, J. Pine, and S. M. Potter, “An extremely rich repertoire of bursting patterns during the development of cortical cultures,” *BMC neuroscience*, vol. 7, no. 1, p. 1, 2006.
- [9] M. Chiappalone, M. Bove, A. Vato, M. Tedesco, and S. Martinoia, “Dissociated cortical networks show spontaneously correlated activity patterns during in vitro development,” *Brain research*, vol. 1093, no. 1, pp. 41–53, 2006.
- [10] M. A. Corner, J. van Pelt, P. Wolters, R. Baker, and R. Nuytinck, “Physiological effects of sustained blockade of excitatory synaptic transmission on spontaneously active

- developing neuronal networks an inquiry into the reciprocal linkage between intrinsic biorhythms and neuroplasticity in early ontogeny,” *Neuroscience & Biobehavioral Reviews*, vol. 26, no. 2, pp. 127–185, 2002.
- [11] Y. Penn, M. Segal, and E. Moses, “Network synchronization in hippocampal neurons,” *Proceedings of the National Academy of Sciences*, vol. 113, no. 12, pp. 3341–3346, 2016.
- [12] A. Bikbaev, R. Frischknecht, and M. Heine, “Brain extracellular matrix retains connectivity in neuronal networks,” *Scientific reports*, vol. 5, 2015.
- [13] M. Chiappalone, A. Novellino, I. Vajda, A. Vato, S. Martinoia, and J. van Pelt, “Burst detection algorithms for the analysis of spatio-temporal patterns in cortical networks of neurons,” *Neurocomputing*, vol. 65, pp. 653–662, 2005.
- [14] J. Van Pelt, M. Corner, P. Wolters, W. Rutten, and G. Ramakers, “Longterm stability and developmental changes in spontaneous network burst firing patterns in dissociated rat cerebral cortex cell cultures on multielectrode arrays,” *Neuroscience letters*, vol. 361, no. 1, pp. 86–89, 2004.
- [15] G. Ramakers, H. Van Galen, M. Feenstra, M. Corner, and G. Boer, “Activity-dependent plasticity of inhibitory and excitatory amino acid transmitter systems in cultured rat cerebral cortex,” *International Journal of Developmental Neuroscience*, vol. 12, no. 7, pp. 611–621, 1994.
- [16] T. K. Hensch, “Critical period plasticity in local cortical circuits,” *Nature Reviews Neuroscience*, vol. 6, no. 11, pp. 877–888, 2005.
- [17] S. Marom and G. Shahaf, “Development, learning and memory in large random networks of cortical neurons: lessons beyond anatomy,” *Quarterly reviews of biophysics*, vol. 35, no. 01, pp. 63–87, 2002.
- [18] D. A. Wagenaar, J. Pine, and S. M. Potter, “Effective parameters for stimulation of dissociated cultures using multi-electrode arrays,” *Journal of neuroscience methods*, vol. 138, no. 1, pp. 27–37, 2004.
- [19] A. Gal and S. Marom, “Entrainment of the intrinsic dynamics of single isolated neurons by natural-like input,” *The Journal of neuroscience*, vol. 33, no. 18, pp. 7912–7918, 2013.
- [20] D. Eytan, N. Brenner, and S. Marom, “Selective adaptation in networks of cortical neurons,” *The Journal of neuroscience*, vol. 23, no. 28, pp. 9349–9356, 2003.
- [21] O. Weihberger, S. Okujeni, J. E. Mikkonen, and U. Egert, “Quantitative examination of stimulus-response relations in cortical networks in vitro,” *Journal of neurophysiology*, vol. 109, no. 7, pp. 1764–1774, 2013.

- [22] P. L. Baljon, M. Chiappalone, and S. Martinoia, “Interaction of electrically evoked responses in networks of dissociated cortical neurons,” *Physical Review E*, vol. 80, no. 3, p. 031906, 2009.
- [23] S. Marom, R. Meir, E. Braun, A. Gal, E. Kermany, and D. Eytan, “On the precarious path of reverse neuro-engineering,” *Frontiers in computational neuroscience*, vol. 3, p. 5, 2009.
- [24] L. Cozzi, P. DAngelo, and V. Sanguineti, “Encoding of time-varying stimuli in populations of cultured neurons,” *Biological cybernetics*, vol. 94, no. 5, pp. 335–349, 2006.
- [25] D. A. Wagenaar, R. Madhavan, J. Pine, and S. M. Potter, “Controlling bursting in cortical cultures with closed-loop multi-electrode stimulation,” *The Journal of neuroscience*, vol. 25, no. 3, pp. 680–688, 2005.
- [26] Z. F. Mainen and T. J. Sejnowski, “Reliability of spike timing in neocortical neurons,” *Science*, vol. 268, no. 5216, p. 1503, 1995.
- [27] D. A. Wagenaar, J. Pine, and S. M. Potter, “Searching for plasticity in dissociated cortical cultures on multi-electrode arrays,” *Journal of negative results in biomedicine*, vol. 5, no. 1, p. 1, 2006.
- [28] E. Kermany, A. Gal, V. Lyakhov, R. Meir, S. Marom, and D. Eytan, “Tradeoffs and constraints on neural representation in networks of cortical neurons,” *The Journal of Neuroscience*, vol. 30, no. 28, pp. 9588–9596, 2010.
- [29] T. V. Bliss and T. Lømo, “Long-lasting potentiation of synaptic transmission in the dentate area of the anaesthetized rabbit following stimulation of the perforant path,” *The Journal of physiology*, vol. 232, no. 2, pp. 331–356, 1973.
- [30] M. Chiappalone, P. Massobrio, and S. Martinoia, “Network plasticity in cortical assemblies,” *European Journal of Neuroscience*, vol. 28, no. 1, pp. 221–237, 2008.
- [31] F. Hamilton, R. Graham, L. Luu, and N. Peixoto, “Time-dependent increase in network response to stimulation,” *PloS one*, vol. 10, no. 11, p. e0142399, 2015.
- [32] M. E. Ruaro, P. Bonifazi, and V. Torre, “Toward the neurocomputer: image processing and pattern recognition with neuronal cultures,” *IEEE Transactions on Biomedical Engineering*, vol. 52, no. 3, pp. 371–383, 2005.
- [33] Y. Jimbo, T. Tateno, and H. Robinson, “Simultaneous induction of pathway-specific potentiation and depression in networks of cortical neurons,” *Biophysical Journal*, vol. 76, no. 2, pp. 670–678, 1999.
- [34] J. le Feber, T. Witteveen, T. M. van Veenendaal, and J. Dijkstra, “Repeated stimulation of cultured networks of rat cortical neurons induces parallel memory traces,” *Learning & memory*, vol. 22, no. 12, pp. 594–603, 2015.

- [35] R. Madhavan, Z. C. Chao, and S. M. Potter, “Plasticity of recurring spatiotemporal activity patterns in cortical networks,” *Physical biology*, vol. 4, no. 3, p. 181, 2007.
- [36] G. G. Turrigiano, “Homeostatic plasticity in neuronal networks: the more things change, the more they stay the same,” *Trends in neurosciences*, vol. 22, no. 5, pp. 221–227, 1999.
- [37] I. Vajda, J. Van Pelt, P. Wolters, M. Chiappalone, S. Martinoia, E. Van Someren, and A. Van Ooyen, “Low-frequency stimulation induces stable transitions in stereotypical activity in cortical networks,” *Biophysical Journal*, vol. 94, no. 12, pp. 5028–5039, 2008.
- [38] D. J. Bakkum, Z. C. Chao, and S. M. Potter, “Spatio-temporal electrical stimuli shape behavior of an embodied cortical network in a goal-directed learning task,” *Journal of neural engineering*, vol. 5, no. 3, p. 310, 2008.
- [39] G. Shahaf and S. Marom, “Learning in networks of cortical neurons,” *The Journal of Neuroscience*, vol. 21, no. 22, pp. 8782–8788, 2001.
- [40] J. le Feber, J. Stegenga, and W. Rutten, “Slow electrical stimuli affect connectivity in cultured neuronal networks,” in *2009 4th International IEEE/EMBS Conference on Neural Engineering*, pp. 546–549, IEEE, 2009.
- [41] S. Otani, O. Blond, J.-M. Desce, and F. Crepel, “Dopamine facilitates long-term depression of glutamatergic transmission in rat prefrontal cortex,” *Neuroscience*, vol. 85, no. 3, pp. 669–676, 1998.
- [42] Q. Gu, “Neuromodulatory transmitter systems in the cortex and their role in cortical plasticity,” *Neuroscience*, vol. 111, no. 4, pp. 815–835, 2002.
- [43] C. Gonzalez-Islas and J. J. Hablitz, “Dopamine inhibition of evoked ipscs in rat prefrontal cortex,” *Journal of Neurophysiology*, vol. 86, no. 6, pp. 2911–2918, 2001.
- [44] E. Biffi, F. Piraino, A. Pedrocchi, G. B. Fiore, G. Ferrigno, A. Redaelli, A. Menegon, and M. Rasponi, “A microfluidic platform for controlled biochemical stimulation of twin neuronal networks,” *Biomicrofluidics*, vol. 6, no. 2, p. 024106, 2012.
- [45] M. Morel, V. Shynkar, J.-C. Galas, I. Dupin, C. Bouzigues, V. Studer, and M. Dahan, “Amplification and temporal filtering during gradient sensing by nerve growth cones probed with a microfluidic assay,” *Biophysical journal*, vol. 103, no. 8, pp. 1648–1656, 2012.
- [46] C. J. Wang, X. Li, B. Lin, S. Shim, G.-l. Ming, and A. Levchenko, “A microfluidics-based turning assay reveals complex growth cone responses to integrated gradients of substrate-bound ecm molecules and diffusible guidance cues,” *Lab on a Chip*, vol. 8, no. 2, pp. 227–237, 2008.

- [47] T. M. Pearce, J. A. Wilson, S. G. Oakes, S.-Y. Chiu, and J. C. Williams, “Integrated microelectrode array and microfluidics for temperature clamp of sensory neurons in culture,” *Lab on a Chip*, vol. 5, no. 1, pp. 97–101, 2005.
- [48] Y. J. Choi, S. Chae, J. H. Kim, K. F. Barald, J. Y. Park, and S.-H. Lee, “Neurotoxic amyloid beta oligomeric assemblies recreated in microfluidic platform with interstitial level of slow flow,” *Scientific reports*, vol. 3, 2013.
- [49] L. J. Millet, M. E. Stewart, J. V. Sweedler, R. G. Nuzzo, and M. U. Gillette, “Microfluidic devices for culturing primary mammalian neurons at low densities,” *Lab on a Chip*, vol. 7, no. 8, pp. 987–994, 2007.
- [50] J. Park, B. K. Lee, G. S. Jeong, J. K. Hyun, C. J. Lee, and S.-H. Lee, “Three-dimensional brain-on-a-chip with an interstitial level of flow and its application as an in vitro model of alzheimer’s disease,” *Lab on a Chip*, vol. 15, no. 1, pp. 141–150, 2015.
- [51] J. Kumamoto, H. Kitahata, M. Goto, M. Nagayama, and M. Denda, “Effects of medium flow on axon growth with or without nerve growth factor,” *Biochemical and biophysical research communications*, vol. 465, no. 1, pp. 26–29, 2015.
- [52] G. W. Arbuthnott and J. Wickens, “Space, time and dopamine,” *Trends in neurosciences*, vol. 30, no. 2, pp. 62–69, 2007.
- [53] B. J. Venton, H. Zhang, P. A. Garris, P. E. Phillips, D. Sulzer, and R. M. Wightman, “Real-time decoding of dopamine concentration changes in the caudate–putamen during tonic and phasic firing,” *Journal of neurochemistry*, vol. 87, no. 5, pp. 1284–1295, 2003.
- [54] G. Brewer, J. Torricelli, E. Evege, and P. Price, “Optimized survival of hippocampal neurons in b27-supplemented neurobasal, a new serum-free medium combination,” *Journal of neuroscience research*, vol. 35, no. 5, pp. 567–576, 1993.
- [55] H. Romijn, F. Van Huizen, and P. Wolters, “Towards an improved serum-free, chemically defined medium for long-term culturing of cerebral cortex tissue,” *Neuroscience & Biobehavioral Reviews*, vol. 8, no. 3, pp. 301–334, 1984.
- [56] J. Ray, D. A. Peterson, M. Schinstine, and F. H. Gage, “Proliferation, differentiation, and long-term culture of primary hippocampal neurons,” *Proceedings of the National Academy of Sciences*, vol. 90, no. 8, pp. 3602–3606, 1993.
- [57] J. W. Park, B. Vahidi, A. M. Taylor, S. W. Rhee, and N. L. Jeon, “Microfluidic culture platform for neuroscience research,” *Nature protocols*, vol. 1, no. 4, pp. 2128–2136, 2006.
- [58] J. W. Park, H. J. Kim, M. W. Kang, and N. L. Jeon, “Advances in microfluidics-based experimental methods for neuroscience research,” *Lab on a Chip*, vol. 13, no. 4, pp. 509–521, 2013.

- [59] P. G. Gross, E. P. Kartalov, A. Scherer, and L. P. Weiner, “Applications of microfluidics for neuronal studies,” *Journal of the neurological sciences*, vol. 252, no. 2, pp. 135–143, 2007.
- [60] S. Kaech and G. Bunker, “Culturing hippocampal neurons,” *Nature protocols*, vol. 1, no. 5, pp. 2406–2415, 2006.
- [61] B. Samel, M. K. Chowdhury, and G. Stemme, “The fabrication of microfluidic structures by means of full-wafer adhesive bonding using a poly (dimethylsiloxane) catalyst,” *Journal of Micromechanics and Microengineering*, vol. 17, no. 8, p. 1710, 2007.
- [62] P. Nath, D. Fung, Y. A. Kunde, A. Zeytun, B. Branch, and G. Goddard, “Rapid prototyping of robust and versatile microfluidic components using adhesive transfer tapes,” *Lab on a Chip*, vol. 10, no. 17, pp. 2286–2291, 2010.
- [63] A. Johnstone, *Microfluidic systems for neuronal cell culture*. PhD thesis, The University of Nottingham, 2015.
- [64] G. A. Bunker, “Trophic interactions between astroglial cells and hippocampal neurons in culture,” *Science*, vol. 209, no. 4458, pp. 809–810, 1980.
- [65] M. Liu, W. Song, P. Li, Y. Huang, X. Gong, G. Zhou, X. Jia, L. Zheng, and Y. Fan, “Galanin protects against nerve injury after shear stress in primary cultured rat cortical neurons,” *PloS one*, vol. 8, no. 5, p. e63473, 2013.
- [66] M. Morel, J.-C. Galas, M. Dahan, and V. Studer, “Concentration landscape generators for shear free dynamic chemical stimulation,” *Lab on a Chip*, vol. 12, no. 7, pp. 1340–1346, 2012.
- [67] Z. Li and M. Sheng, “Some assembly required: the development of neuronal synapses,” *Nature reviews Molecular cell biology*, vol. 4, no. 11, pp. 833–841, 2003.
- [68] S. Lee, B.-E. Yoon, K. Berglund, S.-J. Oh, H. Park, H.-S. Shin, G. J. Augustine, and C. J. Lee, “Channel-mediated tonic gaba release from glia,” *Science*, vol. 330, no. 6005, pp. 790–796, 2010.
- [69] G. Brewer, M. Boehler, R. Pearson, A. DeMaris, A. Ide, and B. Wheeler, “Neuron network activity scales exponentially with synapse density,” *Journal of neural engineering*, vol. 6, no. 1, p. 014001, 2008.
- [70] A. Grabrucker, B. Vaida, J. Bockmann, and T. M. Boeckers, “Synaptogenesis of hippocampal neurons in primary cell culture,” *Cell and tissue research*, vol. 338, no. 3, pp. 333–341, 2009.
- [71] G. Goyal and Y. Nam, “Neuronal micro-culture engineering by microchannel devices of cellular scale dimensions,” *Biomedical Engineering Letters*, vol. 1, no. 2, pp. 89–98, 2011.

- [72] M. Farrant and Z. Nusser, “Variations on an inhibitory theme: phasic and tonic activation of gabaa receptors,” *Nature Reviews Neuroscience*, vol. 6, no. 3, pp. 215–229, 2005.
- [73] I. Mody and R. A. Pearce, “Diversity of inhibitory neurotransmission through gaba a receptors,” *Trends in neurosciences*, vol. 27, no. 9, pp. 569–575, 2004.
- [74] S. Oláh, M. Füle, G. Komlósi, C. Varga, R. Báldi, P. Barzó, and G. Tamás, “Regulation of cortical microcircuits by unitary gaba-mediated volume transmission,” *Nature*, vol. 461, no. 7268, pp. 1278–1281, 2009.
- [75] X. Li, W. Zhou, S. Zeng, M. Liu, and Q. Luo, “Long-term recording on multi-electrode array reveals degraded inhibitory connection in neuronal network development,” *Biosensors and Bioelectronics*, vol. 22, no. 7, pp. 1538–1543, 2007.
- [76] P. Cavelier, M. Hamann, D. Rossi, P. Mobbs, and D. Attwell, “Tonic excitation and inhibition of neurons: ambient transmitter sources and computational consequences,” *Progress in biophysics and molecular biology*, vol. 87, no. 1, pp. 3–16, 2005.
- [77] K. Fuxe, A. B. Dahlström, G. Jonsson, D. Marcellino, M. Guescini, M. Dam, P. Manger, and L. Agnati, “The discovery of central monoamine neurons gave volume transmission to the wired brain,” *Progress in neurobiology*, vol. 90, no. 2, pp. 82–100, 2010.
- [78] K. H. Taber and R. A. Hurley, “Volume transmission in the brain: beyond the synapse,” *The Journal of neuropsychiatry and clinical neurosciences*, vol. 26, no. 1, pp. iv–4, 2014.
- [79] J. Clements, “Transmitter timecourse in the synaptic cleft: its role in central synaptic function,” *Trends in neurosciences*, vol. 19, no. 5, pp. 163–171, 1996.
- [80] P. Sah, S. Hestrin, and R. Nicoll, “Tonic activation of nmda receptors by ambient glutamate enhances excitability of neurons,” *Science*, vol. 246, no. 4931, pp. 815–818, 1989.
- [81] M. J. Wall and M. J. Richardson, “Localized adenosine signaling provides fine-tuned negative feedback over a wide dynamic range of neocortical network activities,” *Journal of neurophysiology*, vol. 113, no. 3, pp. 871–882, 2015.
- [82] E. O. Mann and I. Mody, “Control of hippocampal gamma oscillation frequency by tonic inhibition and excitation of interneurons,” *Nature neuroscience*, vol. 13, no. 2, pp. 205–212, 2010.
- [83] M. Hamann, D. J. Rossi, and D. Attwell, “Tonic and spillover inhibition of granule cells control information flow through cerebellar cortex,” *Neuron*, vol. 33, no. 4, pp. 625–633, 2002.

- [84] K. Lenk, E. Räisänen, and J. A. Hyttinen, “Understanding the role of astrocytic gaba in simulated neural networks,” in *Engineering in Medicine and Biology Society (EMBC), 2016 IEEE 38th Annual International Conference of the*, pp. 6121–6124, IEEE, 2016.
- [85] W. F. M, *Fluid Mechanics*. McGraw-Hill, 2009.
- [86] G. Tamás, A. Lőrincz, A. Simon, and J. Szabadics, “Identified sources and targets of slow inhibition in the neocortex,” *Science*, vol. 299, no. 5614, pp. 1902–1905, 2003.
- [87] J.-m. Zhang, H.-k. Wang, C.-q. Ye, W. Ge, Y. Chen, Z.-l. Jiang, C.-p. Wu, M.-m. Poo, and S. Duan, “Atp released by astrocytes mediates glutamatergic activity-dependent heterosynaptic suppression,” *Neuron*, vol. 40, no. 5, pp. 971–982, 2003.
- [88] M. J. Wall, “Furosemide reveals heterogeneous gaba a receptor expression at adult rat golgi cell to granule cell synapses,” *Neuropharmacology*, vol. 43, no. 4, pp. 737–749, 2002.